Computational Study of the reaction mechanism of the DNA repair enzyme AlkB

A thesis submitted to the University of Manchester for the degree of

Master of Philosophy (MPhil)

in the faculty of Engineering and Physical Science

2011

Luis Enrique Gonzalez Ovalle

School of Chemical Engineering and Analytical Science

TABLE OF CONTENTS

Words count 27,142

LIST OF FIGURES

ABBREVIATIONS

DFT	Density functional theory
HF	Hartree-Fock
MM	Molecular mechanics
NMR	Nuclear magnetic resonance
$P450_{cam}$	Cytochrome P450 from Pseudomonas putida, hydroxylase of camphor
PDB	Protein database
PES	Potential energy surface
QM	Quantum mechanics
QM/MM	Hybrid quantum mechanical molecular mechanics
SCF	Self-consistent field
SRC	Substrate recognition site
TS	Transition state
ZPE	Zero point energy
Ala	Alanine
Arg	Arginine
Asn	Asparagine
Asp	Aspartic acid
Cys	Cysteine
Gln	Glutamine
Glu	Glutamic acid
Gly	Glycine
His	Histidine
Ile	Isoleucine
Leu	Leucine
Lys	Lysine
Met	Methionine
Phe	Phenylalanine
Pro	Proline
Ser	Serine
Thr	Threonine
Trp	Tryptophan
Tyr	Tyrosine

ABSTRACT

The University of Manchester

Faculty of Engineering and Physical Sciences

ABSTRACT OF THESIS submitted by Luis Enrique Gonzalez-Ovalle for the degree of Master of Philosophy (MPhil) and entitled "Computational Study of the reaction mechanism of the DNA repair enzyme AlkB"

Date of submission: 08/09/2011

The AlkB enzyme is one of the most vital nonheme enzymes in the DNA repair mechanism in humans. Because of its importance as a promiscuous substrate recognition enzyme, it is the subject of scientific research into drug development and cancer treatment. However, currently little is known on the catalytic mechanism by the enzyme and the active oxidant in the reaction mechanism. To elucidate the active oxidant and establish a catalytic cycle we performed a series of computational studies, and, in particular, used the quantum mechanics / molecular mechanics (QM/MM) method. A novel mechanism was found, which starts from an iron(IV)-oxo species, whereby an internal rotation of the iron(IV)-oxo group initiated the reaction mechanism and brings the oxidant in close proximity with the substrate. Subsequently, a hydrogen atom abstraction by the iron(IV)-oxo species happens prior to hydroxyl rebound to form hydroxylation products. Our computational study predicts a rate determining hydrogen atom abstraction reaction step followed by concerted rebound to form products. This mechanism shows dramatic differences with other nonheme iron-oxygenases, where no internal rotation is needed and that proceed with significant rebound barriers. The studies also highlight the effects of protein on the reaction mechanism.

In a second set of calculations, we investigated a novel biomimetic model of the nonheme iron enzyme cysteine dioxygenase using density functional theory methods. These systems were recently synthesised and displayed reactivity differences in the presence of chloride as compared to triflate anions. In order to understand these differences, we performed a density functional study and explain the origin of this reactivity difference. Thus, a bulky triflate group causes steric interactions with the isopropyl side groups of the equatorial ligand and consequently thiophenol cannot bind in the favourable equatorial position. As a result, triflate binding cannot give dioxygenation of thiophenol and thiophenyl radical are formed leading to PhSSPh products instead. Our calculations are in good agreement with experimental observation.

Finally, recent studies of the Sorokin group revealed a nonheme diiron phthalocyanine complex capable of hydroxylating the very strong C–H bond in methane. We did a density functional theory study on the mechanism and origin of this efficient reactivity. The exploratory results give a low hydrogen abstraction barrier of 7.9 kcal mol^{-1} from methane by this oxidant that via an concerted mechanism leads to methanol products. The barrier obtained from this study is significantly lower than that found by an iron(IV)-oxo porphyrin cation radical species, which was 26.5 kcal mol^{-1}. Therefore, *N*-bridged diiron complexes are more catalytically active than iron-porphyrins.

DECLARATION

No portion of the work referred to this thesis has been submitted in support of an application for another degree or qualification of this or any other university or other institute of learning.

COPYRIGHT STATEMENT

i. The author of this thesis (including any appendices and/or schedules to this thesis) owns certain copyrights or related rights in it (the "Copyright") and s/he has given The University of Manchester certain rights to use Copyright, including for administrative purposes.

ii. Copies of this thesis, either in full or in extracts and whether in hard or electronic copy, may be made only in accordance with the Copyright, Designs and Patents Acts 1988 (as amended) and regulations issued under it or, where appropriate, in accordance with licensing agreements which the University has form time to time. This page must form part of any such copy made.

iii. The ownership of certain Copyright, patents, designs, trademarks and other intellectual property (the "Intellectual property") and any reproductions of copyright works in the thesis, for example graphs and tables ("Reproductions"), which may be described in this thesis, may not be owned by the author and may be owned by third parties. Such Intellectual Property and Reproductions cannot and must not be made available for use without the prior written permission of the owner(s) of the relevant Intellectual Property and/or Reproductions.

iv. Further information on the conditions under which disclosure, publication and commercialisation of the thesis, the Copyright and any Intellectual Property and/or reproductions described in it may take place is available in the University IP Policy, in any relevant Thesis restriction declarations deposited in the University Library, The Library's regulations and in The University's policy on Presentation of the Theses.

ACKNOWLEGEMENT

It is a pleasure to thank those who made this thesis possible. First of all, my supervisor, Doctor Sam de Visser, whose encouragement, guidance and support from the initial to the final level enabled me to develop an understanding of the subject. I also want to express my gratitude to my college Matthew Quesne, who has made available his support in a number of ways.

Finally, I want to thank all my friends who have support me during this time and specially to Betty Levy, whom without her support I could not start my studies.

CHAPTER 1.

INTRDUCTION

1.1 Preface

The AlkB enzyme is a member of the superfamily of α-ketoglutarate- and iron-dependent dioxygenases (αKG-Fe (II)-dioxygenases) and is one of the most important enzymes in the DNA repair mechanism in humans. This enzyme is the main focus of my work due to its enormous advantage as promiscuous substrate recognition system (Abu-Omar, et al., 2005; Bassan, et al., 2005; Bugg, 2001; Bugg and Ramaswamy, 2008; Decker and Solomon, 2005; Koehntop, et al., 2005; Krebs, et al., 2007). Therefore, it is a key target for scientific research into developing drugs. Surprisingly, the general knowledge of nonheme enzymes and in particular, AlkB is limited.

In this chapter, I will introduce the necessary background information about enzymes, reaction mechanisms, as well as some details of heme and nonheme enzymes, and specially, will focus on the latter type of enzymes and their typical reactions, properties and uses. Later, I will give an overview about DNA and RNA damages and repair and will finish the chapter with an overview of the DNA/RNA repair protein in *Escherichia coli*, AlkB.

1.2 Enzyme

The general definition of an enzyme is substances, usually proteins produced by a living organism, which acts as a biological catalyst of a specific biochemical reaction. The name enzyme comes from the Greek word meaning “in yeast”, and derives from the fact that catalysts are inside a living cell, where they catalyse reactions in the central metabolic pathway in order to keep the cell alive (Horton, 1996; Schulz and Schirmer, 1979; Wilson and Walker, 2009; Zubay, et al., 1995). It is important to keep in mind that the main role of enzymes is to increase the rate of reactions. This important characteristic carries us into the definition of the catalyst, which is known as a substance that accelerates the attainment of equilibrium (Bugg, et al., 1997; Horton, 2006).

Thus, the catalyst lowers the amount of energy necessary to cross a barrier and drive a specific reaction (see Figure 1.1).

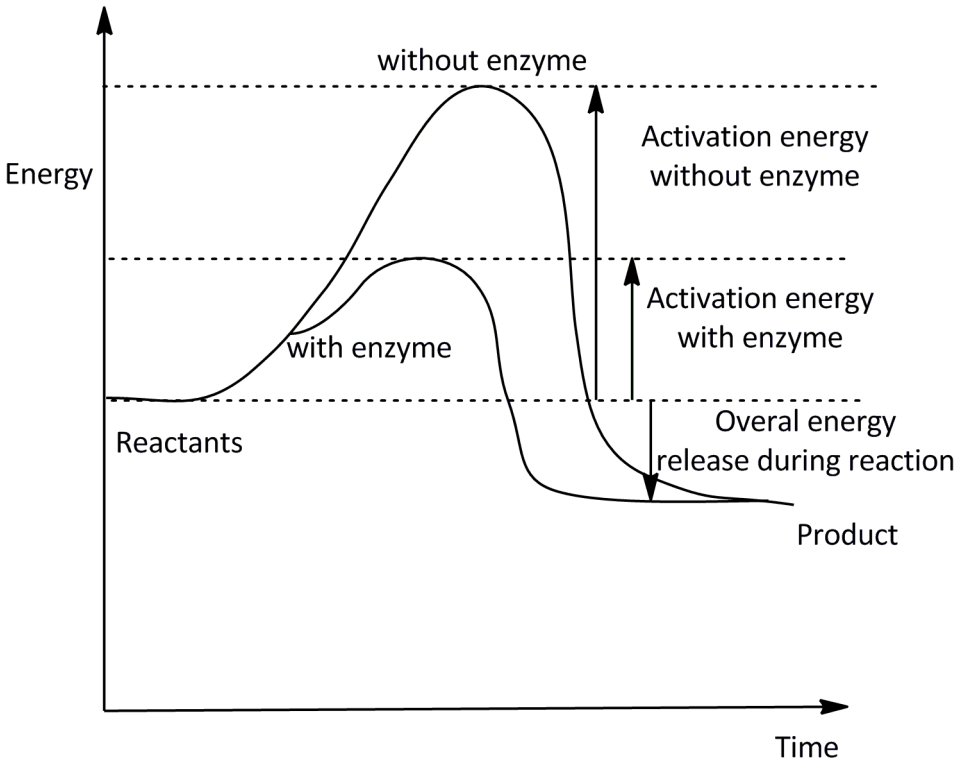

Figure 1.1 Energy landscape of catalysis

1.3 Enzyme Structure and Functions

It has been noted that enzymes have different primary structures. A polypeptide linear sequence chain is formed when two or more amino acids are attached to each other by the use of a peptide bond, which is the basis of the primary structure of the protein (Horton, 1996). The secondary structure, which is built inside of the ribosome, is formed when the linear polypeptide chain is folded, forming the protein three-dimensional structure. Subsequently, a tertiary structure is built, when elements of secondary structure, are joint together and form a catalytically active but stable conformation (Horton, 1996; Schulz and Schirmer, 1979; Wilson and Walker, 2009; Zubay, et al., 1995). A characteristic of this structure is that the hydrophobic amino acid side chain is located inside of the protein whereas the hydrophilic amino acid side chain is on the surface (Jaenicke, 1991). Protein tertiary structures can be characterized as $\alpha - helical\ proteins$, α/β $structures$, or $anti - parallel\ \beta\ structures$. It should be noted that $\alpha - helical\ proteins$ and $\beta - sheets$ are represented by ribbon forms. For example, Hemoglobin, globin oxygen carrier, is a $\alpha - helical$ complex tertiary structure. Flavodoxin, a redox protein with arrangements of $\beta - sheets$ - $\alpha - helix$-parallel $\beta - sheets$ corresponding to structures α/β. Instead, anti-parallel $\beta - sheets$ are arrayed as $\beta - sheets - \beta - turn - anti - parallel\ \beta - sheets$ as is the case of metallo-enzyme superoxido dismutase (Chothia, 1984; Creighton, 1993; Jaenicke, 1991; Schulz and Schirmer, 1979).

It is well known that all enzymes are proteins but not all proteins are enzymes, because enzymes have catalytic activity. As we can observe the active site in the tertiary structure, where the enzymatic activity is performed, is generally a hydrophilic cleft. Often the active site is bonded to some non-protein chemical compounds (cofactors) which are required for a number of specific enzymatic reactions.

The question now is how the enzyme is able to bind the substrate?

In order to answer this question, it is necessary to understand the concept of protein structure and molecular properties. Thus, the main characteristics of the enzyme are its high substrate selectivity. If we consider the chirality of the active site and the shape of the substrate, it is understandable how they can join (Jaenicke, 1991).

1.4 Enzymatic oxidation reactions

In nature, O_2 is essential for life. In process such as cellular respiration, dioxygen is used as a terminal electron acceptor. Besides that, it is well accepted that dioxygen is important in the synthesis of complex molecules by aerobic organisms (Bugg and Ramaswamy, 2008).

Two groups simultaneously discovered the oxygenase enzymes, namely the Osamu Hayaishi group in Japan and the Howard S. Mason from the US, who worked on oxygenases that oxidise a substrate by transferring one oxygen atom from molecular oxygen (Hayaishi, 1994; Hayaishi, 2005; Hayaishi, et al., 1990; Waterman, 2005; Yamamoto, 2006).

There are two types of oxygenases: Monooxygenases, or mixed function oxidase, that transfer one oxygen atom to the substrate, and reduce the other oxygen atom to water, and Dioxygenases, or oxygen transferases, that incorporate both atoms of molecular oxygen (O_2) into the product(s) of the reaction (Bugg, 2003).

1.4.1 Monooxygenases and dioxygenases

There are several classes of monooxygenase enzymes including non-heme, copper-dependent, and metalloporphyrin complexes (Denisov, et al., 2005). It is well known that the use of O_2 in a catalysis has a great advantage due to its oxidation power and because the bond cleavage is highly thermodynamically favourable. However, O_2 on its own is unreactive, since the molecule exists in a triplet ground state. The low reactivity in singlet and triplet ground states is caused by the fact that the reaction is spin forbidden in those states, and therefore requires a high activation energy (Sono, et al., 1996). As noted by Poulos (2005), oxygenases activate dioxygen in such a way that O_2 can participate in reactions it normally would not be involved in. One way to activate dioxygen is through the use of metal cofactors such as iron or copper to perform biological oxidations. In fact, transition metals react directly with triplet O_2 to form a metal (III)-peroxo or metal (II)-superoxo complex that can be converted into a more active metal-oxygen complex such as a metal (IV)-oxo active species. This active oxidant in turn catalyzes either the incorporation of oxygen atoms into organic substrates or to the oxidation of the organic substrates (Poulos, 2005; Sono, et al., 1996). Finally, as Nam (2007) recognised there is a potential economic value if this sort of mechanism is studied and understood, since these high-valent metal-oxo complexes have potential in biotechnology.

1.5 Enzymes that use Fe in active site

Müller and Bröring (2008) classified iron proteins according to their structure into three categories: Iron-sulphur proteins, heme proteins and non-heme proteins. Iron-sulphur proteins are mainly characterised through the binding of cysteinate amino acid residues to the metal, and are involved in electron transfer processes. Heme proteins contain a metal, typically iron, that is ligated to a protoporphyrin IX group of which the four nitrogen ligand atoms coordinate to the iron in one plane of symmetry (Kumar, et al., 2004; Sono, et al., 1996) . These enzymes are involved in electron transfer and oxidation reactions. Finally, Non-heme proteins can be subdivided into mononuclear and binuclear active sites. These enzymes contain metal ion(s) that are coordinated to nitrogen and oxygen based ligands (Müller and Bröring, 2008).

There are two types of transition metal containing enzymes, namely the heme and non-heme enzymes, De Visser (2006). Heme enzymes are generally involved in essential biological processes such as hemoglobin oxygen transport, biosynthesis, and substrate detoxification as is the case with the cytochromes P450 enzymes (Lonsdale, et al., 2009). These enzymes transfer one oxygen atom of molecular oxygen to the substrate and reduce the other oxygen atom to form a water molecule, hence are known as monooxygenases.

By contrast, there are non-heme iron complexes with a pentacoordinated ligand system that act as dioxygenases since they transfer both oxygen atoms of molecular oxygen to one or more substrates (Bollinger Jr, et al., 2005; Bugg, 2003).

Thus, α-ketoglutarate dependent dioxygenases (αKG) play important roles in biological processes such as collagen synthesis and repair of DNA (de Visser, 2006; Knott and Bailey, 1998; Siegel and Martin, 1970).

It has been argued that the biggest dissimilarity of the heme and non-heme enzymes relates to their catalytic cycle, whereby dioxygenases lack cofactors that transfer electrons and/or protons into the active site (Krebs, et al., 2005; Lanzilotta, et al., 2003).

Model calculations on oxo–iron systems of either heme or nonheme systems gave similar geometric features, therefore it was reasoned that the differences in properties between the two model systems arise from electronic differences.

Computational modelling (de Visser, 2006) highlighted the fact that the activation barrier of substrate hydroxylation by a non-heme iron (IV)-oxo oxidant is significantly lower than that found for heme models, such as active site models of cytochrome P450 or horseradish peroxidise (HRP). As a consequence, the αKG model was found to have the capacity to hydroxylate strong C-H bonds due to its extraordinary strong oxygenation capability as compared to heme-type enzymes, such as P450 and HRP.

1.6 Heme-enzymes

In organic synthesis, Monooxygenases and Peroxidases are the main groups of heme enzymes used (Müller and Bröring, 2008). The distal protein pocket of monooxygenases leads the substrate to the porphyrin active site. It is well known that the heme in peroxidases is typically linked to the protein via an iron-histidine bond.

1.6.1 Metal-dependent mono-oxygenases

P450 monooxygenases are a large class of heme enzymes found in most organisms, where they catalyze the specific hydroxylation of inactivated alkanes. The name P450 draws from the fact that an absorbance at 450 nm is observed in the CO bound form (Bugg, 2004).

Computational modelling (Shaik, et al., 1995; Shaik, et al., 1998) showed that the electronic ground state of the iron(IV)-oxo species, termed Compound I (CpdI), contains a nearly degenerate doublet and quartet spin state. As a consequence of this there are two competitive reaction mechanism on either the doublet or the quartet spin state, which has been termed two-state reactivity (Shaik, et al., 2002; Shaik, et al., 2005). It was shown that the reaction takes place via an initial hydrogen atom abstraction followed by radical rebound to form alcohol products. Thus, the quartet spin mechanism was found to proceed via a relatively long-lived radical intermediate that may rearrange and generate by-products whilst the short-lived intermediate on the doublet spin state surface gives unrearranged products directly. Therefore, the population of the doublet and quartet spin states of CpdI of heme enzymes can influences the product distributions, rate coefficients and kinetic isotope effects (de Visser, et al., 2004; de Visser, et al., 2001; Kumar, et al., 2005). By contrast, the iron(IV)-oxo active species in non-heme iron enzymes, e.g. αKG CpdI, has a quintet spin ground state, which is well separated from other spin states (de Visser, 2006), hence the reaction takes place via singlet-state reactivity only.

1.7 Non-heme enzymes

Non-heme iron enzymes participate actively in biochemical processes important for human health such as tissue repair and antibiotic biosynthesis (Cardinale and Udenfriend, 1974; Chen, et al., 1994; Knott and Bailey, 1998; Siegel and Martin, 1970). This family of enzymes is involved in a large amount of catalytic functions due to their versatility of substrate activation (Bugg and Ramaswamy, 2008; Costas, et al., 2004; MacKerell Jr, et al., 1998). It is well known that among the catalytic functions, in which these enzymes participate, include biosynthesis, biodegradation of compounds, and repair mechanisms such as DNA and RNA base repair. A large group of these mononuclear nonheme iron-containing enzymes use α-ketoglutarate as a cosubstrate to act as dioxygenases (Bugg, 2003; Krebs, et al., 2007; Schofield, et al., 2010). The mechanism of these enzymes is characterised by the binding of α-ketoglutarate to an iron (III) centre, while substrate is bound in the vicinity (Branden and Tooze, 1991). After dioxygen binds the iron centre this is followed by decarboxylation of α-ketoglutarate, which in turn, forms an iron(IV)-oxo species, the active oxidant of substrate hydroxylation reactions, and succinate (Abu-Omar, et al., 2005; Lanzilotta, et al., 2003; Lovell, et al., 2003; Ryle and Hausinger, 2002). It has been demonstrated that High-valent iron (IV)-oxo complexes are active oxidants of substrate hydroxylation reactions, for heme and nonheme enzymes (Lonsdale, et al., 2009; Nam, 2007; Sono, et al., 1996).

Although most mononuclear nonheme iron dioxygenases have a 2His/1Asp structural motif (Kamachi, et al., 2004), there are dioxygenases with different ligand binding motif. In fact, dioxygenases such as Acetylacetone Cleaving enzyme (Dke1) has a transition metal active site bound to three histidine groups. Quercetin dioxygenase, instead, has the metal bound to three histidines and one glutamic acid group (Gopal, et al., 2005). Cysteine dioxygenase, another mononuclear nonheme iron dioxygenase, has a 3His metal bounded motif; it is essential for human health (Joseph and Maroney, 2007; Stipanuk, 2004). For instance, neurological disorders related with the reduction of CDO (Perry, et al., 1985) include diseases such as Alzheimer's and Parkinson's (Heafield, et al., 1990). Actually, due to its importance for the human health it has been well studied and research focussed on the understanding of CDO enzyme mechanism (Costello and Lidstrom, 1999; de Visser and Straganz, 2009; Marco, et al., 2004; Phillips, et al., 2006; Pierce, et al., 2007).

The class of non-heme iron proteins is inhomogeneous and therefore often divided into subclasses. A distinction can be made based on the ligands that coordinate to the iron centre.

1.7.1 Mononuclear iron sites

The mononuclear non-heme iron enzymes include in this group are characterised for having an arrangement, where the metal binds to two Histidine and one carboxylate group of the protein. The five different families include in this class are extradiol dioxygenases, Rieske dioxygenases, α-ketoglutarate-dependent hydroxylases, pterin-dependent enzymes and otheroxidases . In this sort of enzymes there are three vacant spaces to bind cofactor, residue or solvent; however, in the resting state those places are occupied by water as a ligand (Karplus, et al., 2006; Müller and Bröring, 2008). The general reaction catalysed by αKDD is given in Figure 1.2 and shows the products alcohol, CO_2 and Succinate.

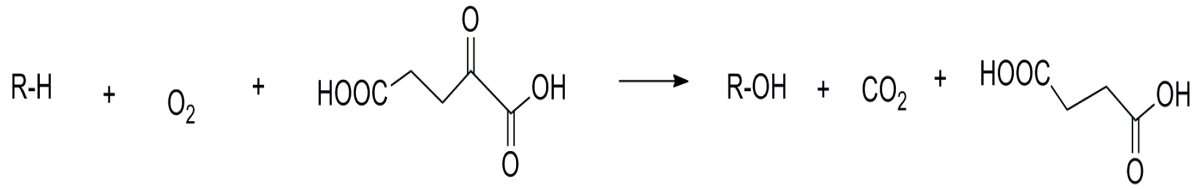

Figure 1.2 Representation of the reaction catalysed by α-ketoglutarate-dependent hydroxylases.

1.7.2 α-Ketoglutarate-dependent dioxygenases

It is often stated that α-Ketoglutarate-dependent dioxygenase (αKDD) are, in fact, one of the biggest families of proteins found in animals, plants and microbes. They contain a transition metal active site that is attached to two histidines, and one carboxylate group (Hausinger, 2004; Purpero and Moran, 2007). Taurine dioxygenase (TauD) is the most intensively studied (αKDD) and is found in bacteria, where it is involved in the biodegradation of taurine. Tau D produces succinate and carbon dioxide using α-Ketoglutarate as a cofactor. This enzyme is characterised for using non-heme iron ion as a cofactor instead of heme iron ion (Müller and Bröring, 2008). The catalytic cycle of TauD is well studied, see e.g. Bassan et al. (2005), Borowski et al. (2004), and Bugg (2004), which starts with dioxygen binding to an Fe(III) centre followed by attack of the terminal oxygen atom on the α-keto position of α-ketoglutarate to form a cyclic peroxy intermediate. This is possible due to the donation of an electron from the non-heme iron (II) to oxygen in order to produce an Iron (III). In turn, succinate is released and an iron (IV)-oxo species is formed through decarboxylation of this intermediate. Even though there are many proposed reaction mechanisms for Fe (II)/α-Ketoglutarate-dependent hydroxylases, one of the most accepted ones is presented in Figure 1.3.

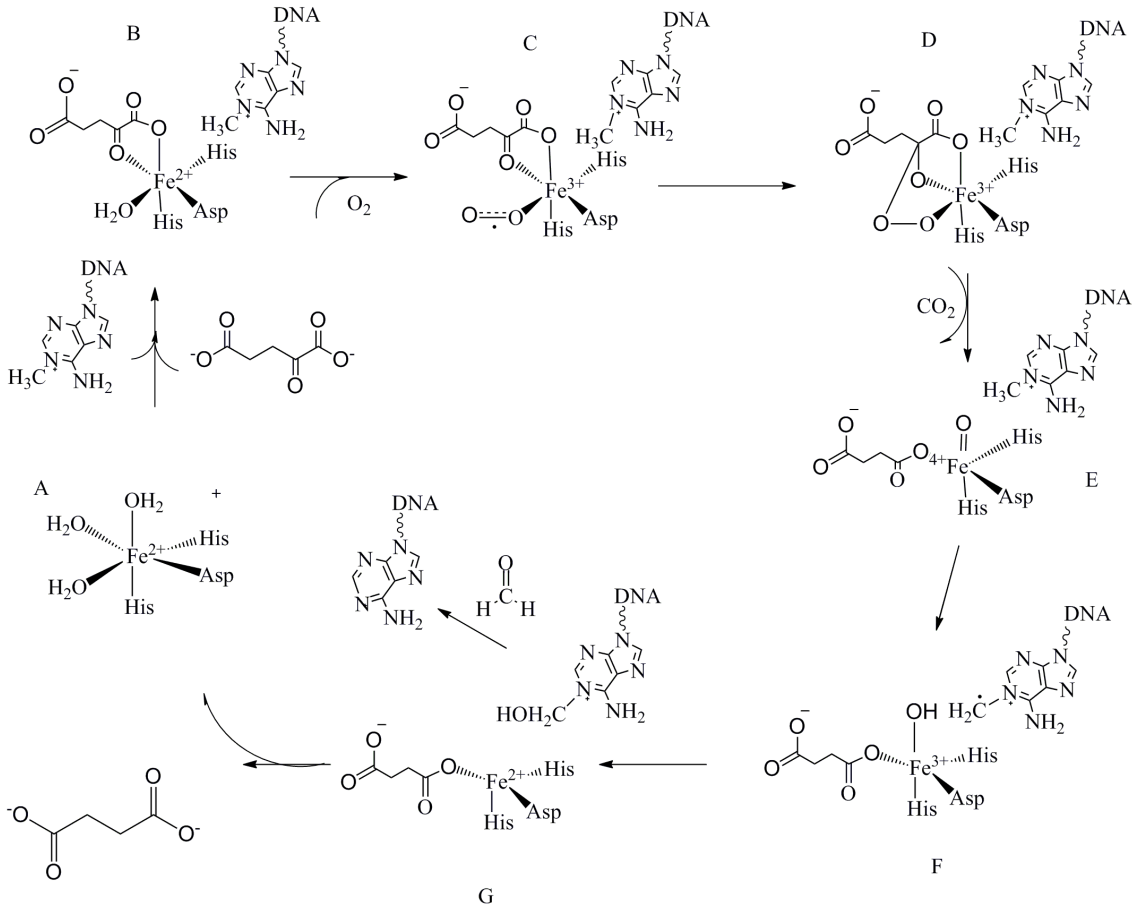

Figure 1.3 Enzymatic mechanisms of α-Ketoglutarate-dependent dioxygenase (αKDD)

Important reactions involving α-Ketoglutarate-dependent iron (II) dioxygenases are biosynthesis of antibiotics and the repair of alkylated nucleic acid (DNA/RNA repair), which is the main topic of this paper.

In order to understand the Scheme of α-Ketoglutarate-dependent iron (II) dioxygenases, it is important to highlight some details. First, the Intermediate (A) shows the His-X-Asp/Glu-Xn-His sequence joined to Fe (II), which is a typical motif between the Fe (II)/αKG-dependent hydroxylases. Furthermore, this metal binding mode is characteristic of this group of enzymes, both the side chains and one face of the metal with the same orientation. The crystal structure shows the binding between Fe (II)-substrate-αKG and three water molecules in the metal coordination sphere. Second, the Intermediate (B) shows the enzyme bonded to Fe (II) and αKG, whereby the five-membered ring is associated with metal-to-ligand charge-transfer transitions (Pavel, et al., 1998). Third, Intermediate (C) symbolize the direct coordination between an enzyme and cosubstrate with the metal ion. Furthermore, it is shown that the bonding of the primary substrate happens nearby in the active site. It is observed the valence

change from Fe (II) to Fe (II) of the metal centre as well as the absorption of O_2 forming the intermediate (C) this stage of the cycle is not well established as well as its subsequent chemistry (Hausinger, 2004). Four, in Intermediate (D), it is well established experimentally that the addition of oxygen reduce the iso-electronic Fe(II)-O_2, Fe(III)-superoxo, or Fe (IV)-peroxo species. Fifth, Intermediates (E), Fe (III) or Fe (IV), in this diagram, bicyclic complex are the product of Nucleophilic attack over the keto group of αKG. Sixth, intermediates (F), the cosubstrate is transformed to a carbonate-succinate mixed to an Fe(III)-hydroxyl radical or Fe(IV)-oxo species when an oxygen atom is bound into the C_1-C_2 carbon–carbon bond of αKG. Finally, intermediate (G), a substrate radical plus an Fe(II)-hydroxide species is formed when the near activated oxygen to the substrate abstracts a hydrogen atom (Hausinger, 2004).

It should be noted that in oxidation reactions where dioxygen is present, transition metals such as iron (II) are the best catalyst. Müller and Bröring (2008) affirm that an iron (III) superoxo intermediate is formed in the catalytic cycle and followed by further reduction of the superoxide to a peroxide in agreement with the mechanism in Figure 1.3 for (αKDD).

1.8 Uses of Non-heme enzymes

Non-heme enzymes play important roles in areas such as pharmaceutical, and biochemical industry. The next part of this section will refer to some of these examples.

1.8.1 Antibiotics biosynthesis

The Fe (II)/αKG-dependent dioxygenases function during the biosynthesis of a diverse range of antibiotics. In addition to catalyzing a variety of hydroxylation reactions, some family members catalyze desaturation, ring expansion, ring formation, and other types of chemical transformations. See Figure 1.4 for examples of antibiotics biosynthesis reactions. The positions of these enzymes in antibiotic pathways vary from the generation of precursors to the modification of more complete intermediates. The following figures describe biochemical studies on the better-studied representatives of the Fe(II)/αKG-dependent dioxygenases involved in antibiotic synthesis; however, it is important to note that sequence analyses are consistent with similar enzymes participating in a number of other pathways (Bodner, et al., 2009; Strieker, et al., 2007; Townsend, 2002; Wackett, 2002; You, et al., 2007). It should be noted that from figure 1.4 to 1.6 the oxidation reaction is characterised by production of Succinate, CO_2 and water in addition with the final biosynthesis product.

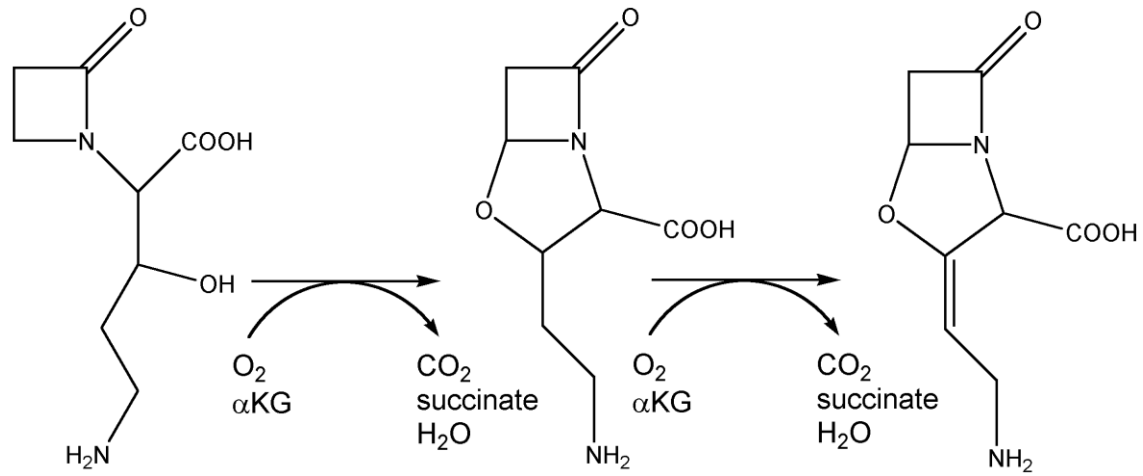

Figure 1.4 Cyclization and desnaturation reaction during the biosynthesis of the β-lactamase inhibitor clavulanic acid by clavaminate synthase

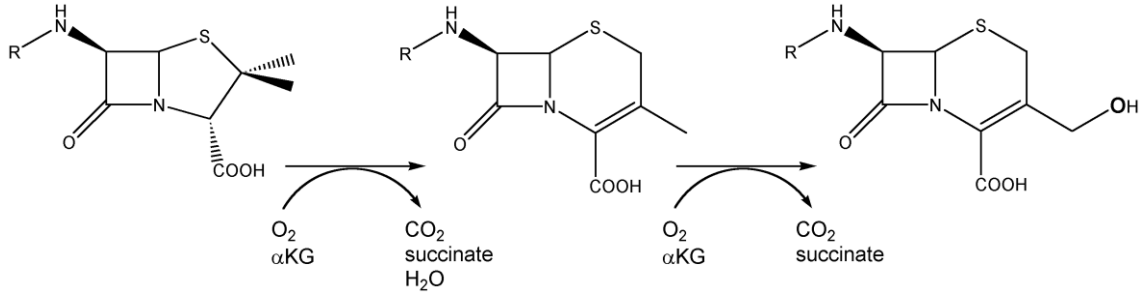

Figure 1.5 Deacetoxycephalosporin C synthase (DAOCS) and deacetylcephalosporin C synthase (DACS) are Fe (II)/αKG-dependent dioxygenases that catalyse sequential reactions starting with penicillin cephalosporin synthesis

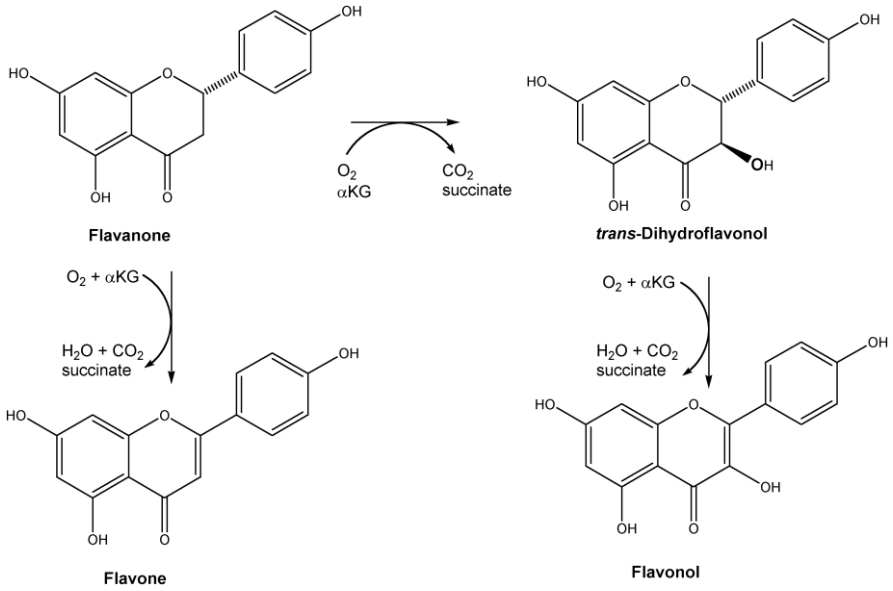

Figure 1.6 Flavanone 3*β*-hydroxylase catalyzes one of the key steps of flavonoid biosynthesis

1.8.2 Hypoxia

Lee et al. (1997) argued that increasing the expression of genes, which encode proteins and tissues, is the natural reaction to hypoxia of the mammalian cells. Proteins such as erythropoiesis that enhances the oxygen carrying capacity of the blood; angiogenesis that delivery of oxygen to hypoxic sites; glycolysis related with the production of energy; xenobiotic related to detoxification (Lee, et al., 1997).

1.8.3 Collagen Cross linking

It is widely known that one of the most important medical applications about Fe (II)/*α*KG-dependent dioxygenases is tissue repair (Pinnell and Martin, 1968; Siegel and Martin, 1970). For example, it has been used to treat health illness such as keratoconus that causes distortion of vision. Bone collagen cross-links are now widely used to measure bone levels in many metabolic bone diseases. It is understood that the enzymatic collagen cross-linking mechanism is co-dependent of the aldehyde formation from specific peptide lysine residues (Knott and Bailey, 1998).

As Siegel and Martin (1970) states that “the enzyme-dependent production of cross-linked collagen and the lysine-derived cross-link precursor allysine (α-aminoadipic δ-semialdehyde) has been demonstrated.” As the reason that the residue that is converted *in vivo* and β-

aminopropionitrile inhibits the conversion *in vivo*, the conclusion shows that the oxidase is the physiologically active enzyme necessary in the cross-linking of collagen first step.

1.8.4 DNA/RNA base repair

Repairing alkylation damages of DNA and RNA is the most recent function learned about Fe (II)/αKG-dependent dioxygenases. Producing a specific kind of DNA enzyme, cells defeat the mutagenic and lethal effects of these alterations. For example, *Escherichia coli* remove the alkyl groups along with the attached adenines to create a basic site in the DNA product. To do this the DNA uses its two distinct 3-methyladenine DNA glycosylases, encoded by *tag* and *AlkA.* On the other hand, A*lkB* encodes a Fe (II)/αKG-dependent dioxygenase that directly repairs 1-alkyladenine and 3- alkyl cytosine lesions in DNA or RNA (Hausinger, 2004). It appeared that the AlkB protein itself is not exclusively responsible for repairing DNA/RNA alkylation damages, perhaps because its own characteristics allow believing that it is possible to be part of a complex that perform such important mission (Chen, et al., 1994). The suggested DNA/RNA repair mechanisms are shown in Figure 1.7 and 1.8.

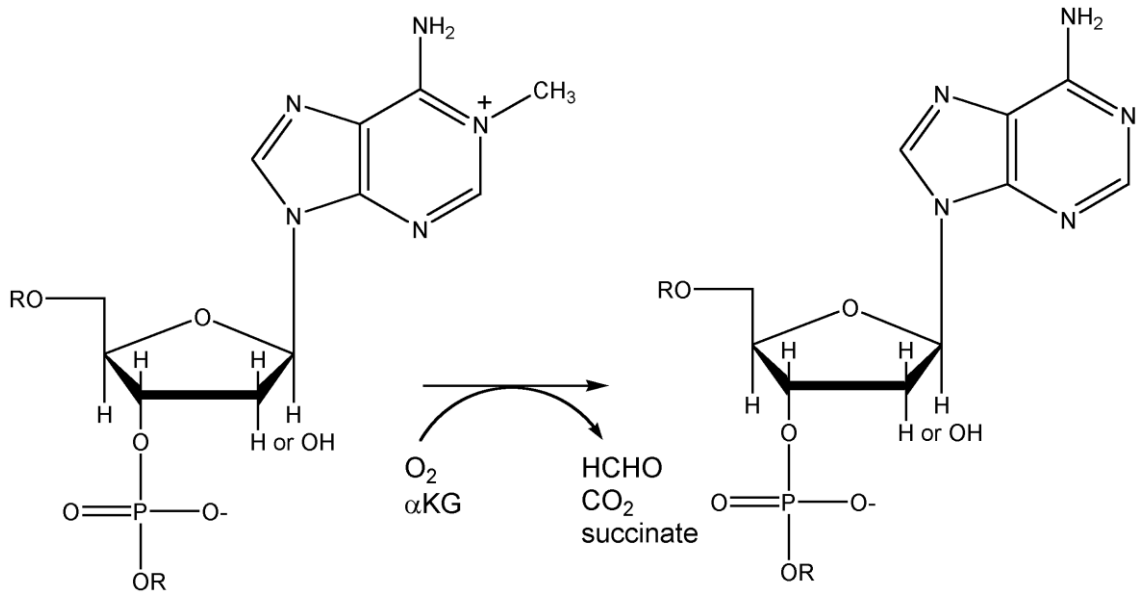

Figure 1.7 Suggested DNA repair mechanism

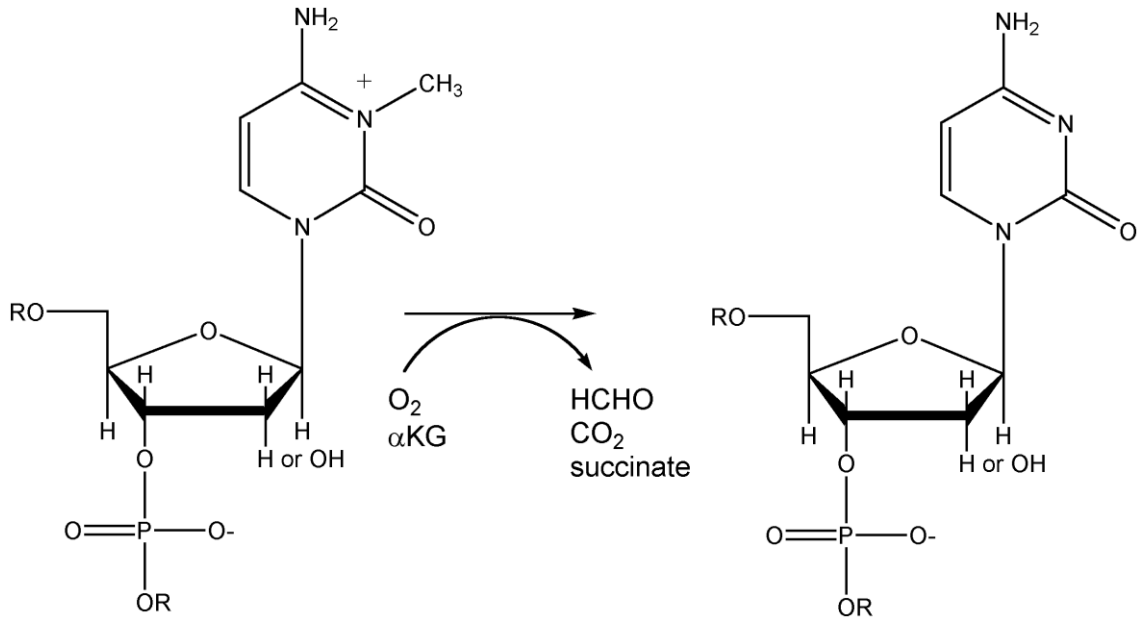

Figure 1.8 Proposed mechanism of DNA/RNA repairing

1.9 The study of AlkB iron enzyme

It has been discussed that DNA cytotoxic and mutagenic problems are caused by methylation (Chen, et al., 1994; Reißner, et al., 2009). AlkB, a DNA repair protein in *Escherichia coli*, is responsible for fixing DNA methylations by oxidation reactions producing formaldehyde from the methyl carbon (Aravind and Koonin, 2001; Guo, et al., 2003; He, et al., 2006; Roy and Bhagwat, 2007). It is mentioned that also exist two other homologous proteins to AlkB, in humans, ABH2 and ABH3, which repair the same sorts of DNA lesions (Falnes, 2004; Falnes, et al., 2004; Mishina and He, 2003). However, in our studies, we will focus in AlkB enzyme. In order to achieve the demethylation, a non-heme mononuclear iron (II), and two cofactors: α-ketoglutarate (αKG) and dioxygen are used by AlkB(Yang, et al., 2009). Lesion of DNA bases such as 1-methyladenine (1-meA), 3-methylcytosine (3-meC), 1-methylguanine (1-meG), and 3-methylthymine (3-meT), are repaired by AlkB(Delaney and Essigmann, 2004). It is well known that AlkB, is characterised by repairing damaged bases in RNA as well as performing job on single-stranded DNA (ssDNA) (Kudrik and Sorokin, 2008; Sorokin, et al., 2009).

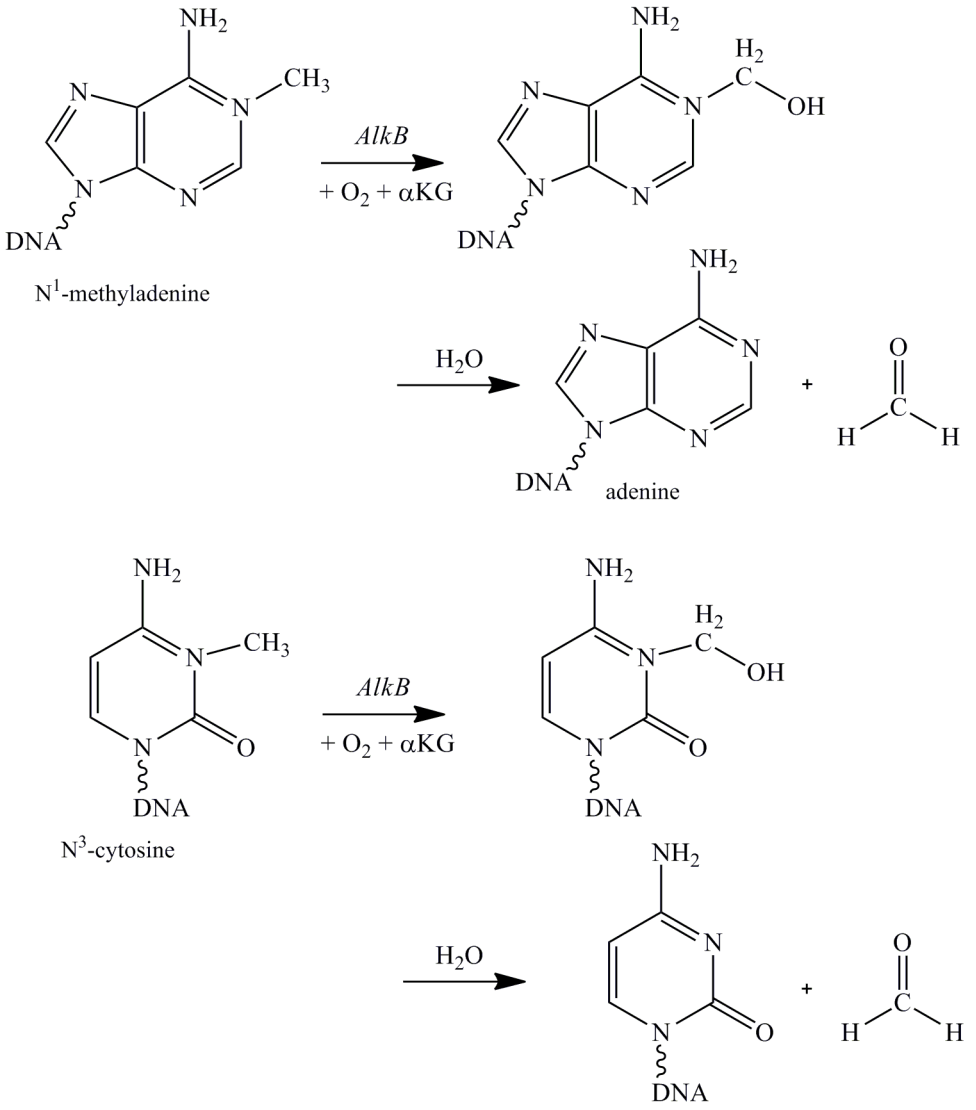

Figure 1.9 Proposed repair mechanisms of N^1methyladenine and N^3-cytosine by AlkB

It has shown that AlkB have a preference of demethylating N^1methyladenine and N^3-cytosine, see Figure 1.9 (Koivisto, et al., 2003). According to Duncan et al, (2002), it is also possible to repair N^1-ethyladenine by AlkB producing adenine with acetaldehyde. Even though, N^3-methylthymine and N^1-methylguanine are also repaired, see Figure 1.10., but less efficient (Delaney and Essigmann, 2004; Falnes, 2004). Figure 1.10 (B) shows how the putative iron -oxo intermediate epoxidizes the exocyclic double bond of the base lesion. Subsequent hydrolytic decomposition of the epoxide intermediate liberates the repaired base and dialdehyde glyoxal (de Visser, 2009). The N^1-adenine and N^3-cytosine positions are involved in hydrogen bonding. It has been argued by Chen et al., (1994) that in a single-stranded oligonucleotide, these positions would be much more susceptible to methylation.

The figure 1.10 shows (A) DNA/RNA alkylations that are known to be repaired by AlkB family enzymes, and (B) Repair mechanism of 1, N^6 ethenoadenine by AlkB

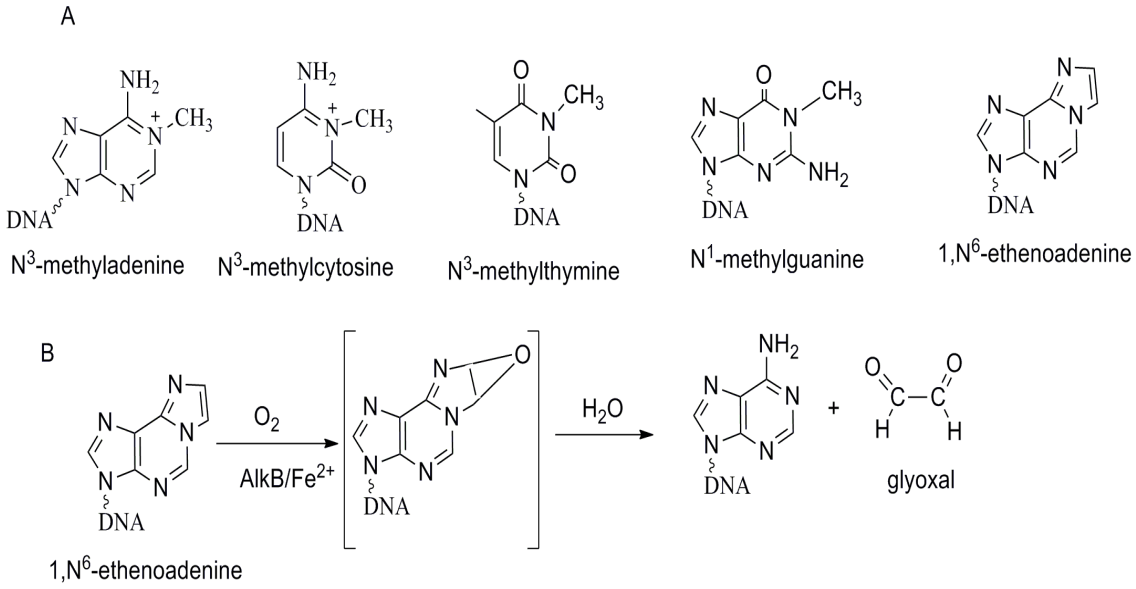

Figure 1.10 Mechanism of repair by AlkB dioxygenase

1.9.1 Characteristics of the Non-Heme Iron (II) Site of AlkB

As noted by Mishina et al., (2004) in the absence of DNA, the geometry of AlkB has a five-coordinate iron (II) while in the presence of ssDNA, iron (II) turn into six-coordinated. Two important observations were made: First, the regulation of the dioxygen activation is likely by substrate binding. Second, the change of the geometry helps to bind dioxygen to iron (II) and in turn iron (II) oxidation.

1.9.2 AlkB Structure

The structure of AlkB comprises of three regions: (1) a catalytic core in the carboxyl-terminal domain, (2) a unique nucleotide-recognition lid, and (3) an N-terminal extension. It was reported that important residues are found in the active side such as Trp69 and His131, which make possible substrate recognition. Tyr76 makes hydrogen bonding interactions with the two phosphates methylated groups, which may facilitate to fix the substrate into the active site (Yu and Hunt, 2007). Mishina et al., (2004) implies that the binding between enzymes and nucleic acid is weak and does not follow any specific manner of sequencing.

1.9.3 AlkB superfamily

The AlkB enzyme was identified in February 2001, through the studies about biochemical activity (Aravind and Koonin, 2001). Additional computational studies analysed and classified it to belong to the superfamily of α-ketoglutarate-dependent dioxygenase (αKDD), and it was found that this DNA repair enzyme superfamily catalyzes a wide variety of oxidation reactions by using a oxygen molecule (Alseth, et al., 2006; Aravind and Koonin, 2001; Borowski, et al., 2004; Elkins, et al., 2002; Hegg and Que, 1997; Sanchez-Pulido and Andrade-Navarro, 2007). Information about this enzyme was used to predict the oxidative demethylation reaction on 1MeA and 3MeC-bases in alkylated DNA strains (Aravind and Koonin, 2001).

1.9.4 AlkB in vivo

Repairing damaged DNA with AlkB is essential as problems in N^1methyladenine and N^3-cytosine cause death of *E. Coli* (Kataoka, et al., 1983) and human cells . It is understood that the produced formaldehyde in the DNA repair mechanism is dangerous (Chen, et al., 1994; Lutz, 1990), as second-hand damage can happen after the reparation; however, it is believed that cells have the capacity of avoiding this situation. As Aravind and Koonin states that this enzyme should be able to remove N^1methyladenine and N^3-cytosine lesions from RNA (Aravind and Koonin, 2001). Damage to RNA by alkylating-agents may cause protein synthesis defects, resulting at the end in apoptosis. Moreover, this repair of damaged RNA is essential and prevents neurodegenerative disorders.

1.10 Summary of project objectives

AlkB repair enzymes, with a nonheme iron centre, bind αKG, dioxygen and methylated DNA to catalyze a hydroxylation reaction, and produce formaldehyde. According to some analytical studies, for the formation process of formaldehyde and CO_2, Fe (II), αKG and molecular oxygen are needed (Borowski, et al., 2004; Riggs-Gelasco, et al., 2004; Yang, et al., 2009). In 2006, Yu et al., classified the AlkB repair enzymes belonging to the αKG dependent dioxygenases and highlighted a nonheme iron active site, where the metal is bound to a 2-His/1-Asp ligand system(Wiener, et al., 2003). Due to the mechanism of substrate activation of AlkB repair enzymes is unknown as well as the origin of the substrate specificity, it is necessary to perform a combined quantum mechanics/molecular mechanics (QM/MM) and density functional theory (DFT) study on substrate activation by AlkB repair enzymes in order to address these issues. Figure 1.11 shows the mechanism to be studied.

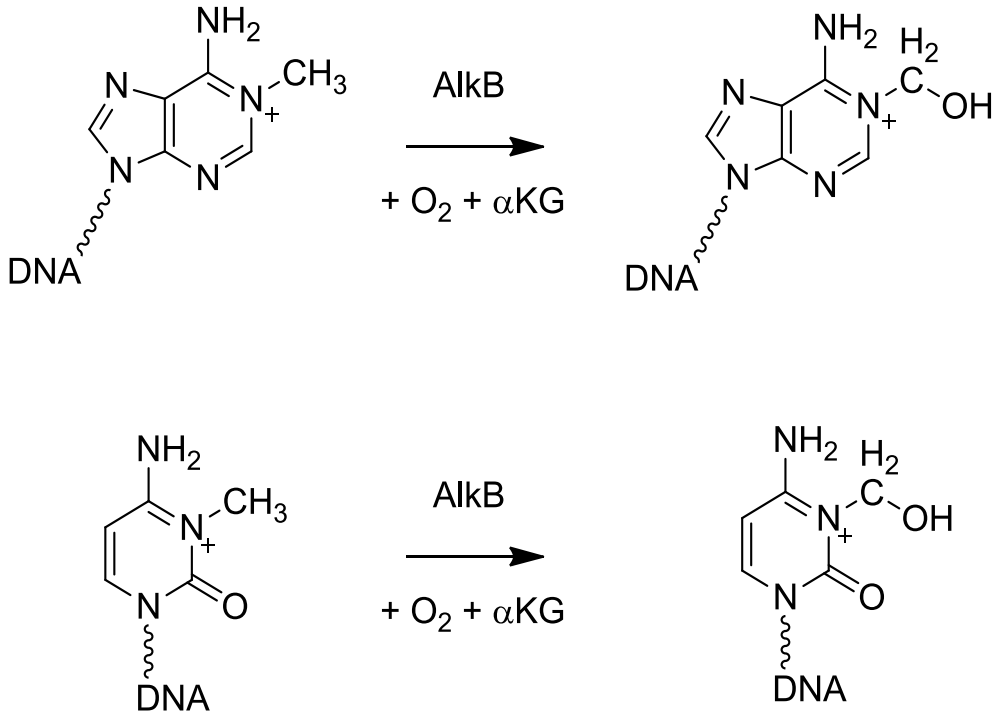

Figure 1.11 DNA base repair mechanisms to be studied in this work.

CHAPTER 2.

COMPUTATIONAL METHODS

2.1 Introduction

In order to understand and predict molecular behaviour, computational procedures were developed which generally fall into three categories: *ab initio* and semi-empirical quantum mechanics (QM) methods and molecular mechanics (MM) methods. The accuracy of the results is dependent on the computational theory that is used. For example, *ab initio* methods start from the Schrödinger equation (Equation 2.1) and do not use information of the chemical properties of the molecules, whereas (semi)empirical methods use thermodynamic and structural parameters (Atkins and Friedman, 2011; Atkins and Friedman, 2005) . Quantum-mechanical (QM) methods are based on the solution of the Schrödinger equation that was introduced by Erwin Schrödinger in 1926.

$$\mathrm{H}\Psi = \mathrm{E}\Psi \tag{2.1}$$

The interactions of all charged particles are described by a Hamiltonian (H) that couple with the movement path of these particles called the wavefunction (Ψ) and has a total energy (E) as eigenvalue. The advantage of QM methods is that with the approximate solution of this equation, it is possible to predict chemical proprieties with reasonable accuracy. In general, wavefunction methods scale with the number of electrons in the chemical system. Consequently, these methods cannot be used to study large systems (>50 atoms) due to their high computational cost. QM *ab initio* methods are generally used for studies of small systems and can reach accuracies of 1 kcal mol^{-1} for thermodynamic properties (Atkins and Friedman, 1997; Atkins and Friedman, 2005; Atkins, et al., 1997; Jensen, 2007; Leach, 2001; Mulholland, 2007; Mulholland, et al., 1993; Schneider, 1998; Siegbahn and Himo, 2009; Szabo and Ostlund, 1996).

MM methods, on the other hand, ignore electron distributions but describe bonds as strings and, therefore, scale more favourably for larger systems, i.e. tens of thousands of atoms. However, their big limitation is that they cannot describe or model bond-breaking/- formation processes (Atkins, 1978; Atkins, 1991; Atkins and Friedman, 1997; Atkins and Friedman, 1997; Atkins and Friedman, 2005; Daudel, et al., 1959; Flurry, 1983; Georgieva and Himo, 2010; Jensen, 2007; Leach, 2001; Mulholland, 2007; Schneider, 1998; Siegbahn and Himo, 2009; Szabo and Ostlund, 1996).

Thus, the method that is selected for the chemical problem is dependent on the level of accuracy necessary, and the size of the system under study.

In order to calculate large systems, i.e. enzymes, specific methods have been developed that combine the speed of MM through the handling of large amounts of atoms with the accuracy

of QM. This method is termed QM/MM and allows one to calculate large molecular systems with reasonable speed and accuracy. In QM/MM the system is split into two main parts: the centre where the active site is located, which is calculated with QM methods, and the outer region of the system that contains the long-range interactions of amino acids and surrounding solvent (Kumar, et al., 2011; Senn and Thiel, 2007; Senn and Thiel, 2009).

Since standard wavefunction methods scale badly for large systems, alternative methods were developed. One of the most successful one of those is the density functional theory method (DFT), where the wavefunction in the Schrödinger equation is replaced by an electron density (ρ). This method scales much more favourably for larger molecules and, these days, chemical systems of 200 atoms can be treated with reasonable accuracy using DFT methods. For instance, using the DFT procedure, free energies of activation were predicted, with high accuracy, as compared to other experimental methods, and at substantially lower computational cost (Falnes, et al., 1999; Kohn, et al., 1996; Lovell, et al., 2003; Parr, 1983; Parr and Yang, 1984). Density functional theory (DFT) has become a useful supporting tool in experimental work, helping in the interpretation of results and conducting new scientific studies (de Visser, 2009).

2.2 Classical Mechanics

It is well known that Newtonian mechanics equations can describe the movement or interaction among objects at the macroscopic level. Classical mechanics uses the concept of energy and classifies it in two: kinetic, related to movement of the particle, and potential energy, related to the position and the forces that influence them (Atkins, 1992; Atkins and De Paula, 2010; Atkins and De Paula, 2011; Barrow, 1996; Jensen, 2007). However, at microscopic level classical mechanics equations are not suitable anymore. Therefore, quantum mechanics was developed in order to describe the system behaviour of molecules, atoms, and electrons (Atkins and Friedman, 1997; Atkins and Friedman, 2011; Atkins and Friedman, 2005; Foresman, et al., 1996; Jensen, 2007).

2.3 Quantum Mechanics

As QM has the ability of representing the behaviour at microscopic level, it is possible to study chemical reactions using these methods in detail. That is, simulate reactions where electrons,

atoms and molecules are involved in QM is characterised by two main principles (Keeler and Wothers, 2008; Levine, 2000; McQuarrie, 2008; Yuryeva, et al., 2007) .

First, the quantization of energy in a particle (electron) is the main result obtained from QM. This means that, the energy levels are restricted to specific values rather than an ensemble average (Keeler and Wothers, 2008).

Second, there is no certainty about the exact location of the particle. The Heisenberg principle connects position and momentum; therefore, it is only possible to offer a probability about its particular position. Because there are, different location probabilities of being the particle situated, it is represented that the particle could appear all over the region of space (Keeler and Wothers, 2008; Levine, 2000; McQuarrie, 2008; Yuryeva, et al., 2007). It is understood that these two principles are associated with the concept of wavefunction, which will be explained later on.

2.3.1 The wavefunction

A wavefunction is a mathematical function that describes the motion and path of an electron/proton over time; consequently, it is a three-dimensional function with coordinates $x, y, and\ z$, which specify its position. Therefore, $x, y\ and\ z$ represent variables of the wavefunction. A wavefunction is generally noted by the Greek letter, (Ψ), and it would be written as $\Psi(x, y, z)$ indicating that it is a function of $x, y, and\ z$.

2.3.2 Probability interpretation of the wavefunction

The square of the wavefunction represent the probability of finding the electron in a specific area in space.

The probability of finding the electron in a small volume δV located at position (x, y, z) is $|\psi(x, y, z)|^2 \delta V$, which is the probability density, per unit volume, and is given by the square of the wavefunction $|\psi(x, y, z)|^2$

2.3.3 Energy

Quantum mechanics is concerned with kinetic and potential energy. Kinetic energy is associated with the motion of a particle with mass (m) moving with velocity (v) and kinetic

energy $=\frac{1}{2}mv^2$. Whilst the potential energy is related with the position of the electron (particle). These concepts will be discussed in further detail later on.

Quantum mechanics solves the Schrödinger Equation, in order to find out the energy levels and wavefunctions as well as information about the variation of potential energy experimented by the particles with respect to the position.

2.3.4 Heisenberg uncertainty principle

It is well understood that quantum mechanics is an improvement over classical mechanics due to the consideration of the Heisenberg uncertainty principle. This principle establishes that it is impossible to know the values of the conjugate properties exactly (Haas and Codd, 1930; Heisenberg, 1930; Heisenberg, et al., 1930). In the case of a particle on a line, Heisenberg showed that the momentum (*p*) that is the velocity and the position (*x*) of the particle are conjugate derivate properties via Planck's constant(h) and was defined as in the Equation 2.2.

$$\Delta p \Delta x \ = \ h \tag{2.2}$$

Thus, for atomic systems, it is impossible exactly know the momentum and position of the particle at the same time, because they are conjugated parameters. In QM, the result of conjugate parameters such as energy (E) and time (t) is also associated to the Planck's constant via $\Delta E \Delta t \ = \ h$. Due to these uncertainty principles, the equations used in classical mechanics are not valid for microsystems. Therefore, new equations considering the Heisenberg principles have been developed to depict atomic and molecular systems (Atkins and Friedman, 1997; Atkins and Friedman, 2005; Flurry, 1983; Grinter, 2005; Kauzmann, 1957).

Heisenberg found that the product of uncertainty momentum Δp_x multiplied by the uncertainty position Δx could never be less than $^{h}/_{4\pi}$ that was expressed as Equation 2.3 (Atkins and Friedman, 1997; Atkins and Friedman, 2005).

$$\Delta p_x \Delta x \geq {}^{h}/_{(4\pi)} = {}^{\hbar}/_{2} \tag{2.3}$$

2.3.5 The Schrödinger equation terms

To understand the details of the Schrödinger equation in the following, I will define often-used terms such as Eigenfunction, Eigenvalues, Observable, Operators, Tunnelling, Hamiltonian,

Position or Coordinate, Linear momentum, Angular momentum, Energy, Kinetic energy, and Potential energy.

2.3.5.1 Eigenfunctions

An Eigenfunction is a function, which is the result of an operation, and is defined as the same function multiplied by a constant. In quantum mechanics, these functions explain the probability distribution of the electron in the nucleus region of the atom, such distribution is associated with a specific energy which in turn, associated with the eigenvalue (Atkins and Friedman, 1997; Atkins and Friedman, 2005; Grinter, 2005; Keeler and Wothers, 2008).

2.3.5.2 Eigenvalues

The scalar value of the eigenfunction is called the eigenvalue. In the case of quantum mechanics they are the possible energy values of the electron in the atom or molecule (Atkins and Friedman, 1997; Atkins and Friedman, 2005; Grinter, 2005; Keeler and Wothers, 2008).

2.3.5.3 Observable

Observables are dynamical variables, which one can measure. In quantum mechanics, these are represented by a mathematical operator, while they are represented by functions in classical mechanics where they are represented by functions. (Atkins and Friedman, 1997; Atkins and Friedman, 2005)

2.3.5.4 Operator

The operator is the symbol that shows what instruction or action need to be taken in a function (Atkins and Friedman, 1997; Atkins and Friedman, 2005; Grinter, 2005; Keeler and Wothers, 2008), see Equation 2.4.

$$\text{Operator operating on Eigenfunction} = \text{Eigenvalue} \times \text{Eigenfunction} \qquad (2.4)$$

2.3.5.5 Hamilton operator

The Hamilton operator or Hamiltonian (H) is the operator that describes all perturbations to the wavefunction of motion and therefore affects the total energy of the system. The Hamiltonian, therefore, contains kinetic energy (W) as well as potential energy (V) functions. The former depends on the motion of the particles (electrons and protons), whereas the latter

is a function of the position of the particle (Atkins and Friedman, 2005; Keeler and Wothers, 2008; Leach, 2001).

$$\mathrm{H} = W + V \tag{2.5}$$

2.3.5.6 Position or coordinate, $\hat{x}$

The particle position operator (x) or (r), represents the particle position along the x-axis as $(\hat{x})$ or $(\hat{r})$. The caret mark (^) differentiates the operator from the observable. Consequently, the expected value $(\bar{x})$,as is shows in Equation 2.6, of the x coordinate for a particle is represented by the wavefunction ψ (Atkins and Friedman, 2005; Grinter, 2005; Keeler and Wothers, 2008).

$$\bar{x} = \int_{all\ space} \psi \hat{x} \psi dx dy dz \equiv \langle \psi | \hat{x} | \psi \rangle \tag{2.6}$$

2.3.5.7 Linear momentum, $\hat{p}_x$

In Equation 2.7, linear momentum (p) of the particle is the product of the mass (m) and the velocity (v) (Atkins and Friedman, 2005; Grinter, 2005; Keeler and Wothers, 2008).

$$p = m \times v \tag{2.7}$$

If it is replaced by the linear momentum in the x direction by differentiation with respect to x multiplied by $-i\hbar \cdot \Big/ _{2\pi}$, then we obtain the following expression:

$$p_x = m \times v_x \Rightarrow \hat{p}_x = -i\hbar \cdot \frac{\partial \psi}{\partial x} \tag{2.8}$$

2.3.5.8 Angular momentum (L)

Angular momentum is given in Equation 2.9; a particle with mass m rotating about a centre is defined as the vector product of the distance from the centre (r) and its linear momentum (p). If the rotation is taking place only in the $xy-$ plane, meaning$(z = 0, p_z = 0)$, we obtain the following angular momentum operator:

$$L = r \times p = xp_y - yp_x \Longrightarrow \hat{L} = i\hbar \left\{ \hat{x}. \frac{\partial \psi}{\partial y} - \hat{y}. \frac{\partial \psi}{\partial x} \right\} \tag{2.9}$$

The total angular momentum of the electron is equal to $\hbar[l(l+1)]^{1/2}$, and the component in the z direction is equal to $m_l\hbar$ (Atkins and Friedman, 1997; Atkins and Friedman, 2005; Grinter, 2005; Keeler and Wothers, 2008)

2.3.5.9 Kinetic energy $\widehat{W}$

In quantum mechanics kinetic energy, Equation 2.10, is related to electron movement with mass (m_e) and charge $(-e)$, it is well known that around the nucleus of charge $(+e)$, which is directly proportional to the square of its velocity (v) (Atkins and Friedman, 1997; Atkins and Friedman, 2005; Grinter, 2005; Keeler and Wothers, 2008).

$$(\widehat{W}) = (m_e\, v)/2 \tag{2.10}$$

2.3.5.10 Potential energy($\hat{V}$)

In quantum mechanics, potential energy is expressed in terms of particle position that means, the distance of the electron from the nucleus. It is noted that the operator of potential energy is the position operator (Atkins and Friedman, 1997; Atkins and Friedman, 2005; Grinter, 2005; Keeler and Wothers, 2008). In this case, the potential energy (V), with two charges of $+e$ and $-e$ separated by the distance r, is replaced by the operator $(\hat{\mathrm{V}})$ in the following Equation 2.11.

$$\mathrm{V} = {-\mathrm{e}^2}/{\mathrm{r}} \Longrightarrow \hat{\mathrm{V}} = {-\mathrm{e}^2}/{\hat{\mathrm{r}}} \tag{2.11}$$

2.3.6 Schrödinger equation

In QM a wavefunction (Ψ) describes the particle characteristics in a system. It is well understood that the shape and size of the wavefunction (Ψ) is determined by all perturbations that influence the system. Thus, the Schrödinger equation illustrates how in the electronic ground state the kinetic and potential energy contributions give the system its minimum energy E (Schrödinger, 1926). In the Hamilton operator, all the perturbations that affect the wavefunction and the energy of the system are included.

It is considered that the Hamiltonian operator describes the interactions of the electron and protons within the molecule. For instance, the Hamiltonian operator for the hydrogen atom is described as:

$$\hat{\mathrm{H}} = -\frac{\hbar^2}{2m_e}\nabla^2 + \frac{e^2}{4\pi\varepsilon_0 R} \tag{2.12}$$

The kinetics energy of the electron with mass me is represented in the first term, whilst the second term is represented the coulombic attraction at distance R between the proton and electron each with charge e.

Planck's constant ħ is divided by 2π and ε_0 is the permittivity in vacuum. The Laplacian ∇ represents the sum of all partial derivatives to each individual coordinate.

$$\nabla^2 = \frac{\partial^2}{\partial x^2} + \frac{\partial^2}{\partial y^2} + \frac{\partial^2}{\partial z^2}. \tag{2.13}$$

There are two ways to describe a system, namely in either Cartesian coordinates using a definite x, y, and z axis, or as internal coordinates, considering the connection between particles via a distance (r), angle (ϕ) and dihedral angle (θ).

It should be noted that the Schrödinger method has three basic steps. First, determine the operator associated with the observable to be calculated. Second, find the eigenfunctions of the operator and finally, ensure that the eigenfunctions are physically acceptable, in which case the corresponding eigenvalues will be the possible, quantised values of the observable.

2.4 Electronic structure calculations

2.4.1 Born-Oppenheimer approximation

To calculate molecular geometries and energies, Electronic-structure calculations use the Schrödinger equation. However, the only chemical systems for which the Schrödinger equation can be solved exactly are the hydrogen atom and the hydrogen molecule cation. In all other cases, it is necessary to make assumptions in order to solve the Schrödinger equation numerically. The Born–Oppenheimer approximation is one assumption base on the fact that the momentum of the electrons is larger than that of the nuclei, due to their considerable mass (Born and Oppenheimer, 1927). Thus, the mass of the electron is more than 1800 times smaller than the mass of a proton; hence, the momentum of the electron will be much larger. As such, the nuclei seem to look rigid in the plane of the fast-moving electrons. In such case, the Born– Oppenheimer approximation assumes that the coordinates and the distance between of the nuclei are constant and only the electrons move. This also implies that the

nucleus-nucleus interactions in the Schrödinger equation are reduced to a constant. Equation 2.13 gives the Hamiltonian describing the electrons in the field of the nuclei.

$$\hat{\mathrm{H}} = -\frac{\hbar^2}{2m_e}\sum_i^{N_e}\nabla_{\mathrm{i}}{}^2 - \sum_i^{N_e}\sum_I^{N_p}\frac{Z_I e^2}{4\pi\varepsilon_0 R_{Ii}} + \frac{1}{2}\sum_{i,j}^{N_e}\frac{e^2}{4\pi\varepsilon_0 r_{ij}} \quad (2.14)$$

In this equation, the kinetic-energy contribution of the electrons is represented in the first term. The second term is the electron–nucleus attraction and the third term represents the electron–electron repulsion. In this Hamiltonian equation the sum of all the interactions of N_e electrons with N_p protons and of N_e electrons with N_e–1 other electrons is considered. It should be noted that for larger molecular systems, the equation increases in complexity.

2.4.2 Hartree-Fock theory

In this section, I will describe how the Schrödinger equation is solved for a system with the Hamiltonian operator and wavefunction mentioned before. It is noted that the Hartree–Fock theory (HF) equations are arranged to solve individual one-electron wavefunctions, that is, for the first electron named 1 in orbital ϕ_a using f_1 , Fock operator, to calculate the orbital energy (ε_a) of an electron in orbital ϕ_a.

$$f_1\phi_a(1) = \varepsilon_a\phi_a(1) \quad (2.15)$$

If the Fock operator is split into three parts, it is obtained: first, a Hamiltonian (h_1), which describes the kinetic energy, one-electron integrals and the expressions for the two-electron integrals, the Coulomb operator (J_u) and the exchange operator (K_u) (Atkins and Friedman, 1997; Atkins and Friedman, 2005; Atkins and Friedman, 2011; Leach, 2001; Rappe and Casewit, 1997; Schrodinger, 1994)

$$f_1 = h_1 + \sum_u\{J_u(1) - K_u(1)\} \quad (2.16)$$

$$J_u(1)\phi_a(1) = \left\{\int \phi_u^*(2)\frac{e^2}{4\pi\varepsilon_0 r_{12}}\phi_u(2)dx_2\right\}\phi_a(1) \quad (2.17)$$

$$K_u(1)\phi_a(1) = \left\{\int \phi_u^*(2)\frac{e^2}{4\pi\varepsilon_0 r_{12}}\phi_a(2)dx_2\right\}\phi_u(1) \quad (2.18)$$

The wavefunction is expressed as a sum of basis functions (θ_j) as a linear combination with specific coefficients. In this case (c_{ji}) of the M basis functions describes the wavefunction (Hall, 1951; Roothaan, 1951; Roothaan, 1951) as follows:

$$\phi_i = \sum_{j=1}^{M} c_{ji}\theta_j \quad (2.19)$$

Using these basis functions, the overlap matrix ($\boldsymbol{S}_{ij}$) and Fock matrix ($\boldsymbol{F}_{ij}$) are calculated as follows:

$$S_{ij} = \int \theta_i^*(1)\theta_j(1)dr_1 \tag{2.20}$$

$$F_{ij} = \int \theta_i^*(1)f_1\theta_j(1)dr_1 \tag{2.21}$$

Those equations are known as the Roothaan equations, which are used for most of the electronic-structure packages in order to obtain the geometry optimisation, which correspond with the minimal electronic energy.

Most programmes follow the next steps in order to obtain the geometry optimisation:

First, a starting structure is defined, i.e. a molecular geometry, is given in the input file, with a set of coordinates that describe all individual atoms of the molecule. Second, a set of basis functions θ_j is selected. Third, a set of trial coefficient c_{ja} is created using the basis functions to calculate the overlap matrix S_{ij} and Fock matrix F_{ij} .

These matrixes are embedded into the secular determinant, Equation 2.22, which is necessary to solve in order to obtain the energies ε_a and the coefficients c_{ja} (Atkins and Friedman, 2011; Atkins and Friedman, 2005; Leach, 2001; Levine, 2005) .

$$det|F - \varepsilon_a S| = 0 \tag{2.22}$$

Finally, when the new coefficients are obtained, they are compared with the previous coefficients. If they are considered identical, the calculation is said to be converged and the process is finished. Otherwise, the process is repeated until the coefficients do converge.

It is important to understand that even though the converged wavefunction is considered the so-called best computational energy, it is still directly connected to the initial geometry. Therefore, it is necessary to perform more calculations to obtain the optimised geometry at its lowest energy point on the potential-energy surface.

After the convergence of the first geometry, the programme alters the coordinates slightly in order to create a new geometry structure, and repeat the same procedure as describe before so as to converge the wavefunction again. Thereafter, it is noted that the first derivative of the energy is used to create a third new geometry. This process is repeated until the first energy

derivative to the nuclear coordinates, the absolute energy, and the change in coordinates do not change anymore.

Configuration interaction (CI) and Møller–Plesset perturbation theory are some of the higher-level *ab initio* methods. A characteristic of these methods is that they take the excitations of electrons from occupied to virtual orbitals into account and enter those perturbations into the wavefunction system in order to get a more precise calculation. These methods occasionally reach accuracy with energies with 1 kcal mol^{-1}, from experiment. However, these sorts of methods only can be used to small systems (less than 20 atoms) due to their high computational cost. Consequently, these methods are not suitable for the system, which will be described in this dissertation.

2.4.3 Geometry optimisation

As we discussed in this chapter earlier, Geometry optimisation is an iterative process where the main objective is to locate a minimum on the potential energy surface. In that way, it is possible to predict equilibrium structures of molecular systems. It is noted that at the minimum, the first derivative of the energy with respect to each coordinate x_i, is equal to zero (Foresman, et al., 1996).

$$\frac{\partial f}{\partial x_i} = 0 \tag{2.23}$$

$$\frac{\partial^2 f}{\partial x_i^2} > 0 \tag{2.24}$$

This iterative process of geometry optimisation must satisfy the following criteria:

First, the consecutive changes in the geometry must not lower the energy by which it was specified. Second, in order to ensure that the optimisation is close to the potential energy surface (PES) bottom, the energy gradient at the optimised geometry must closely approach zero.

Working with small molecules, this means, less that 100 atoms, this approach is very efficient and the computer cost is low rather whereas for big molecules the results can be the opposite (Foresman, et al., 1996).

A popular software package for the description of molecules with QM methods is Gaussian 03 (G03), which we have mainly used in this work. It is mainly characterised for two reasons: First,

when the optimisation process start, an approximate Hessian is built that is improved using the first derivative calculated in every point. Second, According to Schlegel (1982), Gaussian 03 uses the regular Berny optimisation algorithm where it applies the second derivatives in its calculations (Foresman, et al., 1996).

2.4.4 Transition state

A transition state is the lowest energy maximum that connects two local minima; therefore, it is a first-order saddle point with a maximum a long one degree of freedom (the reaction coordinate) and a minimum energy along all other degrees of freedom. Experimentally, transition states cannot be characterised because their lifetime is too short, however, the free energy of activation, i.e. the energy between the transition state and the reactant structure connects to the rate constant for the chemical reaction.

Specific methods have been developed allow searching for the transition states. Generally, the method that we have applied is the following.

Initially, we ran a geometry scan between the reactant and product geometries, and *vice versa,* whereby the reaction coordinate was fixed at specific intervals while at the same time the rest of the structure was fully optimised. An example of a thus obtained geometry scan is given in Figure 2.1. This geometry scan connects reactants with products and shows a maximum along the scan.

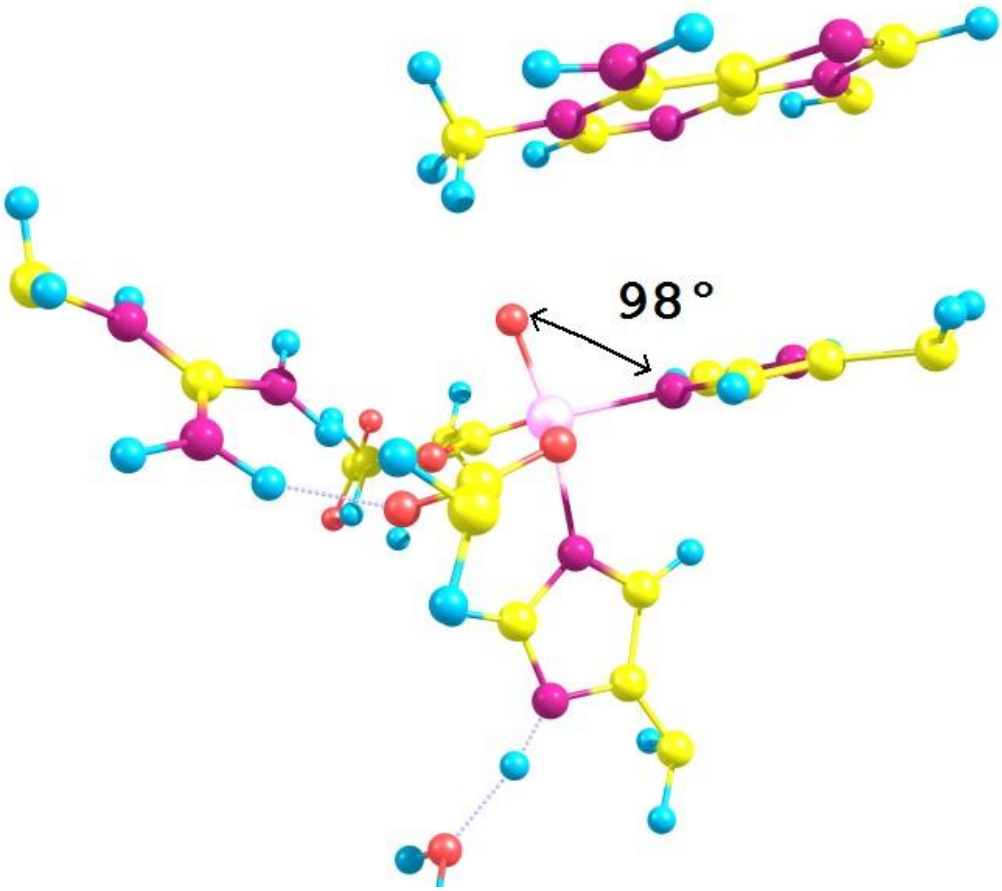

Figure 2.1 Geometry scan

Subsequently, we took the geometry at the maximum point along the geometry scan, and we did a full transition state search. A following frequency calculation characterised the transition state as a first order saddle point with one imaginary frequency for the correct mode.

It is important to understand that the height of the barrier, transition state, separating reactants and products relates directly to the overall reaction rate. Additionally, the positions of the minima along the reaction coordinate provide the equilibrium geometries of reactant and products (Foresman, et al., 1996; Leach, 2001; Matouschek, et al., 1989; Pechukas, 1981).

It should be noted that transition states (maxima) are points for which the second derivative are less than zero along one degree of freedom. See Equation 2.25

$$\frac{\partial^2 f}{\partial x_i^2} < 0 \tag{2.25}$$

2.4.5 Vibration analysis

In computational chemistry, a vibrational analysis is carried out with the aim of verifying the information obtained from the geometry optimisation, and transition state searches. Although a minimum energy structure has no imaginary frequencies, a transition state has a single one. In this case, this single imaginary frequency is visualised in a software package, e.g. ChemCraft, and it is confirmed that it is the correct vibration along the reaction coordinate (Zhurko and Zhurko, 2005).

Vibrational analysis also offers information about the zero-point energy (Atkins and Friedman, 1997; Leach, 2001; Pechukas, 1981). Zero-point energy is a characteristic of quantum mechanics. ZPE has a direct implication with the Heisenberg uncertainty principle as in the so-called zero-point energy the system still has a minimum energy, that is, the particle is never at a standstill but instead is moving around. Therefore, it is impossible to establish its exact location even in its minimum energy.

As the expression, which gives the probability density of the particle, suggest that the location of the particle is not punctual but is spread out over the area.

$$|\psi_1(x)|^2 \tag{2.26}$$

Inclusion of electron correlation generally leads to improved values for vibrational frequencies (Scott and Radom, 1996).

2.5 Calculation methods used in QM studies

2.5.1 Basis sets

Often QM calculations involve atomic functions as a basis sets. In particular, Slater type orbitals would be the first choice to use, since the solution of the Schrödinger equation gives those types of wavefunctions for the hydrogen atom. However, from a computational integration point of view these kinds of functions are difficult to manage (Leach, 2001), therefore, Gaussian-type functions are commonly used as an alternative. Gaussian basis sets have the form exp $(-\alpha r^2)$, were α is a constant that establishes the radial extent r of the this function (de Visser, 2009; Foresman, et al., 1996; Leach, 2001). Thus, a zeroth-order Gaussian g_s (s-orbital angular symmetry), and three first-order Gaussian functions (p-orbitals symmetry) have the following shapes:

$$g_s(\alpha, r) = \left(\frac{2\alpha}{\pi}\right)^{\frac{3}{4}} e^{-\alpha r^2} \tag{2.27}$$

$$g_x(\alpha, r) = \left(\frac{128\alpha^5}{\pi^3}\right)^{\frac{1}{4}} xe^{-\alpha r^2} \tag{2.28}$$

$$g_y(\alpha, r) = \left(\frac{128\alpha^5}{\pi^3}\right)^{\frac{1}{4}} ye^{-\alpha r^2} \tag{2.29}$$

$$g_z(\alpha, r) = \left(\frac{128\alpha^5}{\pi^3}\right)^{\frac{1}{4}} ze^{-\alpha r^2} \tag{2.30}$$

While the six second-order functions are represented by the following expressions

$$g_{xx}(\alpha, r) = \left(\frac{2048\alpha^7}{\pi^3}\right)^{\frac{1}{4}} x^2 e^{-\alpha r^2} \tag{2.31}$$

$$g_{xy}(\alpha, r) = \left(\frac{2048\alpha^7}{\pi^3}\right)^{\frac{1}{4}} xye^{-\alpha r^2} \tag{2.32}$$

It is noted that whereby the 3d atomic orbitals, not all second-order functions have identical angular symmetry. For that reason, they combine to the following expressions:

$$g_{3zz-rr} = \frac{1}{2}\left(2g_{zz} - g_{xx} - g_{yy}\right) \tag{2.33}$$

$$g_{xx-yy} = \sqrt{\frac{3}{4}}\left(g_{xx} - g_{yy}\right) \tag{2.34}$$

Furthermore, the sixth linear combination in a *s* function is expressed as follows:

$$g_{rr} = \sqrt{5}\left(g_{xx} + g_{yy} + g_{zz}\right) \tag{2.35}$$

The molecular orbitals are then a linear combination of these basis functions.

The basis set $(STO - 3G)$ is considered the minimum basis sets as it was found that the minimum set which represent exactly each Slater type orbital is the one which include three Gaussians functions for each atomic orbital. Unfortunately, these minimum bases sets have some limitations. First, atoms at left-hand-side *versus* right-hand-side of the periodic table are described in the same way even though they have different electronic configuration. Second,

the minimum set basis is not able to depict non-spherical characteristics of the electronic distribution. Finally, the size contraction or expansion of the functions is not allowed, in other words, it is not possible to be adjusted to the changes in the molecular environment (Jensen, 2007; Leach, 2001).

A double zeta basis set is one option to solve those problems. This basis function allow to solve the anisotropic difficulty as in this case, it is likely to obtain more linear combinations for $P_x, P_y,$ and P_z. It is understood that the basis sets coefficients, contracted/diffused functions, are calculated by Self-consistent Field calculation (SCF) (Leach, 2001).

The *split valence* double zeta basis set $(3-21G)$ that uses three Gaussian functions to describe the core orbitals. In this case, three Gaussian functions also characterize the valence electrons distributed as follows: two Gaussian functions for the contracted part, and one Gaussian function for the diffuse part (Ditchfield, et al., 1971; Leach, 2001).

The *polarisation functions* basis sets, it is characterised for having a higher angular quantum number. Thus, hydrogen has p orbitals and first and second-row elements have d orbitals. This basis sets function solves the problem of perturbation in the charge distribution. In this case, the nomenclature changes adding an asterisk $(*)$ in the regular basis set. $(6-31G^*)$ used for heavy atoms, $(6-31G^{**})$ indicate use of the polarisation for hydrogen and helium (Leach, 2001).

Furthermore, the addition of diffuse basis function is needed in order to deal with anions and molecules that contain lone-pair orbitals, which usually are more diffuse than the normal orbital configuration. These basis set function are symbolised with a $(+)$ symbol. In this case, the diffuse basis set function is $(3-21+G)$ that have additional single set of diffuse s and p –type Gaussian functions. If in the diffuse functions are incorporated for hydrogen and heavy metals, it is symbolised as $(++)$ (Jensen, 2007; Leach, 2001).

Transition metal complexes, such as those described in this dissertation require special basis sets for the transition metal. We used the Los Alamos type double- ζ quality basis set (LACVP) on iron for geometry optimisations and frequencies, while we did single point energy calculations with a triple-ζ type LACV3P+ basis set that contains a set of diffuse functions. Note that these Los Alamos-type basis sets contain a core potential, where the inner 1s, 2s and 2p electrons on the metal have been replaced by point charges. Although this seems to simplify the electronic description of the metal, it actually cancels out relativistic effects and hence

gives good structures and energies. Generally, a double ζ quality basis set (LACVP on Fe, 6-31G on first row elements) is sufficient for geometry optimizations. Test calculations (de Visser, 2009; Kumar, et al., 2010) showed little different along a potential energy profile when relative energies are calculated with a triple-ζ basis set as compared to double-ζ basis set.

2.5.2 *ab initio* methods

It is well known that the term *ab initio* means "from the beginning" a Latin word. The *ab initio* calculation is one of the main methods to solve the Schrodinger equation. The accuracy of this approximation method depends upon the model chosen for the wavefunction. It is noted that due to its high accuracy this calculation methods are not suggested for large molecules due to it high computational cost (Atkins and Friedman, 1997; Atkins and Friedman, 2011)

The main characteristic of *ab initio* methods is that it does not use any experimental data. Therefore, this method only uses quantum mechanics principles to perform its calculations. That is, *ab initio* calculation base upon in physical constants such as Planck's constant, the electron and nuclei charges and masses, and the speed of light (Foresman, et al., 1996; Ghosh, et al., 2003; Wadt and Hay, 1985).

New development in *ab initio* methods allow to perform prediction calculation in systems with over hundreds of atoms in a relative short of time (Foresman, et al., 1996).

2.5.3 Semi-empirical methods

Semi-empirical calculation methods is characterised by two main aspects. First, the incorporation of data information obtained experimentally. Second, it uses for its calculations a simplified form of Hamiltonian (Atkins and Friedman, 1997; Atkins and Friedman, 2005; Foresman, et al., 1996).

Semi-empirical methods differ from *ab initio* calculations due to its reasonable computational cost, and acceptable accuracy in its results, which generally offer a comparatively good quality of molecular predictions or chemical structures. However, the method falls short in calculating energies and rate constants accurately, and, therefore, is lesser suitable for chemical systems we investigated. Because we did not use semi-empirical methods in our work, I will not discuss this in detail here.

2.5.4 Density functional theory

Density functional theory, depicts the energies as a function of the electron density, and differs from the wavefunction method described above (Ziegler, 1991). Kohn et al developed a methodology based on a series of one-electron equations, which allows the use of electron density and total energy calculations (Hohenberg and Kohn, 1964; Kohn, et al., 1996; Kohn and Sham, 1965).

The advantages of using the DFT methodology include the reduction of computer cost, and the reasonable conformity between the data obtained using DFT and the experimental information of large chemical systems (de Visser, 2009; Siegbahn, 2003).

The total energy (E_{el}) of a DFT calculation is represented by the following equation:

$$E_{el} = -\frac{1}{2}\sum_i \int \phi_i(r_1)\nabla^2\phi_i(r_1)dr_1 + \sum_A \int \frac{Z_A}{|R_A - r_1|}\rho(r_1)\,dr_1 + \frac{1}{2}\int \frac{\rho(r_1)\rho(r_2)}{|r_1 - r_2|}dr_1 dr_2 + E_{xc} \quad (2.36)$$

The first term in this equation represents kinetic energy, the second term the electron–nucleus attractions, the next term is the Coulomb interactions between the electrons and the last one the exchange-correlation term (E_{xc}) (Ziegler, 1991).

Because the exchange-correlation functional is generally unknown, some approximate equations have been developed in order to determine its contribution to DFT calculations. Generally, the exchange-correlation component is split into an exchange energy term and correlation energy expression.

$$E_X^{Slater} = -\frac{9}{4\alpha_{ex}}\left(\frac{3}{4\pi}\right)^{1/3}\sum_\gamma \int \left[\rho_1^\gamma(r_1)\right]^{4/3} dr_1 \quad (2.37)$$

The exchange scale factor α_{ex} in equation (2.37) has the value of $^2/_3$ for an electron gas.

The correlation energy functional factor E_C^{VWN} developed by Vosko, Wilk and Nusair represents the correlation energy per electron in a gas $\varepsilon_c\left[\rho^\alpha, \rho_1^\beta\right]$ with spin densities ρ_1^α and ρ_1^β (Vosko, et al., 1980)

$$E_C^{VWN} = \int \rho_1(r_1)\varepsilon_c\left[\rho_1^\alpha(r_1), \rho_1^\beta(r_1)\right]dr_1 \quad (2.38)$$

Even though there have been new developments to obtain a local density approximation, the most common methods is via the correlation combination of Slater exchange and Vosko et al. It is important to understand that in this case, those correlations come straight from the homogenous electron-gas equations.

Though there are different functional correlations available to perform this sort of calculation, the most accepted approaches are those that have been developed by Becke, Lee, Yang and Parr (LYP correlation functional) (Lee, et al., 1988) and Perdew and Wang (PW91 correlation functional), (Perdew and Wang, 1992).

A great advance in computational chemistry was occurred when Becke developed the well known hybrid density functional procedures (Becke, 1993). Therefore, Becke mainly compared information from an experimental test-set, which includes ionisation energies, proton and electron affinities, against DFT calculated values. The results demonstrated the high accuracy of the method. Albeit there are many combinations possible, it is well demonstrated that, the most commonly used is the B3LYP method. The hybrid density functional method B3LYP has the following form:

$$E_{XC}^{B3LYP} = AE_X^{Slater} + (1 + A)E_X^{HF} + B\Delta E_X^{Becke} + E_C^{VWN} + C\Delta E_C^{LYP} \qquad (2.39)$$

Thus, this equation includes the Slater and Vosko– Wilk–Nusair local density approximation functions, the Hartree–Fock exchange, and a correction term for the exchange due to Becke and one for correlation from Lee, Yang and Parr.

The coefficients A, B, and C are obtained through benchmarking the calculated energies at the B3LYP/6–31G* level of theory with the experimentally obtained ionisation energies and electron affinities.

Technically, therefore, the B3LYP method is not considered as an *ab initio* method as it includes information from experiments, which contrast full ab initio methods that do not take any prior knowledge of experiment into account. The B3LYP method has been demonstrated to give reasonably accurate results with low computational cost. Although, in general, the accuracy of DFT is not as good as high-level ab initio methods, such as coupled cluster methods, their speed in combination with reasonable accuracy makes them a very popular and useful methodology.

2.6 Molecular mechanics methods

The main characteristics of MM methods is their capacity of working with large chemical systems at very low computer cost (Leach, 2001), mainly because the electronic activity is ignored.

Thus, the MM model used to calculate the energy, considers the arrangements of the atoms, that is, their hybridisation state and the environment surrounding it.

It is important to highlight that in MM the potential energy contributors such angle bending, dihedral torsion, bonding, antibonding stretching, and electrostatic interactions are considered (Foresman, et al., 1996; Leach, 2001).

2.6.1 Force fields

A functional force field equation that represents the potential energy $V(r^N)$ as a function of the nuclear position r of N particles (atoms) is described as:

$$V(r^N) =$$

$$\sum_{bonds} \frac{k_i}{2}\left(l_i - l_{i,0}\right)^2 + \sum_{angles} \frac{k_i}{2}\left(\theta_i - \theta_{i,0}\right)^2 + \sum_{torsions} \frac{V_n}{2}(1 + \cos(n_\omega - \gamma)) +$$

$$i=1Nj=i+1N4\varepsilon ij\sigma ijrij12-\sigma ijrij6+qiqj4\pi\varepsilon 0rij \quad (2.40)$$

In this equation, the first term is associated with the interaction between the pair of bound atoms, with l_i the bond length and $l_{i,0}$ the reference value. The second term is the sum of valence angles, while the third term represents the torsion energy, and the last one is the non-bonded term, which is calculated between all pairs of atoms (i, j). It should be noted that non-bonded term, in some force field, are expressed as a Coulomb potential for electrostatic interactions or by a Lennard-Jones potential for van der Waals interactions.

2.6.2 Molecular dynamics simulation

Molecular dynamics simulations (MD), integrate Newton's laws of motion, and are useful when the study objective is to find information about the conformational properties of the system and their evolution over time. In other words, MD gives information about how the position and velocities of the particles (atoms) changes over a period of time.

The Newton's equation (Equation 2.41) of motion relates the force (F_i), mass(m_i) and acceleration (a_i) of the particle (i). It is well understood that the trajectory of the particle is found solving the following differential equation:

$$\frac{d^2x_i}{dt^2} = \frac{Fx_i}{m_i} \quad (2.41)$$

2.7 Quantum mechanics and molecular mechanics methods

The quantum-mechanics/molecular-mechanics (QM/MM) methodology is characterised by splitting the system into two regions, and inner core (the QM region) and the outer region (MM region). Thus, the enzymatic system is, in fact, divided into two regions: an inner central part, which is formed mainly by the catalytic centre better known as the active site, and the area, which is constituted by the rest of the protein surrounding and solvent. In QM/MM the inner region is the region of interest and is calculated with accurate, *ab initio* or DFT method, whereas the outer region is included through long-range interactions and salvation effects only.

QM/MM is widely used to treat biological systems, which are characterised for being the largest enzymatic systems, keeping the high accuracy of DFT or *ab initio* methods (Senn and Thiel, 2007; Senn and Thiel, 2009).

The calculation procedure, generally, is to treat using accurate computational methods, such as DFT or *ab initio*, while the external area is calculated using molecular mechanics (MM) method based upon classical empirical potentials.

We have applied this method to the AlkB repair enzyme, where we have split our chemical system into two regions:

(1) The inner core, calculated with B3LYP and a double-ζ basis set that contains the active site and the components that contribute to the reaction mechanism.
(2) The outer region, calculated with MM methods and the universal force field (Casewit, et al., 1992; Casewit, et al., 1992; Rappe, et al., 1992) that helps the active site rigid through molecular interactions and influence the reaction through long-range interactions (charge, dipole, etc).

CHAPTER 3.

Mechanism of DNA base repair by nonheme iron(IV)-oxo species, a quantum mechanics/molecular mechanics study‡

‡ Luis Enrique Gonzalez-Ovalle, Reza Latifi, Matthew D. Quesne and Sam P. de Visser, "*Mechanism of DNA base repairs by nonheme iron(IV)-oxo species, a quantum mechanics/molecular mechanics study.*" Manuscript in preparation

3.1 Abstract

We present the first quantum mechanics / molecular mechanics (QM/MM) study on AlkB repair enzymes. These enzymes belong to the group of nonheme iron dioxygenases and demethylate alkylated DNA bases in the body. We find a novel mechanism that starts with a rotation of the iron(IV)-oxo group prior to methyl group hydroxylation. In addition to the QM/MM calculations, we report density functional theory calculations on active site models of this enzyme for a range of methylated DNA-base demethylation reactions. Our calculations predict a rate determining hydrogen atom abstraction reaction and highlight the effects of protein on the reaction mechanism.

3.2 Introduction

Nonheme iron dioxygenases are important enzymes in nature that catalyze the biosynthesis of antibiotics in microbes and are involved in oxygen sensing and collagen cross-linking processes in mammals (Abu-Omar, et al., 2005; Bruijnincx, et al., 2008; Bugg, 2001; Bugg and Ramaswamy, 2008; Costas, et al., 2004; Ryle and Hausinger, 2002; Solomon, et al., 2000). They generally contain a nonheme iron active centre that is bound to the protein via a facial triad of two histidine and one carboxylate based (Asp/Glu) amino acids (Que, 2000). The nonheme iron dioxygenases utilize a co-substrate (α-ketoglutarate, αKG) on an iron centre to convert molecular oxygen into a high-valent iron(IV)-oxo species. This active species has been characterized by resonance Raman and Mössbauer spectroscopy and was found to react by hydrogen atom abstraction with a large kinetic isotope effect (Proshlyakov, et al., 2004; Riggs-Gelasco, et al., 2004).

The AlkB repair enzymes belong to the class of nonheme iron dioxygenases and repair methylated DNA (and RNA) bases that have been damaged by intra- or extracellular chemicals, in particular alkylating agents (Falnes, et al., 2002; Trewick, et al., 2002; Yi, et al., 2009). The most common methylation product of DNA strains contains the base N^3-methyladenine, which has dramatic effects on the biological system since it blocks DNA replication (Mishina, et al., 2006). Chemicals such as methylmethane sulfonate and methyl halides have been shown to generate N^1-methyladenine and N^3-methylcytosine. These methylated bases prevent formation of Watson-Crick base-pairs and as a consequence are toxic. The function of AlkB repair enzymes is to remove the methyl groups from the positions in N^1-methyladenine and N^3-methylcytosine via a mechanism shown in Figure 3.1 (Mishina and He, 2006).

The AlkB repair enzymes contain a nonheme iron centre that binds αKG, molecular oxygen and methylated DNA and catalyze the hydroxylation of the methyl group, which in a subsequent step is released as formaldehyde. Isotopic labelling and product distributions show that Fe(II), αKG and molecular oxygen are needed in the process and that formaldehyde and CO_2 are formed (Falnes, et al., 2002; Trewick, et al., 2002; Yi, et al., 2009). Crystallographic data provided further evidence that AlkB repair enzymes belong to the αKG dependent dioxygenases and highlighted a nonheme iron active site, where the metal is bound to a 2-His/1-Asp ligand system (Yu, et al., 2006). Currently the mechanism of substrate activation of AlkB repair enzymes is unknown and neither is the origin of the substrate specificity. To address these issues we have performed a combined quantum mechanics/molecular mechanics (QM/MM) and density functional theory (DFT) study on substrate activation by AlkB repair enzymes.

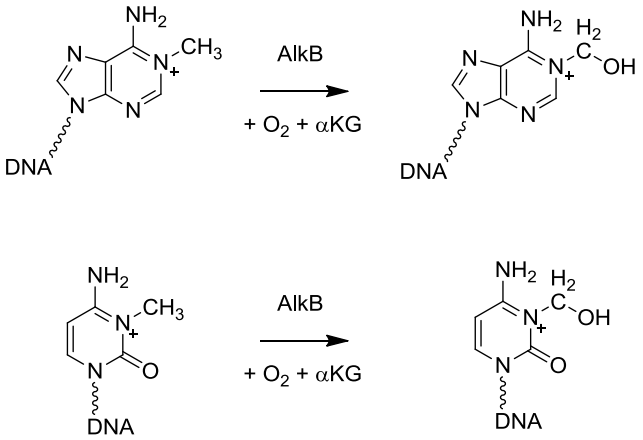

Figure 3.1 DNA base repair mechanisms studied in this work.

3.3 Computational methods

All DFT calculations were done using extensively tested and benchmarked methods (de Visser, 2010; Kumar, et al., 2010). Geometries were optimized in *Gaussian*-03 (Frisch, et al., 2004) and followed by a frequency calculation using the unrestricted B3LYP method (Becke, 1993; Lee, et al., 1988) in combination with a double-ζ quality LACVP basis set on Fe coupled to 6-31G on the rest of the atoms, basis set B1 (Hay and Wadt, 1985). A subsequent single point calculation used an LACV3P+ basis set on Fe and 6-311+G* on the rest of the atoms, basis set B2. Energies reported here, use the latter energy and include a correction for the zero-point energy as taken from the frequency calculations. Single point calculations in a dielectric constant of ε= 4.7 were done, but generally no dramatic differences from the gas-phase results are found.

In a second set of calculations, we ran a series of QM/MM calculations starting from the 3I2O protein databank (pdb) file (Yu and Hunt, 2009). This is a substrate bound AlkB repair enzyme monomer that contains a small single stranded DNA chain of with three bases. The pdb was modified by replacing the iron(III)-αKG active site by an iron(IV)-oxo succinate group whereby αKG was replaced by succinate and CO_2 removed from the chemical system. The water molecule that originally filled the sixth binding site of the metal was replaced by an oxo group and the corresponding bond distance was set to 1.65 Å prior to the geometry optimisation. Subsequently, hydrogen atoms and solvent (with sphere of radius of 8 Å) were added to the chemical system to generate a system with a total 6,359 atoms. Apart from the two histidine groups that are bound to the metal, all other histidine side chains were doubly protonated. Furthermore, we made sure that all arginine and lysine side chains were protonated and all glutamic acid and aspartic acid side chains were deprotonated. A molecular mechanics equilibration and heating to 298 K was performed using the FF94 force field (Wang, et al., 2004). This created a QM/MM structure with overall neutral charge.

Several low energy snapshots from the molecular dynamics simulation were selected as starting points for the QM/MM calculations. These calculations employed the ONIOM program package (Maseras and Morokuma, 1995) as implemented in *Gaussian*-03. The QM region was described by B3LYP/B1 and the universal force field (UFF) was selected for the MM region. Previous QM/MM studies of our group showed that these methods correctly reproduced reactivities and spectroscopic parameters (Godfrey, et al., 2008; Porro, et al., 2009). The QM region contained the iron(IV)-oxo group, methyl-imidazole groups for His_{131} and His_{187}, acetate for succinate and Asp_{133}, methylguanidinium for Arg_{210}, and N^1-methyladenine as the substrate, see Figure 3.2. Since His_{131} is hydrogen bonded to a water molecule, this water molecule was also included in the QM region to give a total number of QM atoms of 70. Both QM and MM regions were fully optimized during the calculations.

It was shown that enzymatic iron(IV)-oxo oxidants have a quintet spin ground state that is well separated from other spin states (de Visser, 2006; de Visser, 2006), therefore, we focused our studies on the quintet spin state mechanisms only.

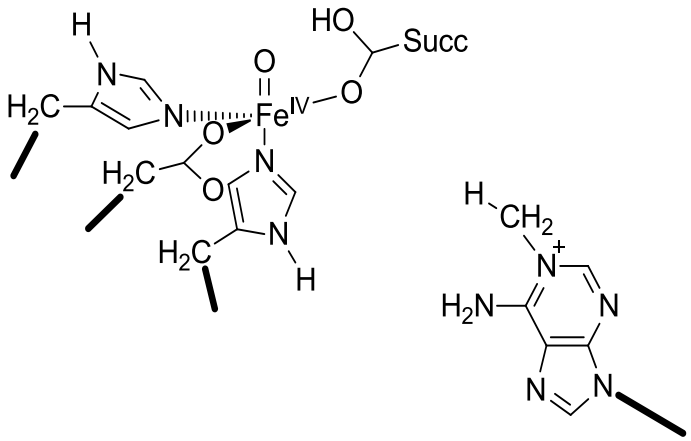

Figure 3.2 Selected QM region in the QM/MM calculations

3.3 Results and discussion

As found previously, the active species of AlkB repair enzymes and analogous nonheme iron dioxygenases is an iron(IV)-oxo species (Borowski, et al., 2004). Therefore, we generated and optimized the iron(IV)-oxo species initially and from there continued the hydrogen atom abstraction reactions from substrate. However, before discussing the reactivity patterns, let us first focus on the oxidant itself. Figure 3.3 gives DFT and QM/MM optimized geometries of the iron(IV)-oxo species of AlkB repair enzymes. Since the sixth ligand position of the metal contained a water molecule in the pdb file, in the set-up of the QM/MM calculation we replaced this water molecule by an oxo group. However, during the geometry optimization, a 90^{o} rotation of the Fe=O bond occurs, see Figure 3.3. Thus, the oxo group moves to a position in close proximity of the substrate, thereby enabling easier hydrogen abstraction. The calculated iron(IV)-oxo species has an Fe–O distance of 1.659 (QM/MM) and 1.649 (DFT) Å in good agreement with previous calculations and experimental estimates (de Visser, 2006; Godfrey, et al., 2008; Proshlyakov, et al., 2004; Riggs-Gelasco, et al., 2004; Ye and Neese, 2011). The electronic structure is almost identical to calculations found using DFT methods with spin densities and charges that are almost identical.

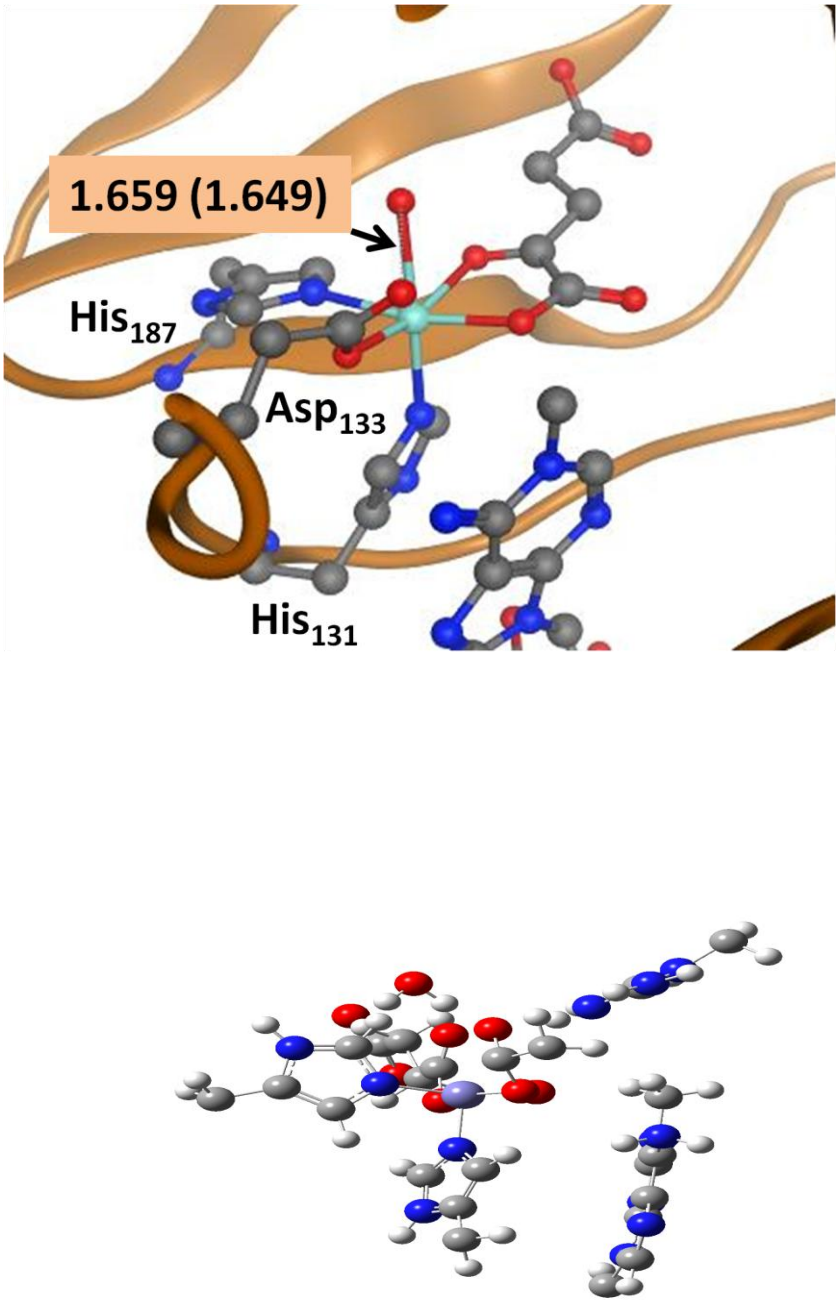

Figure 3.3 Optimized geometries of the iron(IV)-oxo species of AlkB repair enzymes as calculated with QM/MM and DFT (values in parenthesis). Bond lengths are in Ångstroms. Panel (a) gives the starting structure, whereas panel (b) gives the QM/MM optimized geometry.

Subsequently, we calculated hydrogen atom abstraction from N^1-methylguanine, N^1-methyladenine, N^3-methylcytosine and N^3-methylcytosine using DFT methods and N^1-methyladenine hydroxylation by an iron(IV)-oxo system with QM/MM. Figure 3.4 shows the optimized geometry of the hydrogen atom abstraction barriers obtained with DFT methods.

Our calculated hydrogen abstraction barrier for N^1-methyladenine of 19.8 kcal mol^{-1} is close in energy to the one reported by Gauld and co-workers (20.9 kcal mol^{-1}) (Liu, et al., 2009). This barrier, however, is quite high and much higher than calculated barrier heights of enzymatic systems seen before (Lonsdale, et al., 2010; Schöneboom, et al., 2004; Senn and Thiel, 2009). By contrast, the barrier heights for hydrogen atom abstraction from N^3-methylcytosine, N^1-methylguanine and N^3-methylthymine are 6.8, 10.9 and 16.0 kcal mol^{-1}, respectively. Therefore, dramatic differences in methyl hydroxylation barriers are found in the various DNA bases. It should be noted here that these barriers are gas-phase barriers without the protein environment included.

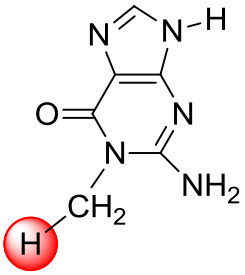

$\Delta E^{\ddagger}$ = 10.9 kcal mol^{-1}

N^1-methylguanine

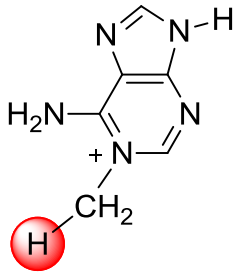

$\Delta E^{\ddagger}$ = 19.8 kcal mol^{-1}

N^1-methyladenine

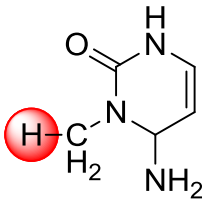

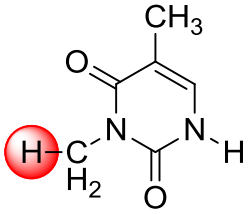

Figure 3.4 Barrier heights of DFT (UB3LYP/B1) optimized geometries of hydrogen atom abstraction of methylated DNA bases by an iron(IV)-oxo species. Energies calculated in kcal mol^{-1} at UB3LYP/B2//UB3LYP/B1.

To find out whether the barrier height, and consequently the rate constant of the reaction, is affected by the substrate binding pocket and long-range electrostatic interactions as appear in an enzyme, we decided to do additional QM/MM calculations on this mechanism. Due to the high barrier of N^1-methyladenine in the gas-phase, we investigated this mechanism with QM/MM using the modified 3I20 pdb file. Moreover, since the QM/MM optimized iron(IV)-oxo species gives a rotated orientation with respect to the gas-phase, we considered an alternative

mechanism, which is schematically displayed in Figure 3.5. This mechanism shows similarities to the one calculated before for the nonheme halogenase enzyme αKG dependent halogenase (Borowski, et al., 2010; de Visser, 2006). Thus, we predict molecular oxygen to bind the sixth coordination site of the metal but during the catalytic cycle the iron(IV)-oxo will point to another direction than the oxygen binding site, namely into the direction of the substrate. This implies that the oxo group will be trans to His_{187} in the catalytically active oxidant rather than His_{131}.

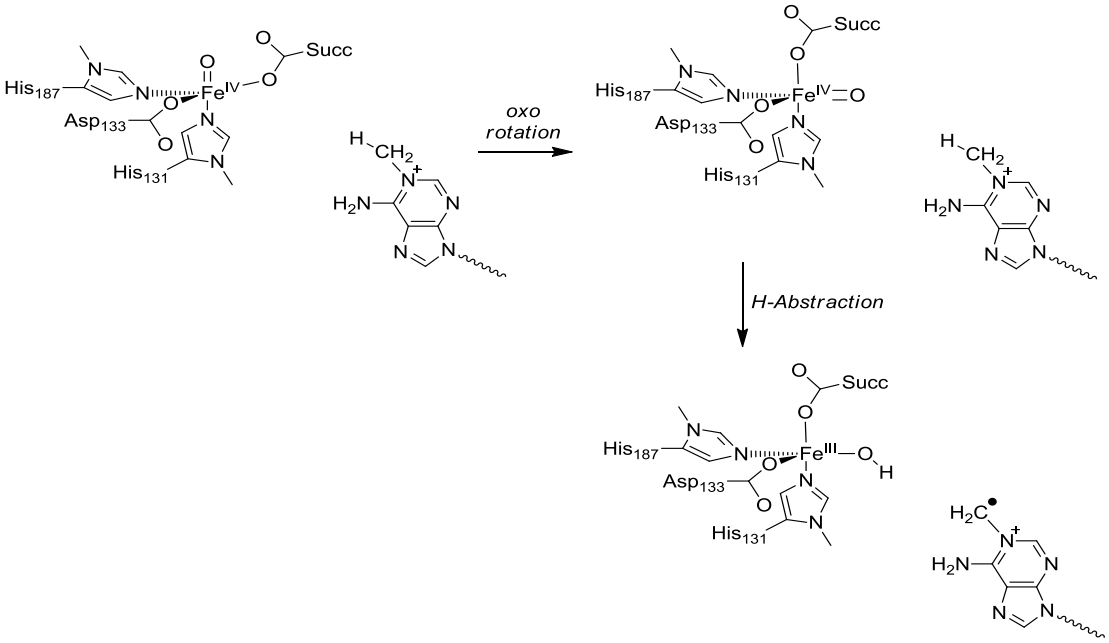

Figure 3.5 Reaction mechanism derived from QM/MM.

Initially, we started a geometry optimization of the iron(IV)-oxo species in QM/MM starting with the oxo-group trans to His_{131}. However, during the optimization the structure fell to the more stable conformation where His_{187} was trans to the oxo group. A geometry scan for the rotation of the iron(IV)-oxo group from the position trans to His_{131} to the one trans to His_{187} revealed continuously downward slope without rotational barrier.

Subsequently, we investigated the hydrogen atom abstraction from methyladenine substrate by the iron(IV)-oxo species and the obtained geometry scan is given in Figure 3.6. The reaction starts on the right-hand-side of Figure 3.6 with the iron(IV)-oxo species. Initially, minor energy changes are seen along the geometry scan, but when the distance becomes shorter than 1.4 Å the energy steeply rises until a maximum of approximately 31 kcal mol^{-1}. This barrier is significantly higher in energy to the direct mechanism described above, where 19.8 kcal mol^{-1} was found. There are several reasons for this. Firstly, no zero-point correction was added to

the QM/MM barrier height. This is important in hydrogen abstraction barriers, since the reaction results in the loss of a high-energy vibrational mode (C-H vibration), which costs about 3 kcal mol^{-1} (de Visser, et al., 2002; de Visser, et al., 2002). Secondly, there is the effect of the environment on the barrier heights and rate constants through long-range electrostatic interactions.

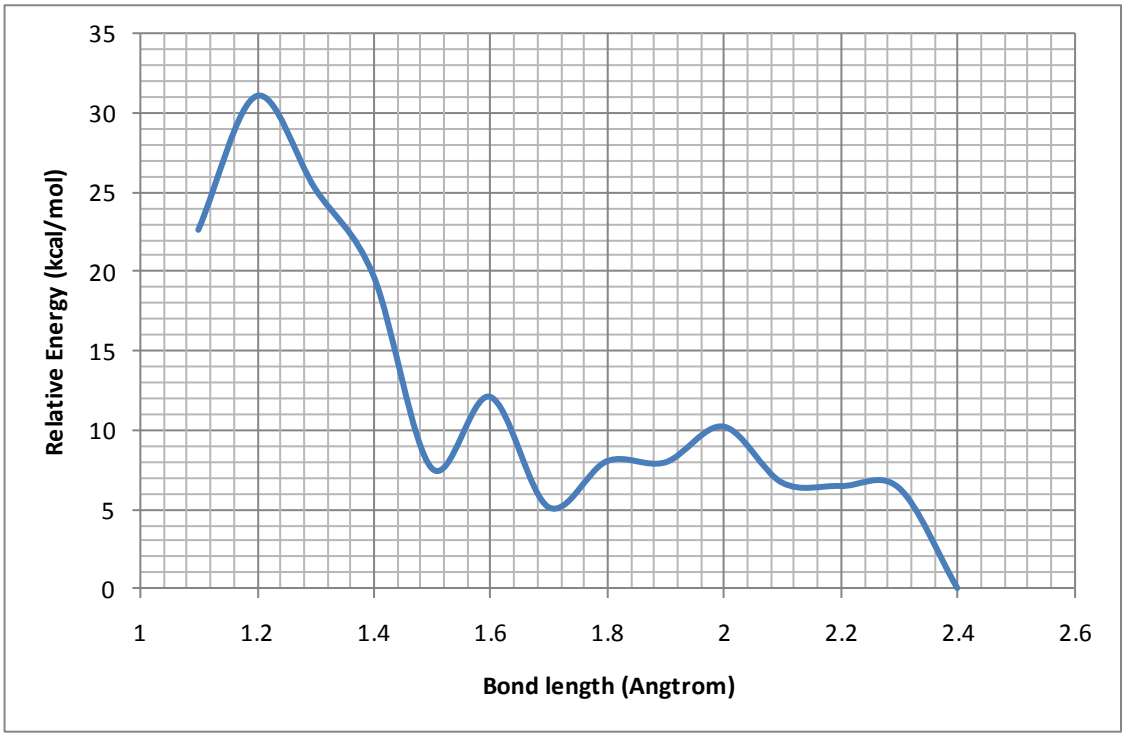

Figure 3.6 Geometry scan for the hydrogen atom abstraction from methylated adenine base by iron(IV)-oxo oxidant using QM/MM methods. Each point in the scan refers to a full geometry optimization in ONIOM with a fixed O–H distance. Energies are calculated relative to the iron(IV)-oxo species (trans to His_{187}) in kcal mol^{-1}.

3.4 Concluding and remarks

In summary, we have performed a series of QM/MM and DFT calculations on the mechanism of hydroxylation of methylated DNA bases by a nonheme iron DNA base repair enzyme. The calculations give a novel mechanism, whereby the initial rotation of the iron(IV)-oxo group aligns the oxidant with the substrate prior to the hydrogen atom abstraction process followed by rebound of the hydroxyl group to form alcohol products. QM/MM and DFT studies are in good agreement and show that the various methylated DNA bases give dramatic differences in hydrogen abstraction barrier heights. A hydrogen bonded arginine amino acid facilitates the rotation from oxo trans to His_{131} to trans to His_{187} and thereby brings the oxo group in close proximity of the methyl group of the DNA base.

CHAPTER 4.

Axial and equatorial ligand effects on biomimetic cysteine dioxygenase model complexes ‡

‡ Luis Enrique Gonzalez-Ovalle, Matthew D. Quesne, David P. Goldberg and Sam P. de Visser, "*Biomimetic models of cysteine dioxygenases enzymes: structure and function*." Manuscript in preparation.

4.1 Abstract

Density functional theory calculations are presented on biomimetic model complexes of cysteine dioxygenase for the first time. Recent studies of the Goldberg group [Y.M. Badiei, M.A. Siegler, D.P. Goldberg, J. Am. Chem. Soc. 133 (2011) 1274–1277] gave evidence of a nonheme iron biomimetic model of cysteine dioxygenase using an *i*-Pr-BIP(*i*-Pr-BIP = *i*-propyl-bis(imino)pyridine) equatorial tridentate ligand. Addition of thiophenol, an anion – either chloride or triflate – and molecular oxygen, leads to several possible stereoisomers of this cysteine dioxygenase biomimetic. Experimental studies revealed big differences in reactivity patterns using chloride as compared to triflate as the binding anion. Our DFT calculations show that the origin of these reactivity differences is caused by the preference of anion and thiophenol binding to the chemical system. Thus, the bulky *i*-propyl substituents of the *i*-Pr-BIP prevent binding of thiophenol in the equatorial position using triflate as the additional counter ion. By contrast, smaller anions, such as chloride, can bind in several ligand positions and give isomers with similar stability. Our calculations explain the observance of thiophenol dioxygenation by this biomimetic system and explain why this does not occur with a triflate anion bound to the system.

4.2 Introduction

Nonheme iron enzymes are versatile oxidants that catalyze a range of vital processes for human health. These enzymes are involved in repair mechanisms, biosynthesis as well as biodegradation of compounds. Generally, they use molecular oxygen on an iron centre and transfer either one or both oxygen atoms to a substrate, whereby a monoxygenation, dioxygenation or dehydrogenation type of reaction occurs. Nature has developed a large arsenal of these nonheme iron enzymes with big differences in ligand orientation and binding as well as functional properties (Bruijnincx, et al., 2008; Bugg, 2001; Bugg and Ramaswamy, 2008; Costas, et al., 2004; Solomon, et al., 2000). Research in this area, therefore, is widespread and the field is developing fast. As such, research on nonheme iron containing enzymes and synthetic analogues (biomimetic compounds) is important for the understanding of biochemical reaction mechanisms but also for industrial (biotechnological) applications.

An extensively studied class of nonheme iron enzymes is the α-ketoglutarate dependent dioxygenases, which anchor the metal via a facial 2-His-1-Asp ligand orientation to the protein (Bugg, 2003; Krebs, et al., 2007; Schofield and Zhang, 1999). These enzymes catalyze the

biosynthesis of several antibiotics in bacteria, including vancomycin, fosfomycin and carbapenem (Bodner, et al., 2009; Choroba, et al., 2000; Higgins, et al., 2005), as well as the DNA and RNA repair mechanisms in mammals (Falnes, et al., 2002; Mishina, et al., 2006; Trewick, et al., 2002). Another enzyme in the class of nonheme iron dioxygenases is cysteine dioxygenase (CDO) that is involved in the detoxification and metabolism of cysteine in the body (Joseph and Maroney, 2007; Stipanuk, 2004; Straganz and Nidetzky, 2006). CDO contains an unusual ligand system where the metal is bound to three histidine ligands of the protein via a 3-His facial ligand orientation, i.e. it lacks the carboxylate ligand that is so common in nonheme iron dioxygenases. Substrate cysteinate binds the metal in a bidentate fashion through the thiolate and amine groups and is locked in hydrogen bonding interactions via several nearby-located polar amino acids. Figure 1 displays the active site of substrate bound CDO as taken from the 2IC1 protein databank (pdb) structure(Ye, et al., 2007). Similar to the nonheme iron dioxygenases the protein binds the metal in a facial orientation and the ligand position *trans* to His_{86} is vacant and is reserved for molecular oxygen. A series of computational studies in our groups have given insight into the CDO ligand system and its mechanism of substrate activation (de Visser and Aluri, 2007; de Visser and Straganz, 2009; Kumar, et al., 2011). These studies showed that replacing the 3-His ligand system of CDO by a 2-His-1-Asp ligand system disrupts the dioxygenation process of cysteine and, in particular, leads to weakening of the Fe–S bond. It appears, therefore, that the 3-His ligand system is essential for optimal dioxygenation of cysteine.

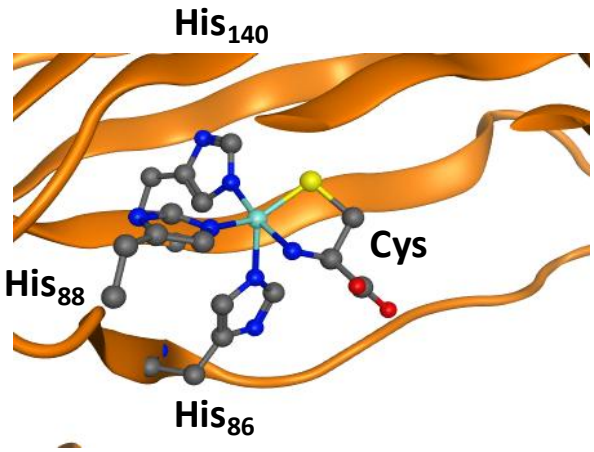

Figure 4.1 Extract of the active site of CDO as taken from the 2IC1 pdb file [18]. Amino acids are labelled as in the pdb.

In biomimetic chemistry, active site analogues are created with the aim to understand the basic features of enzyme active site structures (Abu-Omar, et al., 2005; Bruijnincx, et al., 2008; Costas, et al., 2004; Kryatov, et al., 2005; Nam, 2007). Recently, a biomimetic model of CDO enzymes was published and spectroscopically characterized that contains an Fe(II)-*i*-Pr-BIP ligand: *i*-Pr-BIP = *i*-propyl-bis(imino)pyridine, Figure 4.2 (Badiei, et al., 2011; Jiang, et al., 2010). The studies focused on the relative orientation of thiophenol and dioxygen on the metal centre. Thus, the *i*-Pr-BIP ligand occupies three ligand positions of the metal in the same plane of symmetry and the dioxygen moiety that will bind last to the metal centre occupies the equatorial position with respect to the nitrogen atoms of the *i*-Pr-BIP ligand. The remaining two ligand positions are occupied by thiophenolate (SPh^-) and an anion, which is either Cl^- or $CF_3SO_3^-$ (triflate). Consequently, these complexes have two possible stereoisomers (Figure 4.2) for the Fe (III)-superoxo complex, i.e. [$Fe^{III}O_2$ (*i*-Pr-BIP)(SPh)(L)] with L = Cl^- or $CF_3SO_3^-$ (OTf^-), which are designated **A** and **B**, respectively. It also should be noted that in contrast to the facial triad of histidine ligands in CDO enzymes, the *i*-Pr-BIP ligand coordinates in one plane of symmetry thereby leaving the axial ligand position vacant for either substrate or an anion. The experimental studies revealed dramatic differences in reactivity patterns by changing the ligand L from Cl^- to $CF_3SO_3^-$, whereby the chloride ligated complex reacted by forming disulfide products, whereas the triflate ligated system gave sulfinic acid products (Badiei, et al., 2011; Jiang, et al., 2010). These differences were assigned to the axial versus equatorial ligand effects of the oxidant.

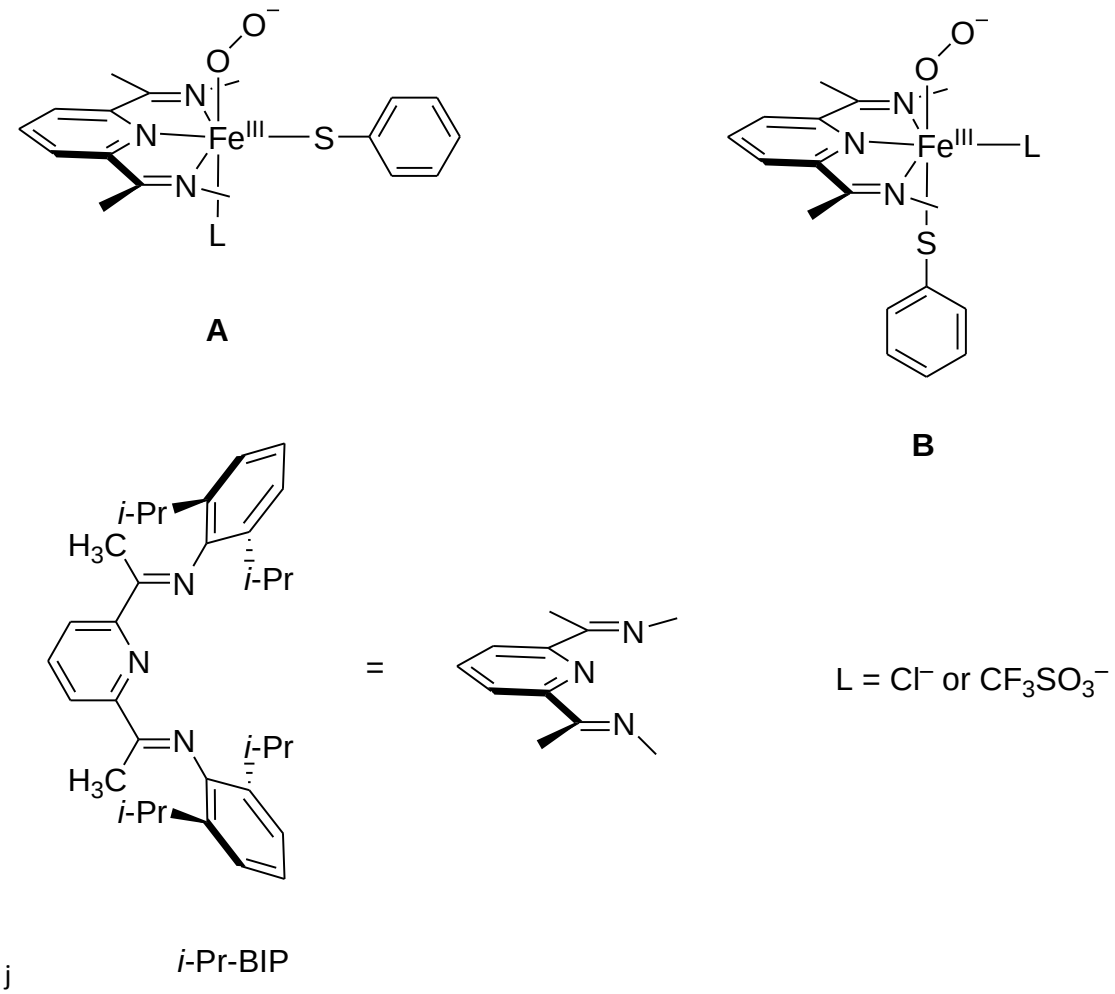

Figure 4.2 Models investigated in this study.

The effect of axial and equatorial ligands on heme and nonheme iron oxidants is well documented (Bukowski, et al., 2005; Costas, et al., 2004; de Visser, 2009; Decker and Solomon, 2005; Hirao, et al., 2008; Que Jr and Ho, 1996; Roelfes, et al., 2003; Shaik, et al., 2007; Solomon and Zhang, 1992) . Thus, heme monooxygenases such as the cytochromes P450 contain an iron-heme active centre where the heme is linked to the protein via an axial cysteinate ligand (Dawson, et al., 1976; Poulos, 1996). By contrast, heme peroxidases have an axially ligated histidine group, which has been proposed to be the key reason for their differences in catalytic function (Dawson, 1988; Green, et al., 2004; Woggon, 2005). These studies proposed the cysteinate to act with a "push"-effect, while histidine with a "pull"-effect. The push/pull-effect of the axial ligand was shown to be the key reason for the reactivity differences of P450s vis-à-vis peroxidases. Indeed, a series of density functional theory calculations confirmed that peroxidase models reacted with much higher barriers in aliphatic hydroxylation and epoxidation reactions using the same substrate (Shaik, et al., 1995; Shaik, et

al., 2005). In biomimetic models, the effect of the axial ligand on spectroscopic properties (*trans*-influence) as well as on reactivity patterns (*trans*-effect) was demonstrated by Gross and co-workers(Czarnecki, et al., 1996; Gross, 1996; Gross and Nimri, 1994) using studies of styrene epoxidation by a range of iron(IV)-oxo porphyrin cation radical systems. Subsequent studies of Nam et al (Nam, et al., 2004; Song, et al., 2005) showed differences in oxidative properties of iron(IV)-oxo oxidants with chloride *trans* to the oxo group as compared to those with acetonitrile, leading to reactivity differences of those oxidants with *cis* versus *trans* olefins, the regioselectivity of aliphatic over aromatic hydroxylation, as well as epoxidation versus hydroxylation processes. Further studies also revealed an axial ligand effect on reactivity and spectroscopic parameters in a selection of nonheme iron complexes (Anastasi, et al., 2007; Fukuzumi, et al., 2010; Hirao, et al., 2008; Jackson, et al., 2008; Jensen, et al., 2007; Sastri, et al., 2007; Zhou, et al., 2008). Recent, combined experimental and computational studies on the reactivity of manganese(V)-oxo embedded in a corrolazine ligand system identified a pronounced axial ligand effect on the rate constant of hydrogen atom abstraction from dehydroanthracene as a function of the axial ligand (Prokop, et al., 2010). This ligand effect was characterized as to occur due to differences in electron affinity of the oxidant as well as the pK_a strength of the protonated species. Following a series of computational studies on the axial ligand effect on heme iron (IV)-oxo complexes (de Visser, 2006; de Visser, 2006; de Visser, et al., 2009), the equatorial ligand effect on nonheme iron(IV)-oxo complexes (de Visser and Nam, 2008), and the axial ligand effect on nonheme iron(IV)-oxo complexes (de Visser, et al., 2011), we have decided to investigate the equatorial and axial ligand effect of the CDO biomimetic model displayed in Figure 4.2, which we will report in this work.

4.3 Computational methods

The studies presented in this work use density functional theory methods as implemented in the *Gaussian*-03 program package (Frisch, et al., 2004). Following previous experience in the field (de Visser, 2006; de Visser, 2006; de Visser, et al., 2011; de Visser and Nam, 2008; de Visser, et al., 2009), we initially used the unrestricted hybrid density functional method UB3LYP (Becke, 1993; Lee, et al., 1988) in combination with a double-ζ quality LANL2DZ basis set on iron that includes a core potential and 6-31G on the rest of the atoms (Hay and Wadt, 1985), basis set BS1. We performed a full geometry optimization (without constraints) followed by an analytical frequency. All structures were confirmed as local minima and had no imaginary frequencies. Subsequent geometry optimization and frequency calculations were

done with a triple-ζ quality basis set: BS2 represents a triple-ζ LACV3P+ basis set on iron and 6-311+G* on the rest of the atoms and BS3 is 6-311+G* on all atoms. It should be noted that very little differences in energy and optimized geometries are obtained between UB3LYP/BS2//UB3LYP/BS1 calculations as compared to those found for UB3LYP/BS2 optimizations, therefore, we will focus on the latter results only in this paper. All calculations were done for the lowest lying singlet, triplet and quintet spin states, since it was shown that nonheme iron complexes can react via two-state-reactivity patterns (Hirao, et al., 2006). To test the effect of the environment on the ordering and relative energies of the various spin states, we did single point calculations using the polarized continuum model (PCM) with a dielectric constant of ε = 35.7 mimicking an acetonitrile solution at UB3LYP/BS2. Vibrational frequencies reported here were scaled with the recommended scaling factor of 0.96 (Scott and Radom, 1996).

4.4 Results and discussion

We started our investigation with a series of calculations on $^{1,3,5}\mathbf{A}_{L}$ (L = Cl^- and OTf^-) and the optimized geometries are given in Figure 2. For both complexes the quintet spin state is the ground state and it is well separated from the other spin states: the triplet spin state is higher in energy by 11.7 kcal mol^{-1} for $\mathbf{A}_{Cl}$ and 11.5 kcal mol^{-1} for $\mathbf{A}_{OTf}$, whereas the closed-shell singlet spin states are considerably higher in energy (by 25.6 and 31.8 kcal mol^{-1}, respectively). Optimized geometries are in line with previous computational studies on Fe(III)-superoxo complexes that typically found O–O distances in the range of 1.323 – 1.370 Å (Annaraj, et al., 2009; de Visser, 2009; Jensen, et al., 2005; Nakashima, et al., 2006; Rydberg, et al., 2004). The Fe–Cl distance is in a narrow range from 2.420 – 2.438 Å, which is in good agreement with previous studies of iron(IV)-oxo porphyrin cation radical systems that also had an axially ligated Cl^- anion (de Visser, 2006). There is some fluctuation in the Fe–S bond length between the three different spin states, however, this follows from the molecular orbital occupations, *vide supra*.

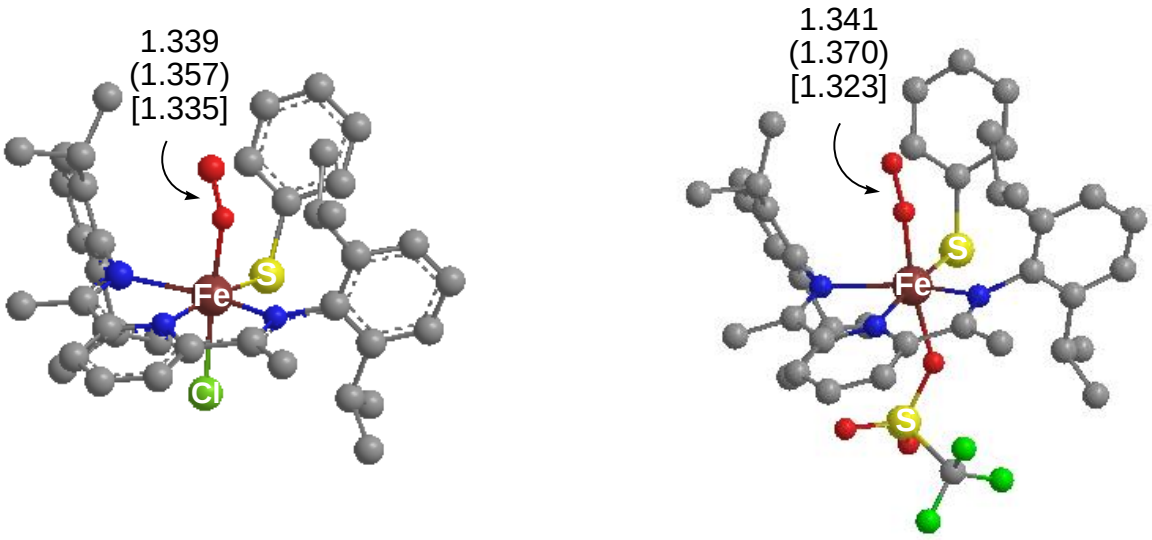

r_{FeO} = 1.801 (1.912) [2.018]
r_{FeCl} = 2.420 (2.437) [2.438]
r_{FeS} = 2.451 (2.271) [2.364]

$^{1}\mathbf{A}_{Cl}$ ($^{3}\mathbf{A}_{Cl}$) [$^{5}\mathbf{A}_{Cl}$]

r_{FeO} = 1.819 (1.906) [2.043]
r_{FeOTf} = 2.050 (2.068) [2.101]
r_{FeS} = 2.469 (2.261) [2.381]

$^{1}\mathbf{A}_{OTf}$ ($^{3}\mathbf{A}_{OTf}$) [$^{5}\mathbf{A}_{OTf}$]

Figure 4.3 Optimized geometries of $^{1,3,5}\mathbf{A}_{Cl}$ (left-hand-side) and $^{1,3,5}\mathbf{A}_{OTf}$ (right-hand-side) with bond lengths in angstroms.

To understand these spin state energetics and the differences between models $\mathbf{A}_{Cl}$ and $\mathbf{A}_{OTf}$, consider in Figure 3 the high-lying occupied and virtual orbitals for both systems as taken from the triplet spin calculations. The metal-type orbitals originate from a linear combination of the 3*d* atomic orbitals on iron with ligand based orbitals. The lowest lying orbital is the π^*_{xy} orbital for the interaction of the metal with the axial ligand. A bit higher in energy are the π^*_{xz} and π^*_{yz} orbitals; the former is in the plane of the Fe–O–O group and interacts with a π-orbital on the axial ligand, while the π^*_{yz} orbital interacts with both the axial ligand and the proximal oxygen atom. Higher in energy are two σ^* orbitals: one for the antibonding interaction of the axial ligand and the proximal oxygen atom with the iron (σ^*_{z2}) and the second for the antibonding interactions of the metal with the BIP and sulphide ligands (σ^*_{x2-y2}). Two antibonding orbitals along the superoxo bond are also depicted in Figure 3 ($\pi^*_{OO,yz}$ and $\pi^*_{OO,xz}$), which are occupied with three electrons. The metal-based orbitals are occupied with five electrons; hence, the system is characterized as an Fe (III)-superoxo complex.

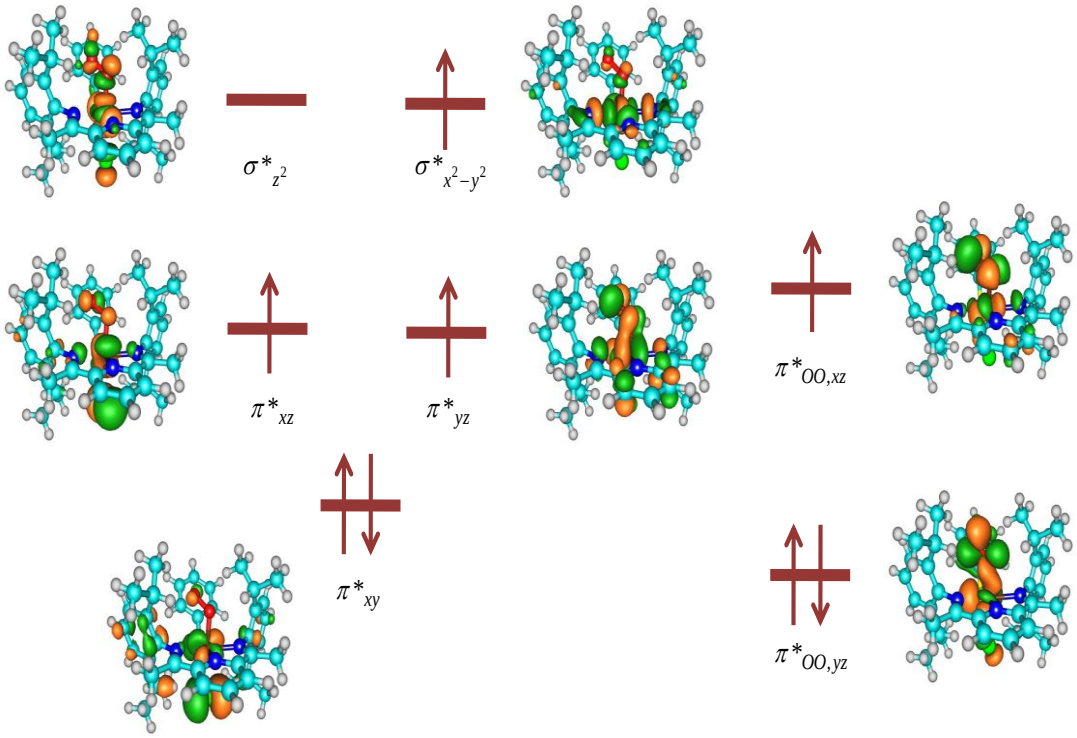

Figure 4.4 High-lying occupied and low-lying virtual orbitals of $^5A_{Cl}$

The quintet spin state has orbital occupation $\pi^*_{xy}{}^2\ \pi^*_{xz}{}^1\ \pi^*_{yz}{}^1\ \sigma^*_{x2-y2}{}^1\ \pi^*_{OO,yz}{}^2\ \pi^*_{OO,xz}{}^1$ and includes the ferromagnetic coupling of the $\pi^*_{OO,xz}$ electron with three metal based unpaired electrons. The lowest lying triplet spin state, by contrast, has $\pi^*_{xy}{}^2\ \pi^*_{yz}{}^2\ \pi^*_{xz}{}^1\ \pi^*_{OO,yz}{}^2\ \pi^*_{OO,xz}{}^1$ and distinguishes from the quintet spin state essentially by the transfer of one electron from σ^*_{x2-y2} to π^*_{yz}. Both of these states, therefore, can be characterized as Fe (III)-superoxo complexes. The singlet-spin state, by contrast, is an Fe (II)-peroxo complex with orbital occupation $\pi^*_{xy}{}^2\ \pi^*_{xz}{}^2\ \pi^*_{yz}{}^2\ \pi^*_{OO,yz}{}^2$. We made several attempts to swap orbitals and calculate a low-spin Fe (III)-superoxo complex but all our calculations converged back to the Fe (II)-peroxo situation instead. It appears therefore that there is no lower lying low-spin state for these complexes. The orbital occupation and spin state ordering is in line with previous experimental and computational studies of six-coordinate iron(III)-superoxo complexes that were characterized as high-spin states (Baerends, 1989; de Visser, 2006; Emerson, et al., 2007; Georgiev, et al., 2008; Green, 2006; Jensen, et al., 2010; Lee, et al., 2010; Mukherjee, et al., 2010; Shaik, et al., 2005; Siegbahn, et al., 2004). Furthermore, the iron (III)-*i*-Pr-BIP(X) complex with X = Cl^- or OTf^- was characterized as a high-spin state (Badiei, et al., 2011), in support with what we find here. Our optimized geometries are also in support of the orbital occupations, and, for instance, in the quintet spin state due to single occupation of a σ^*_{x2-y2} orbital with antibonding character along the Fe–SPh axis, the Fe–S distances are elongated with respect to

the triplet spin state, where this orbital is virtual. The same trend is also observed for $^{1,3,5}\mathbf{A}_{OTf}$. On the other hand, occupation of the σ^*_{z2} orbital in the quintet spin state would have elongated the Fe–O and Fe-axial ligand distances considerably, as observed before (Baerends, 1989; de Visser, 2006). The geometries, therefore, support the assignment of a singly occupied σ^*_{x2-y2} orbital and virtual σ^*_{z2} orbital in the quintet spin states.

The group spin densities (Figure 4.5) give further evidence for the assignment of the orbital occupations of Figure 4.4 above. In the triplet spin state the unpaired spin density on the superoxo group is 0.92 for both $^3\mathbf{A}_{Cl}$ and $^3\mathbf{A}_{OTf}$, which is coupled to an unpaired electron on the metal; the spin density on iron is 0.91 in $^3\mathbf{A}_{Cl}$ and 0.87 in $^3\mathbf{A}_{OTf}$. These spin densities confirm the single occupation of the π^*_{xz} and $\pi^*_{OO,xz}$ orbitals in these triplet spin states. In the quintet spin states, by contrast, the metal unpaired spin density has increased to 3.07 and 3.30 for $^5\mathbf{A}_{Cl}$ and $^5\mathbf{A}_{OTf}$, respectively. Technically (Figure 4.4), the metal is involved in all four singly occupied molecular orbitals, although the contribution is small in $\pi^*_{OO,xz}$. In the quintet spin states there is also significant spin density on the BIP ligand system (0.30 in $^5\mathbf{A}_{Cl}$ and 0.33 in $^5\mathbf{A}_{OTf}$), which further supports the assignment of a singly occupied σ^*_{x2-y2} orbital.

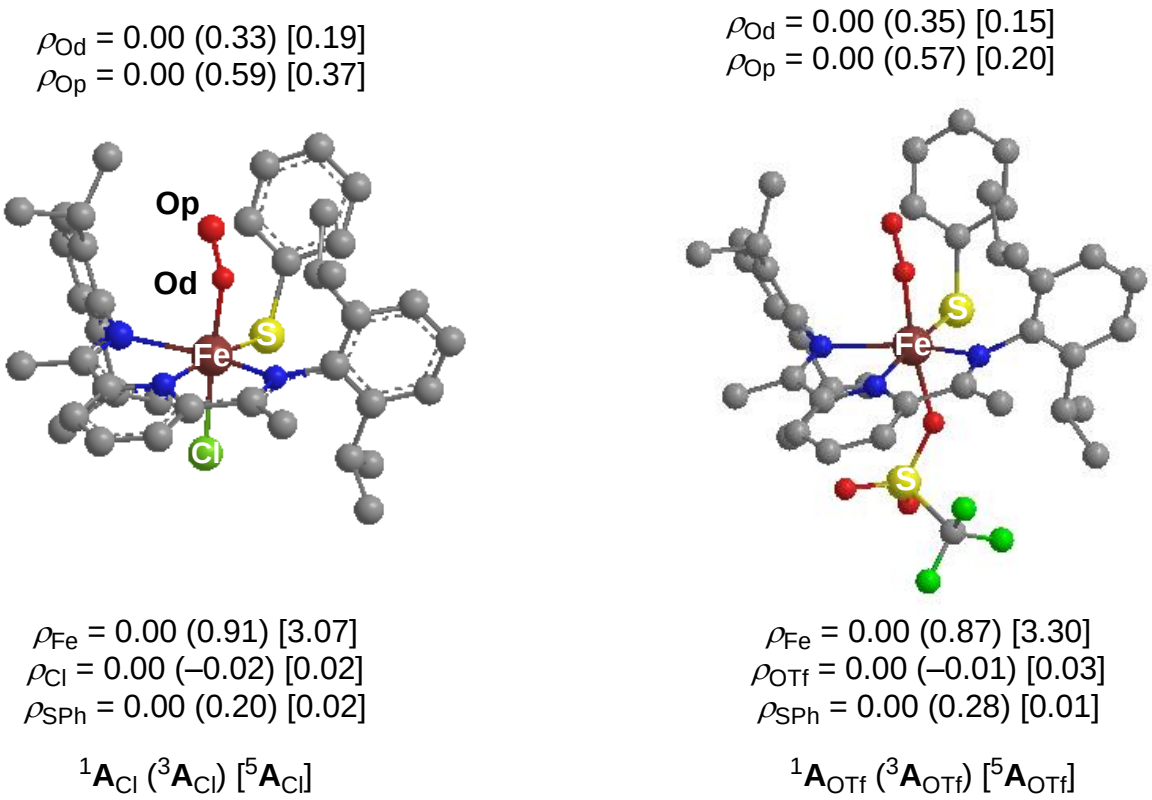

Figure 4.5 Group spin densities calculated at UB3LYP/B2//UB3LYP/B1 for $^{1,3,5}\mathbf{A}_{Cl}$ (left-hand-side) and $^{1,3,5}\mathbf{A}_{OTf}$ (right-hand-side)

Subsequently, we investigated the isomers $^{1,3,5}\mathbf{B}_{Cl}$ and $^{1,3,5}\mathbf{B}_{OTf}$, which have the axial and equatorial ligands swapped as compared to structure $\mathbf{A}_L$ (L = Cl^- or OTf^-), Figure 4.2, i.e. the thiophenolate is put in the axial position of the iron(III)-superoxo and the anionic ligand (Cl^- or OTf^-) is in the equatorial position. Optimized geometries of the lowest lying singlet, triplet and quintet spin state structures are depicted in Figure 4.6. Similarly, to the results described above on $^{1,3,5}\mathbf{A}_{Cl}$, also for $\mathbf{B}_{Cl}$ the quintet spin state is the ground state followed by the triplet spin state and the closed-shell singlet spin state. Relative energies of the three spin states and their ordering is close to those observed reported above for $^{1,3,5}\mathbf{A}_{Cl}$: $^5\mathbf{B}_{Cl}$ (0.0 kcal mol^{-1}), $^3\mathbf{B}_{Cl}$ (8.2 kcal mol^{-1}) and $^1\mathbf{B}_{Cl}$ (27.0 kcal mol^{-1}).

Geometrically, there are similarities as well as differences between the structures $^{1,3,5}\mathbf{A}_{Cl}$, on the one hand, and $^{1,3,5}\mathbf{B}_{Cl}$, on the other hand. Despite the fact that the dioxygen bond length is virtually the same in all complexes, actually the metal-ligand distances show big differences. Thus, the metal-oxygen bond is significantly elongated from 1.912 Å in $^3\mathbf{A}_{Cl}$ to 2.027 Å in $^3\mathbf{B}_{Cl}$ and from 2.018 Å in $^5\mathbf{A}_{Cl}$ to 2.223 Å in $^5\mathbf{B}_{Cl}$. At the same time elongation of the Fe–S bond occurs from 2.271 Å in $^3\mathbf{A}_{Cl}$ to 2.382 Å in $^3\mathbf{B}_{Cl}$ and from 2.364 Å in $^5\mathbf{A}_{Cl}$ to 2.972 Å in $^5\mathbf{B}_{Cl}$. The latter structure, therefore, has a very weak thiophenolate bound and with a bond length of that magnitude cannot be considered as a covalent bond. In the triflate bound isomers ($^{3,5}\mathbf{B}_{OTf}$) this situation is even worse and the thiophenolate has dissociated completely from the metal and is optimized with a distance of around 6 Å. Hence, $^{3,5}\mathbf{B}_{OTf}$ are pentacoordinate iron (III)-superoxo complexes. The reason for this is the considerable steric strain from the di-*iso*-propylphenyl groups that are attached to the BIP ligand. The group spin densities of these complexes are also characterized as Fe (II)-superoxo with a nearby thiophenol radical, i.e. an electron transfer from thiophenol to the metal has taken place. This electron transfer fills the π^*_{xz} orbital with a second electron in both the triplet and quintet spin states. A single point calculation in a dielectric constant does not change the spin and charge distributions dramatically and keeps the system in a Fe(II)-superoxo-*i*-Pr-BIP-(OTf) with a nearby $SPh^\bullet$ radical. Therefore, the $Fe^{II}O_2$-*i*-Pr-BIP (OTf) complex can abstract electrons from thiophenolate to give $SPh^\bullet$, whereby the latter can form PhS–SPh complexes in a bimolecular reaction of two thiophenol radicals.

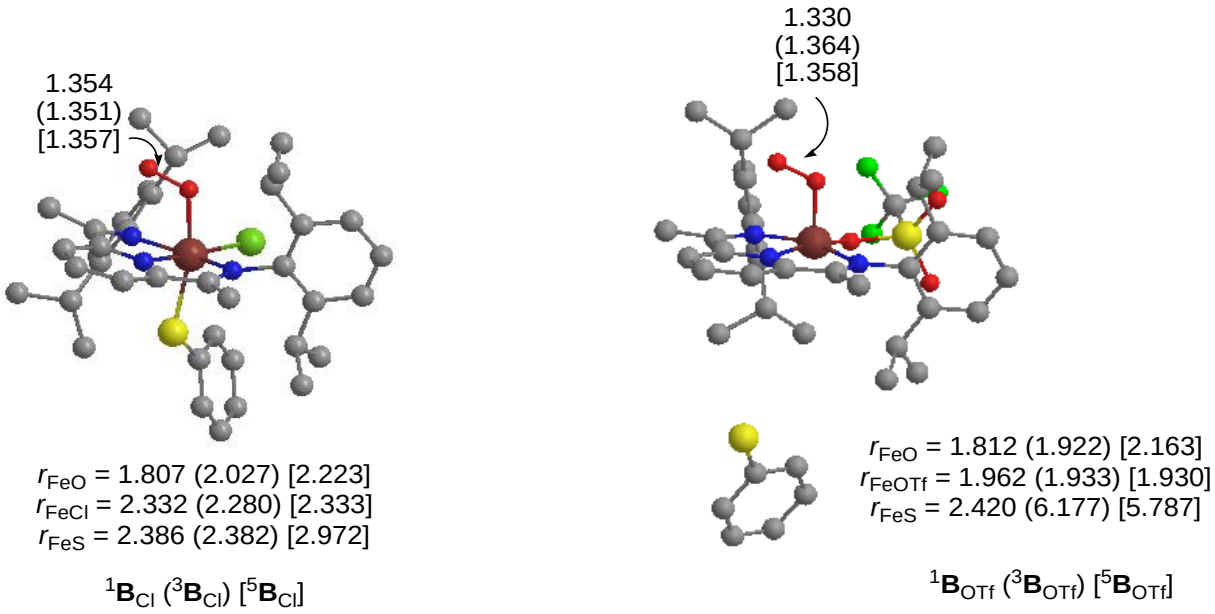

Figure 4.6 Optimized geometries of $^{1,3,5}\mathbf{B}_{Cl}$ (left-hand-side) and $^{1,3,5}\mathbf{B}_{OTf}$ (right-hand-side) with bond lengths in angstroms

Green showed the applicability of Badger's rule for the correlation of Fe–O stretch vibrations with the strength of the Fe–O bond length for a series of heme and nonheme iron (IV)-oxo complexes (Green, et al., 2004). Further studies in our group showed that calculated vibrational frequencies for metal-oxo complexes fit experimental observations well and, for instance, reproduce experimental $^{16}O_2/^{18}O_2$ vibrational shifts (de Visser, 2008; Godfrey, et al., 2008; Karamzadeh, et al., 2010). To find out whether this is similar for iron (III)-superoxo complexes we extracted and analyzed the vibrational frequencies of $^5\mathbf{A}_{Cl}$, $^5\mathbf{A}_{OTf}$ and $^5\mathbf{B}_{Cl}$. Thus, the superoxo stretch vibration (ν_{OO}) is located at 1095, 1082, and 1043 cm^{-1}, respectively, for $^5\mathbf{A}_{Cl}$, $^5\mathbf{A}_{OTf}$ and $^5\mathbf{B}_{Cl}$. Thus, in these three complexes the strength of the axial ligand gradually decreases from Cl^- to OTf^- to PhS^-. It appears, therefore, that the superoxo stretch vibration drops when a weaker axial ligand is selected. On the other hand, the Fe–O frequency for these iron (III)-superoxo complexes increases along this trend from 243 to 271 to 322 cm^{-1} for $^5\mathbf{A}_{Cl}$, $^5\mathbf{A}_{OTf}$ and $^5\mathbf{B}_{Cl}$, respectively. Consequently, a trans-influence on the spectroscopic features shifts the Fe–O and O–O stretching frequencies dependent on the nature of the axial ligand.

An oxygen atom transfer reaction from complexes **A** or **B** to give sulfoxide or sulfinic acid products leads to initial dioxygen bond breaking. In previous work, we showed that the hydrogen atom abstraction reaction by iron (IV)-oxo porphyrin cation radical oxidants is proportional to the strength of the C–H bond that is broken as well as with the O–H bond that is formed (de Visser, 2010; Kumar, et al., 2010; Shaik, et al., 2008). In a similar vein, we predict

complex $^5\mathbf{A}_{Cl}$ to be more efficient in oxygen atom transfer reactions to substrates since the superoxo bond is weaker; hence, it should be easier to break in the process. To test this we ran a geometry scan for the attack of the terminal oxygen atom of the superoxo group on the sulphur atom of SPh^- for $^5\mathbf{A}_{Cl}$ and $^5\mathbf{A}_{OTf}$ and the results are given in Figure 6. As follows, both reactions efficiently lead to a bicyclic ring structure, whereby an S–O bond is formed and the O–O bond is still intact, although weakened. This mechanism was also found for CDO enzymes using DFT and QM/MM methods (Aluri and de Visser, 2007; de Visser and Straganz, 2009; Kumar, et al., 2011). Indeed, as predicted from the optimized geometries of $^5\mathbf{A}_{Cl}$ and $^5\mathbf{A}_{OTf}$, the barrier height for oxygen attack on sulphur is smaller for $^5\mathbf{A}_{Cl}$ than $^5\mathbf{A}_{OTf}$.

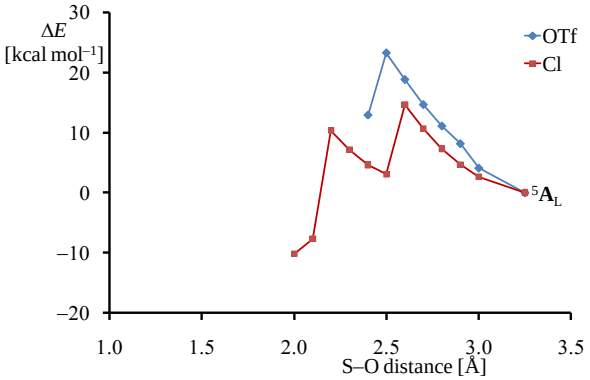

Figure 4.7 Geometry scans for the attack of superoxo on the SPh^- group in ^5A_L(L = Cl^- or OTf^-). Each point in the figure represents a full geometry optimization (UB3LYP/LANL2DZ) with fixed S–O distance in Gaussian. Energies are relative to ^5A_L (L = Cl^- or OTf^-).

So how do our computations match the experiments reported on these particular systems. First of all, the crystal structure of Fe(III)-*i*-Pr-BIP with either chloride or triflate bound gave a structure of the **B**-type with chloride bound, but of **A**-type with triflate bound. These structures, of course, are pentacoordinated and no molecular oxygen is attached to the metal centre. Nevertheless, we will compare the results obtained in this work with the pentacoordinate crystal structures from ref (Badiei, et al., 2011). The relative energy between structures $^5\mathbf{A}_{Cl}$ and $^5\mathbf{B}_{Cl}$ is calculated to be 1.2 kcal mol^{-1} in favour of structure **A**. Technically, therefore, both isomers should exist side-by-side unless the anion binding is determined in an earlier step in its biosynthesis. By contrast, for the triflate structure $^5\mathbf{A}_{OTf}$ is well lower in energy than $^5\mathbf{B}_{OTf}$ by 23 kcal mol^{-1} due to the dissociation of the thiophenol from the metal centre. It appears therefore that the cavity within the *i*-Pr-BIP ligand is small to fit the thiophenolate ligand. By contrast, small anions, such as chloride, fit into the cavity easily. As a consequence, the triflate bound structure resides in an orientation with the thiophenolate in the *cis*-position (equatorial), i.e. in a position adjacent to the superoxo group. Because of this, the substrate

will be accessible for attack by dioxygen and efficient dioxygenation of the substrate may occur. This is indeed what Goldberg and co-workers observed with this oxidant. By contrast, in the chloride bound structure, where the thiophenolate is in the *trans*-position (axial), it will be located too far away from molecular oxygen to enable reactivity. However, these stable complexes may have a finite lifetime and during the course of that lifetime, collisions of two $^{5}\mathbf{A}_{Cl}$ structures may occur that lead to disulfide product complexes.

4.5 Concluding remarks

In summary, the key feature that determines dioxygenation of thiophenol by nonheme iron complexes is the availability of a *cis*-binding site on the metal adjacent to the dioxygen binding position. Stereochemical interactions of ligands as are the case in structure **B** prevent binding of thiophenolate in an appropriate position and consequently cannot bind it. However, these complexes can donate electrons rather than binding substrate that will then lead to formation of PhS–SPh products.

Density functional theory calculations are presented on biomimetic model complexes of cysteine dioxygenase. Our studies show that it is vital to have a thiolate substrate bound in the *cis*-position of the dioxygen moiety. Preventing substrate binding through Stereochemical interactions of other ligands prevents substrate dioxygenation. However, the iron (III)-superoxo complex is a good electron acceptor and easily abstracts electrons from thiophenols so that they can react further to form PhS–SPh via a bimolecular reaction.

CHAPTER 5.

Methane hydroxylation by a biomimetic methane monooxygenase system with a *N*-bridged-diiron-oxo centre

5.1 Abstract

In the final project that I will discuss in this dissertation, I show results of a computational study on a biomimetic model complex that is capable of hydroxylating methane. The enzyme methane monooxygenase (MMO) is an important bacterial enzyme that is able to activate the very strong C–H bond in methane. Recent studies of the Sorokin group highlighted a biomimetic model complex with an *N*-bridged diiron porphyrin conformation that is able to efficiently hydroxylate methane. We investigated this model using density functional theory and find that this biomimetic model complex reacts with a low hydrogen abstraction barrier of only 7.9 kcal mol^{-1} via a concerted mechanism to give products. This barrier is considerably lower than that found by an iron(IV)-oxo porphyrin cation radical species, where a barrier of 26.5 kcal mol^{-1} was found. That means that *N*-bridged diiron complexes are more catalytically active than iron-porphyrins.

5.2 Introduction

Methanotrophs are bacteria that metabolise methane and as a result they have important roles in the industrial production of bioremediation destroying or controlling contaminants. (Brigmon, 2002; Costello and Lidstrom, 1999; Hanson and Hanson, 1996; Marco, et al., 2004). Methanotrophs also have important roles in global warming (Murrell, et al., 2000).

Methane monooxygenase (MMO) is one of the few enzymes that are able to oxidise the extremely strong C-H bond of methane. MMO enzymes come in two varieties, namely as cytoplasmic soluble MMO (sMMO) and particulate MMO (pMMO). The cytoplasmic soluble methane monooxygenase (sMMO) contains a diiron cluster i.e. two iron ions which react with oxygen and oxidize methane to produce methanol (Bollinger Jr, 2010; Kovaleva, et al., 2007; Merkx, et al., 2001). In contrast to the well studied sMMO, the knowledge of membrane bound pMMO is very limited and the mechanism is controversial. It has been suggested by Balasubramanian, et al. (2010) that the oxidation of methane in the nature should take place on a dicopper centre rather than diiron, due to the absence of iron in the membrane of the protein.

The active site of sMMO contains a diiron centre, where the iron atoms are bridged by a carboxylate group of glutamate side chain, as well as a hydroxide ion, and an acetate ion. In

addition, the metal atoms are coordinated by two histidine groups, three glutamine residues, and a water molecule (Rosenzweig, et al., 1995).

So far, very few biomimetic model complexes have been generated with potency in substrate hydroxylation that is competitive with the MMO enzymes. Recent studies of the Sorokin group (Kudrik and Sorokin, 2008; Sorokin, et al., 2009; Sorokin, et al., 2010; Sorokin, et al., 2009; Sorokin, et al., 2008) established methane hydroxylation by an *N*-bridged diiron phthalocyanine complex, Figure 5.1. Thus, a phthalocyanine ring is an aromatic ring similar to porphyrin, but whereby the *meso*-CH groups are replaced by nitrogen atoms. Studies with the bridging nitrogen atom replaced by oxygen, or mononuclear iron-phthalocyaninces showed little activity in substrate hydroxylation, therefore, the bridging nitride group is essential for reactivity. In addition, Sorokin and co-workers found the oxidant to react efficiently with benzene to give phenol products in good yield. To gain insight into the reaction mechanism of methane hydroxylation by the model shown in Figure 5.1 we performed a density functional theory study on the oxidant and its catalytic activity towards methane.

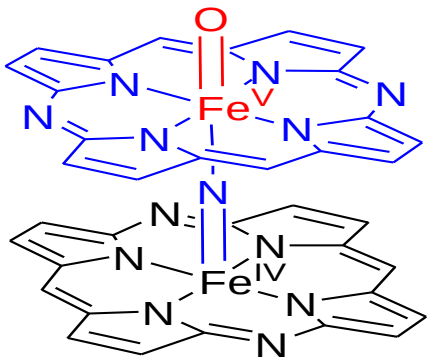

Figure 5.1 *N*-bridged diiron phthalocyanine oxidant studied in this work.

Let me highlight some important points that are related to computational studies on MMO complexes using DFT methods (Siegbahn and Blomberg, 1999). In the past, a range of DFT calculations have been performed on MMO enzymes that established reaction mechanisms, minimum energy structures and reaction rate constants using mimics of biological structures with central metal ion (Kumar, et al., 2011; Siegbahn and Blomberg, 1999; Siegbahn and Blomberg, 2010; Siegbahn and Crabtree, 1997; Siegbahn, et al., 1998; Song, et al., 2005). The model chosen is generally dependent on the size of the chemical system and usually includes the active site and its immediate surroundings. Obviously, the more atoms the model contains, the more accurate the results are, but the calculations also scale with the number of electrons, so that there will be an upper limit of model size that makes the calculation doable. This

evaluation allows one to put experimental information and theoretical computer modelling side-by-side (Siegbahn and Blomberg, 1999).

The computational results are benchmarked against experiment and the model is validated. One such method compares the optimised structures, in which the effects of the protein are included, versus experimental protein structures. Furthermore, often spectroscopic data is available from enzymatic structures, such as electron paramagnetic resonance (EPR) information on the spin state. DFT calculations that have been under close scrutiny by experimentalists include those related to the mechanisms of CH_4 activation, and in particular by MMO enzymes (Siegbahn and Blomberg, 1999). The analysed systems in their study used models of between 40 and 50 atoms in the active site, whereby only the first-shell amino acid ligands were considered in the calculations, while the surrounding is treated with a homogeneous dielectric medium. The thus obtained results were in very good agreement with experiment and are characterised by high accuracy (Blomberg and Siegbahn, 2001).

A later study on MMO that featured a larger active site model was performed on O-O bond cleavage and alkane hydroxylation mechanism by MMO enzymes and gave some interesting results that were different from the initial studies. Large differences on the structure for O-O bond cleavage were found between the new DFT calculations and the calculations made before. It was suggested this was due to the lack of key hydrogen bonding interactions that stabilized the intermediate considerably and lowered barrier heights. Thus, the driving force has calculated to be approximately 5 kcal mol^{-1}. This in turn, could explain the dependency of pH in this study. In fact, this is characterized by the understanding that hydrogen abstraction state obtained from the theoretical calculations, and compared with experimental data (Siegbahn, 2001; Siegbahn, 2006). In conclusion those studies show the sensitivity on the outcomes depending upon the model that has been considered.

Even though in the majority of the studies on MMO a diiron core as the central metal cluster in the active site is considered, in pMMO a dinuclear copper site appears. Yoshizawa and Shiota (2006) investigated the conversion of methane to methanol at the mononuclear and binuclear copper sites of pMMO using a combined DFT and QM/MM study. They identify the formation of a copper-oxo intermediate in the catalytic cycle responsible for methane hydroxylation. QM and QM/MM calculations are used in the methane hydroxylation reaction in mononuclear and dinuclear copper sites of pMMO. In this study, the authors suggest possible mechanisms, in which, the formation of a reactive copper−oxo is found. Molecular oxygen (O_2) binds to a Cu^{I}

species to give a Cu^{II}–superoxo species. This is followed by a proton transfer from a nearby tyrosine residue to form a Cu^{II}–hydroperoxo complex, which is converted into a Cu^{III}–oxo species and a water molecule via abstraction of a proton from a tyrosine residue. It should be noted that when a oxygen molecule (O_2) is added to the dicopper site, it is transformed into a bis(μ-oxo)dicopper species. The pMMO system reacts efficiently with methane to form methanol with the Cu^{III}–oxo species as the active oxidant (Yoshizawa and Shiota, 2006). It was found that the σ* orbital is important factor in the homolytic cleavage of a C−H bond of methane since it is localized along the Cu−O bond region in the triplet state. Finally, this study also identified a second possible oxidant, namely the mixed-valent bis(μ-oxo)$Cu^{II}Cu^{III}$ species that reacts with methane and plays an important role in C−H activation (Yoshizawa and Shiota, 2006).

5.3 Computational methods

The methods used for this project are similar to those from the previous chapter. We used the unrestricted B3LYP density functional method in combination with a double-ζ quality LACVP basis set on iron that contains a core potential for geometry optimizations and frequencies. Single point calculations were done using a triple-ζ quality LACV3P+ basis set on iron (with core potential) and 6-311+G* on the rest of the atoms. All calculations were done for the lowest lying singlet, triplet, quintet, septet and nonet spin state surfaces. Geometry scans were performed by keeping one degree of freedom (the reaction coordinate) fixed, while at the same time minimizing all other degrees of freedom. The DFT calculations were carried out using *Gaussian*-03.

5.4 Results and discussion

The optimised geometries of the reactants and products in the singlet spin state for the *N*-bridged diiron phthalocyanine oxidant structure are illustrated in Figure 5.2 and Figure 5.3, respectively. The values given in these figures are in Ångstroms. The calculation was run using unrestricted DFT, but converged to a closed shell spin state. The diiron distance is 3.561 Å with a long Fe–N bond of 2.018 Å between the iron(V)-oxo group bridging nitride atom, whereas the other Fe–N distance is 1.543 Å, which is typical for a double bond. Note as well that the two phthalocyanine rings are not parallel but about 17.8° twisted as based on a dihedral angle (N–Fe1–Fe2–N). The Fe–O bond is 1.621 Å in length, which is typical for iron(IV)-oxo and iron(V)-oxo oxidants (Kudrik and Sorokin, 2008; Sorokin, et al., 2009; Sorokin, et al., 2010;

Sorokin, et al., 2009; Sorokin, et al., 2008). Methane approaches from the top and forms a weak hydrogen bond (2.300 Å). Methane approaches from the top and forms a weak hydrogen bond (2.300 Å).

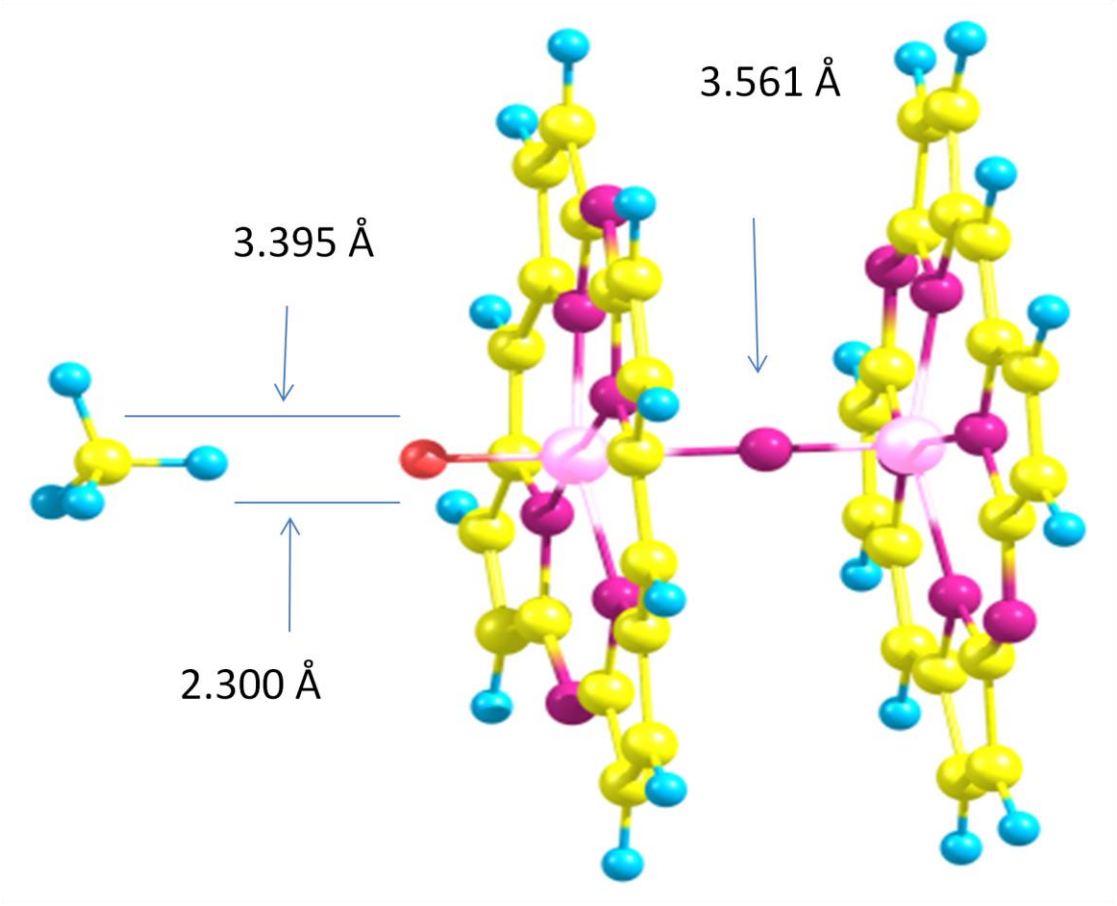

Figure 5.2 Optimised geometry of the singlet spin reactant of the *N*-bridged diiron phthalocyanine oxidant

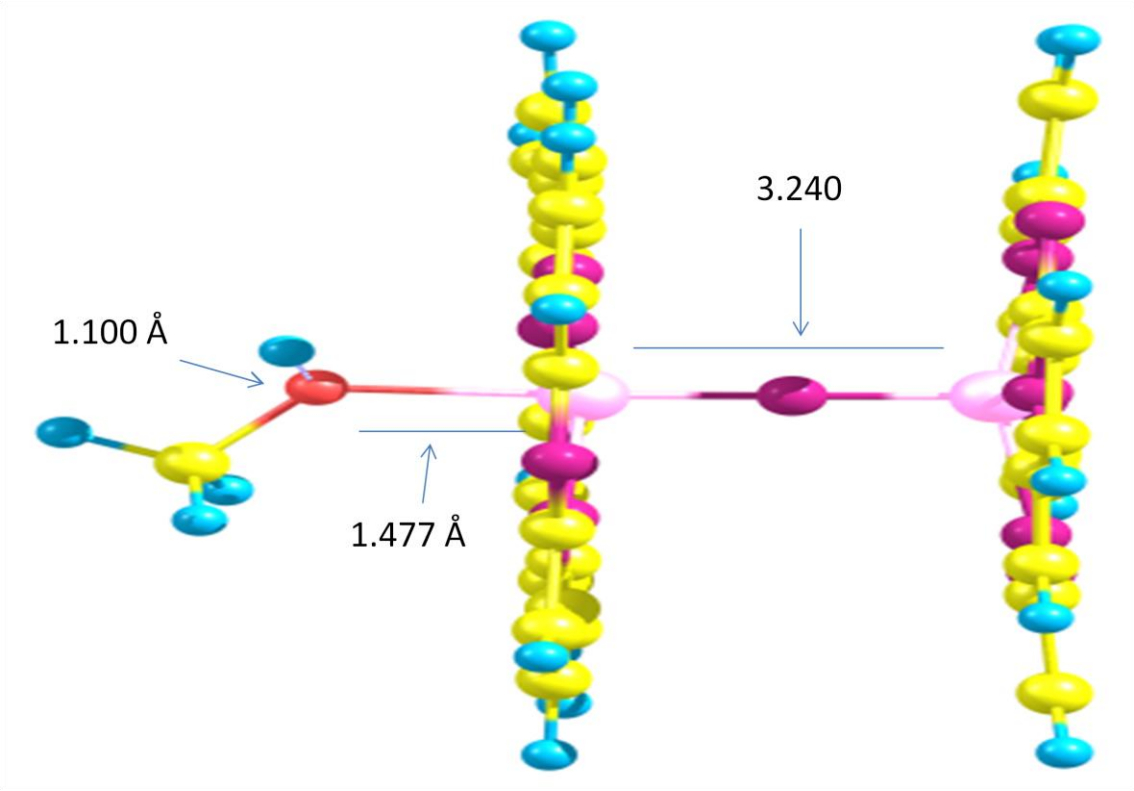

Figure 5.3 Optimised geometry of the singlet spin product complex

The optimized geometry of the product, shows typical features of a methanol bound to an iron centre. The Fe–O distance is long (2.090 Å) typical for a weak interaction. The Fe–N distance of the metal bound to methanol has shortened to 1.640 Å, while the other Fe–N distance of the other phthalocyanine group has elongated to 1.600 Å. Therefore, the nitride bridge has changed from Fe–N=Fe to Fe–N–Fe conformation. Thus, electron transfer from the substrate into the Fe–N–Fe bond releases so much energy that it overcomes the energy to break the C–H bond of methane. Consequently, the diiron phthalocyanine is a powerful oxidant that reacts with strong C–H bonds of substrates.

Subsequently, we ran a geometry scan from reactants to products and the result is given in Figure 5.4. The maximum of the scan is about 7.9 kcal mol^{-1} above the reactant energy. It should be noted that the full geometry optimisation of the transition state was not complete at the time of writing of this dissertation, however we do not expect dramatic changes from the geometry scan. If this is true than the *N*-bridged diiron phthalocyanine complex is a much more powerful oxidant than the iron(IV)-oxo heme cation radical species of cytochrome P450. Calculations on methane hydroxylation by a P450 model complex gave barriers of about 26.5 kcal mol^{-1}, hence considerably higher in energy. During the geometry scan shown in Figure 5.4 the rebound step took place en route to the product complex. This implies that the reaction is

concerted via an initial hydrogen atom abstraction step with a facile rebound. The mechanism is different from that in P450 enzymes, where a definitive stepwise mechanism was found with a stable radical intermediate.

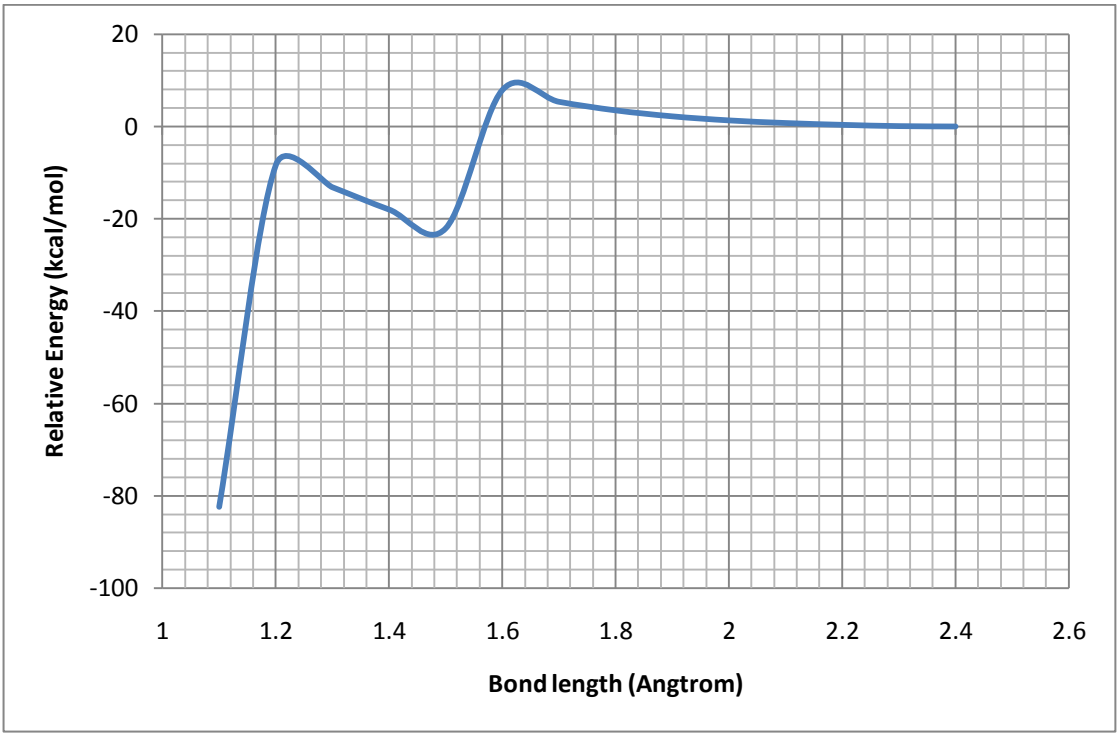

Figure 5.4 Geometry scan for hydrogen atom abstraction from methane by a *N*-bridged diiron complex.

5.5 Concluding remarks

We did exploratory calculations on methane hydroxylation by a *N*-bridged diiron complex, Our work finds low hydrogen abstraction barriers with a concerted mechanism leading to products. We note considerable changes in bond length along the Fe–N–Fe bond during the reaction mechanism, which may be the key reason for the low barrier height. Further studies will be required on other spin state surfaces and with methods with larger basis sets as well as the effect of solvent on the reaction mechanism.

CHAPTER 6.

Conclusions and future prospects

In this dissertation, I present a series of computational studies on enzyme and biomimetic model reactions using a variety of methods and techniques. Let me summarize the results per chapter:

Chapter 3 Mechanism of DNA base repair by nonheme iron(IV)-oxo species, a quantum mechanics/molecular mechanics study

Using QM/MM methods, we established a novel mechanism of substrate hydroxylation in a DNA base repair enzyme. The mechanism starts from an iron(IV)-oxo species with an internal rotation followed by hydrogen atom abstraction. The rotation is facilitated by a hydrogen bonded arginine amino acid side chain and moves iron(IV)-oxo species from a position trans to His_{131} to one that is trans to His_{187}. The internal rotation brings the oxo group in close proximity of the methylated group of the DNA base.

Further studies are ongoing and focus on the transition state for hydrogen atom abstraction. In addition, we will investigate alternative spin states, including the triplet and septet spin states.

Chapter 4 Axial and equatorial ligand effects on biomimetic cysteine dioxygenase model complexes

In summary, we find that the accessibility of the *cis*-binding site of thiophenol in a cysteine dioxygenase model complex is essential for efficient dioxygenation of the substrate in nonheme iron complexes. Furthermore, the bulky isopropyl side groups of the equatorial ligand of the metal prevent triflate and thiophenol binding to the appropriate binding sites and prevent dioxygenase activity.

Chapter 5 Methane hydroxylation by a biomimetic methane monooxygenase system with a *N*-bridged-diiron-oxo centre

Exploratory calculation on a *N*-bridged diiron phthalocyanine complex in methane hydroxylation are presented. The work gives a concerted reaction mechanism with a very low hydrogen abstraction barrier that is significantly lower to that found for cytochrome P450 enzymes. We have highlighted possible reasons for this low rate constant of the reaction.

REFERENCES

Abu-Omar, M.M., Loaiza, A. and Hontzeas, N. (2005) Reaction mechanisms of mononuclear non-heme iron oxygenases, *Chem. Rev.*, **105**, 2227-2252.

Alseth, I.*, et al.* (2006) A new protein superfamily includes two novel 3 methyladenine DNA glycosylases from Bacillus cereus, AlkC and AlkD, *Mol. Microbiol.*, **59**, 1602-1609.

Aluri, S. and de Visser, S.P. (2007) The mechanism of cysteine oxygenation by cysteine dioxygenase enzymes, *J. Am. Chem. Soc.*, **129**, 14846-14847.

Anastasi, A.E.*, et al.* (2007) Electronic structure of bispidine Iron (IV) oxo complexes, *Inorg. Chem.*, **46**, 6420-6426.

Annaraj, J.*, et al.* (2009) Structural Characterization and Remarkable Axial Ligand Effect on the Nucleophilic Reactivity of a Nonheme Manganese (III)–Peroxo Complex, *Angew. Chem., Int. Ed.*, **48**, 4150-4153.

Aravind, L. and Koonin, E.V. (2001) The DNA-repair protein AlkB, EGL-9, and leprecan define new families of 2-oxoglutarate-and iron-dependent dioxygenases, *Genome Biol*, **2**, 1-0007.0008.

Atkins, P.W. (1978) *Molecular quantum mechanics : an introduction to quantum chemistry*. Clarendon Press, Oxford.

Atkins, P.W. (1991) *Quanta : a handbook of concepts*. Oxford University Press, Oxford.

Atkins, P.W. (1992) *Physical chemistry*. Oxford University Press, Oxford.

Atkins, P.W. and De Paula, J. (2010) *Physical chemistry*. W.H. Freeman, New York.

Atkins, P.W. and De Paula, J. (2011) *Physical chemistry for the life sciences*. Oxford University Press, Oxford.

Atkins, P.W. and Friedman, R. (1997) *Molecular quantum mechanics*. Oxford University Press, Oxford.

Atkins, P.W. and Friedman, R. (2005) *Molecular quantum mechanics*. Oxford University Press, Oxford.

Atkins, P.W. and Friedman, R. (2011) *Molecular quantum mechanics*. Oxford University Press, Oxford.

Atkins, P.W. and Friedman, R.S. (1997) *Molecular quantum mechanics*. Oxford University Press, Oxford ; New York.

Atkins, P.W. and Friedman, R.S. (2005) *Molecular quantum mechanics*. Oxford University Press, Oxford ; New York.

Atkins, P.W., Friedman, R.S. and NetLibrary, I. (1997) *Molecular quantum mechanics*. Oxford University Press Oxford.

Badiei, Y.M., Siegler, M.A. and Goldberg, D.P. (2011) O(2) Activation by Bis(imino)pyridine Iron(II)-Thiolate Complexes, *J. Am. Chem. Soc.*, **133**, 1274-1277.

Baerends, E.J. (1989) Full Potential Lcao X-Alpha Calculations - a Citation Classic Commentary on Self-Consistent Molecular Hartree-Fock-Slater Calculations .1. The Computational-Procedure by Baerends,E.J., Ellis,D.E., Ros,P., *Cc/Phys Chem Earth*, 14-14.

Balasubramanian, R*., et al.* (2010) Oxidation of methane by a biological dicopper centre, *Nature*, **465**, 115-119.

Barrow, G. (1996) Physical Chemistry, WCB. McGraw-Hill, New York.

Bassan, A*., et al.* (2005) A Density Functional Study on a Biomimetic Non-Heme Iron Catalyst: Insights into Alkane Hydroxylation by a Formally HO-FeV-O Oxidant, *Chem. Eur. J.*, **11**, 692-705.

Becke, A.D. (1993) Density-functional thermochemistry. III. The role of exact exchange, *Chem. Phys*, **98**, 5648-5652.

Becke, A.D. (1993) Density-functional thermochemistry. III. The role of exact exchange, *J. Chem. Phys.*, **98**, 5648-5652.

Blomberg, M.R.A. and Siegbahn, P.E.M. (2001) A Quantum Chemical Approach to the Study of Reaction Mechanisms of Redox-Active Metalloenzymes, *J Phys Chem B*, **105**, 9375-9386.

Bodner, M.J*., et al.* (2009) Non-heme iron oxygenases generate natural structural diversity in carbapenem antibiotics, *J. Am. Chem. Soc.*, **132**, 12-13.

Bollinger Jr, J.M. (2010) Biochemistry: Getting the metal right, *Nature*, **465**, 40-41.

Bollinger Jr, J.M*., et al.* (2005) Mechanism of Taurine: Ketoglutarate Dioxygenase (TauD) from *Escherichia coli*, *Eur. J. Inorg. Chem.*, **2005**, 4245-4254.

Born, M. and Oppenheimer, R. (1927) Zur quantentheorie der molekeln, *Ann Phys-Berlin*, **389**, 457-484.

Borowski, T., Bassan, A. and Siegbahn, P.E.M. (2004) Mechanism of Dioxygen Activation in 2-Oxoglutarate-Dependent Enzymes: A Hybrid DFT Study, *Chem. Eur. J.*, **10**, 1031-1041.

Borowski, T*., et al.* (2010) Mechanism of Selective Halogenation by SyrB2: A Computational Study, *J. Am. Chem. Soc.*, **132**, 12887-12898.

Branden, C. and Tooze, J. (1991) *Introduction to protein structure*. Garland New York.

Brigmon, R.L. (2002) Methanotrophic bacteria: use in bioremediation, *Ency. Environ. Microbiol.*

Bruijnincx, P.C.A., van Koten, G. and Gebbink, R.J.M.K. (2008) Mononuclear non-heme iron enzymes with the 2-His-1-carboxylate facial triad: recent developments in enzymology and modeling studies, *Chem Soc Rev*, **37**, 2716-2744.

Bugg, T. (2004) *Introduction to enzyme and coenzyme chemistry*. Wiley-Blackwell.

Bugg, T., Kuhl, W. and Pee, K.H. (1997) *Introduction to enzyme and coenzyme chemistry*. Wiley Online Library.

Bugg, T.D.H. (2001) Oxygenases: mechanisms and structural motifs for O2 activation, *Curr. Opin. Chem. Biol.*, **5**, 550-555.

Bugg, T.D.H. (2003) Dioxygenase enzymes: catalytic mechanisms and chemical models, *Tetrahedron*, **59**, 7075-7101.

Bugg, T.D.H. and Ramaswamy, S. (2008) Non-heme iron-dependent dioxygenases: unravelling catalytic mechanisms for complex enzymatic oxidations, *Curr. Opin. Chem. Biol.*, **12**, 134-140.

Bukowski, M.R*., et al.* (2005) A thiolate-ligated nonheme oxoiron (IV) complex relevant to cytochrome P450, *Science*, **310**, 1000.

Cardinale, G.J. and Udenfriend, S. (1974) Prolyl hydroxylase, *Adv. Enzymol. Relat. Areas Mol. Biol.*, 245-300.

Casewit, C., Colwell, K. and Rappe, A. (1992) Application of a universal force field to organic molecules, *J. Am. Chem. Soc.*, **114**, 10035-10046.

Casewit, C., Colwell, K. and Rappé, A. (1992) Application of a universal force field to main group compounds, *J. Am. Chem. Soc.*, **114**, 10046-10053.

Chen, B.J., Carroll, P. and Samson, L. (1994) The Escherichia coli AlkB protein protects human cells against alkylation-induced toxicity, *J. Bacteriol.*, **176**, 6255.

Choroba, O.W., Williams, D.H. and Spencer, J.B. (2000) Biosynthesis of the vancomycin group of antibiotics: involvement of an unusual dioxygenase in the pathway to (S)-4-hydroxyphenylglycine, *J. Am. Chem. Soc.*, **122**, 5389-5390.

Chothia, C. (1984) Principles that determine the structure of proteins, *Annu. Rev. Biochem.*, **53**, 537-572.

Costas, M*., et al.* (2004) Dioxygen activation at mononuclear nonheme iron active sites: enzymes, models, and intermediates, *Chem. Rev.*, **104**, 939-986.

Costello, A.M. and Lidstrom, M.E. (1999) Molecular characterization of functional and phylogenetic genes from natural populations of methanotrophs in lake sediments, *Appl. Environ. Microbiol.*, **65**, 5066.

Creighton, T.E. (1993) *Proteins: Structures and molecular properties*. WH Freeman.

Czarnecki, K*., et al.* (1996) Direct Resonance Raman Evidence for a Trans Influence on the Ferryl Fragment in Models of Compound I Intermediates of Heme Enzymes, *J. Am. Chem. Soc.*, **118**, 2929-2935.

Daudel, R., Lefebvre, R.A. and Moser, C. (1959) *Quantum chemistry: methods and applications*. Interscience Publishers, New York,.

Dawson, J.H. (1988) Probing Structure-Function Relations in Heme-Containing Oxygenases and Peroxidases, *Science*, **240**, 433-439.

Dawson, J.H.*, et al.* (1976) Magnetic circular dichroism studies. 43. Oxidized cytochrome P-450. Magnetic circular dichroism evidence for thiolate ligation in the substrate-bound form. Implications for the catalytic mechanism, *J. Am. Chem. Soc.*, **98**, 3707-3709.

de Visser, S.P. (2006) The axial ligand effect of oxo-iron porphyrin catalysts. How does chloride compare to thiolate?, *J Biol Inorg Chem*, **11**, 168-178.

de Visser, S.P. (2006) Differences in and comparison of the catalytic properties of heme and non-heme enzymes with a central oxo-iron group, *Angew Chem Int Edit*, **45**, 1790-1793.

de Visser, S.P. (2006) Differences in and Comparison of the Catalytic Properties of Heme and Non Heme Enzymes with a Central Oxo–Iron Group, *Angew. Chem.* , **118**, 1822-1825.

de Visser, S.P. (2006) Propene Activation by the Oxo-Iron Active Species of Taurine/ -Ketoglutarate Dioxygenase (TauD) Enzyme. How Does the Catalysis Compare to Heme-Enzymes?, *J. Am. Chem. Soc.*, **128**, 9813-9824.

de Visser, S.P. (2006) Substitution of Hydrogen by Deuterium Changes the Regioselectivity of Ethylbenzene Hydroxylation by an Oxo–Iron–Porphyrin Catalyst, *Chem.--Eur. J.*, **12**, 8168-8177.

de Visser, S.P. (2006) What factors influence the ratio of C-H hydroxylation versus C=C epoxidation by a nonheme cytochrome P450 biomimetic?, *J. Am. Chem. Soc.*, **128**, 15809-15818.

de Visser, S.P. (2008) Is the Oxo Peroxodiiron Intermediate of a Ribonucleotide Reductase Biomimetic a Possible Oxidant of Epoxidation Reactions?, *Chem.--Eur. J.*, **14**, 4533-4541.

de Visser, S.P. (2009) Chapter 2 Introduction to Quantum Behaviour - A Primer. In, *Quantum Tunnelling in Enzyme-Catalysed Reactions*. Roy. Soc. Chem., pp. 18-35.

de Visser, S.P. (2009) Elucidating enzyme mechanism and intrinsic chemical properties of short-lived intermediates in the catalytic cycles of cysteine dioxygenase and taurine/alpha-ketoglutarate dioxygenase, *Coord. Chem. Rev.*, **253**, 754-768.

de Visser, S.P. (2009) Trends in Substrate Hydroxylation Reactions by Heme and Nonheme Iron (IV)-Oxo Oxidants Give Correlations between Intrinsic Properties of the Oxidant with Barrier Height, *J. Am. Chem. Soc.*, **132**, 1087-1097.

de Visser, S.P. (2010) Trends in Substrate Hydroxylation Reactions by Heme and Nonheme Iron(IV)-Oxo Oxidants Give Correlations between Intrinsic Properties of the Oxidant with Barrier Height, *J. Am. Chem. Soc.*, **132**, 1087-1097.

de Visser, S.P. and Aluri, S. (2007) The mechanism of cysteine oxygenation by cysteine dioxygenase enzymes, *J. Am. Chem. Soc.*, **129**, 14846-+.

de Visser, S.P., Kumar, D. and Shaik, S. (2004) How do aldehyde side products occur during alkene epoxidation by cytochrome P450? Theory reveals a state-specific multi-state scenario where the high-spin component leads to all side products, *J. Inorg. Biochem.*, **98**, 1183-1193.

de Visser, S.P*., et al.* (2011) The Axial Ligand Effect on Aliphatic and Aromatic Hydroxylation by Non-heme Iron(IV)-oxo Biomimetic Complexes, *Chem-Asian J*, **6**, 493-504.

de Visser, S.P. and Nam, W. (2008) The Effect and Influence of cis-Ligands on the Electronic and Oxidizing Properties of Nonheme Oxoiron Biomimetics. A Density Functional Study, *J Phys Chem A*, **112**, 12887-12895.

de Visser, S.P., Ogliaro, F. and Shaik, S. (2001) How does ethene inactivate cytochrome P450 en route to its epoxidation? A density functional study, *Angew. Chem.*, **113**, 2955-2958.

de Visser, S.P*., et al.* (2002) Hydrogen Bonding Modulates the Selectivity of Enzymatic Oxidation by P450: Chameleon Oxidant Behavior by Compound I, *Angewandte Chemie*, **114**, 2027-2031.

de Visser, S.P*., et al.* (2002) What factors affect the regioselectivity of oxidation by cytochrome P450? A DFT study of allylic hydroxylation and double bond epoxidation in a model reaction, *J. Am. Chem. Soc.*, **124**, 11809-11826.

de Visser, S.P. and Straganz, G.D. (2009) Why Do Cysteine Dioxygenase Enzymes Contain a 3-His Ligand Motif Rather than a 2His/1Asp Motif Like Most Nonheme Dioxygenases?, *J Phys Chem A*, **113**, 1835-1846.

de Visser, S.P., Tahsini, L. and Nam, W. (2009) How Does the Axial Ligand of Cytochrome P450 Biomimetics Influence the Regioselectivity of Aliphatic versus Aromatic Hydroxylation?, *Chem.--Eur. J.*, **15**, 5577-5587.

Decker, A. and Solomon, E.I. (2005) Dioxygen activation by copper, heme and non-heme iron enzymes: comparison of electronic structures and reactivities, *Curr. Opin. Chem. Biol.*, **9**, 152-163.

Delaney, J.C. and Essigmann, J.M. (2004) Mutagenesis, genotoxicity, and repair of 1-methyladenine, 3-alkylcytosines, 1-methylguanine, and 3-methylthymine in alkB *Escherichia coli*, *P Natl Acad Sci USA*, **101**, 14051.

Denisov, I.G*., et al.* (2005) Structure and chemistry of cytochrome P450, *Chem. Rev.*, **105**, 2253-2278.

Ditchfield, R., Hehre, W. and Pople, J.A. (1971) Self consistent molecular orbital methods. IX. An extended Gaussian type basis for molecular orbital studies of organic molecules, *J. Chem. Phys.*, **54**, 724.

Duncan, T*., et al.* (2002) Reversal of DNA alkylation damage by two human dioxygenases, *Proc. Natl. Acad. Sci. U. S. A.*, **99**, 16660.

Elkins, J.M*., et al.* (2002) X-ray crystal structure of Escherichia coli taurine/ -ketoglutarate dioxygenase complexed to ferrous iron and substrates, *Biochemistry*, **41**, 5185-5192.

Emerson, J.P., Farquhar, E.R. and Que, L. (2007) Structural “Snapshots” along Reaction Pathways of Non-Heme Iron Enzymes, *Angew. Chem., Int. Ed.*, **46**, 8553-8556.

Falnes, P.Ø. (2004) Repair of 3-methylthymine and 1-methylguanine lesions by bacterial and human AlkB proteins, *Nucleic Acids Res.*, **32**, 6260.

Falnes, P.Ø*., et al.* (2004) Substrate specificities of bacterial and human AlkB proteins, *Nucleic Acids Res.*, **32**, 3456.

Falnes, P.O., Johansen, R.F. and Seeberg, E. (2002) AlkB-mediated oxidative demethylation reverses DNA damage in *Escherichia coli*, *Nature*, **419**, 178-182.

Falnes, P.Ø., Johansen, R.F. and Seeberg, E. (1999) AlkB-mediated oxidative demethylation reverses DNA damage in *Escherichia coli*, *Biochemistry*, **38**, 15278-15286.

Flurry, R.L. (1983) *Quantum chemistry : an introduction*. Prentice-Hall, Englewood Cliffs, N.J.

Foresman, J.B., Frisch, Æ. and Gaussian, I. (1996) Exploring chemistry with electronic structure methods.

Frisch, M*., et al.* (2004) Gaussian 03, revision D. 01, *Gaussian, Inc.: Wallingford, CT*.

Fukuzumi, S*., et al.* (2010) Contrasting Effects of Axial Ligands on Electron Transfer Versus Proton Coupled Electron Transfer Reactions of Nonheme Oxoiron (IV) Complexes, *Chem.--Eur. J.*, **16**, 354-361.

Georgiev, V*., et al.* (2008) A comparison of the reaction mechanisms of iron- and manganese-containing 2,3-HPCD: an important spin transition for manganese, *J. Biol. Inorg. Chem.*, **13**, 929-940.

Georgieva, P. and Himo, F. (2010) Quantum chemical modeling of enzymatic reactions: The case of histone lysine methyltransferase, *J. Comput. Chem.*, **31**, 1707-1714.

Ghosh, A., Persson, B.J. and Taylor, P.R. (2003) Ab initio multiconfiguration reference perturbation theory calculations on the energetics of low-energy spin states of iron (III) porphyrins, *J. Biol. Inorg. Chem.*, **8**, 507-511.

Godfrey, E., Porro, C.S. and de Visser, S.P. (2008) Comparative quantum mechanics/molecular mechanics (QM/MM) and density functional theory calculations on the oxo-iron species of taurine/α-ketoglutarate dioxygenase, *J Phys Chem A*, **112**, 2464-2468.

Gopal, B*., et al.* (2005) The crystal structure of a quercetin 2, 3-dioxygenase from *Bacillus subtilis* suggests modulation of enzyme activity by a change in the metal ion at the active site (s), *Biochemistry*, **44**, 193-201.

Green, M.T. (2006) Application of Badger's Rule to Heme and Non-Heme Iron−Oxygen Bonds: An Examination of Ferryl Protonation States, *J. Am. Chem. Soc.*, **128**, 1902-1906.

Green, M.T., Dawson, J.H. and Gray, H.B. (2004) Oxoiron(IV) in chloroperoxidase compound II is basic: Implications for P450 chemistry, *Science*, **304**, 1653-1656.

Grinter, R. (2005) *The quantum in chemistry: an experimentalist's view*. Wiley.

Gross, Z. (1996) The effect of axial ligands on the reactivity and stability of the oxoferryl moiety in model complexes of Compound I of heme-dependent enzymes, *J. Biol. Inorg. Chem.*, **1**, 368-371.

Gross, Z. and Nimri, S. (1994) A pronounced axial ligand effect on the reactivity of oxoiron (IV) porphyrin cation radicals, *Inorg. Chem.*, **33**, 1731-1732.

Guo, J.D., Luo, Y. and Himo, F. (2003) DNA repair by spore photoproduct lyase: A density functional theory study, *J Phys Chem B*, **107**, 11188-11192.

Haas, A.E. and Codd, L.W. (1930) *Quantum chemistry; a short introduction in four non-mathematical lectures*. R.R. Smith, New York,.

Hall, G.G. (1951) The Molecular Orbital Theory of Chemical Valency .8. A Method of Calculating Ionization Potentials, *Proc. R. Soc. London, A*, **205**, 541-552.

Hanson, R.S. and Hanson, T.E. (1996) Methanotrophic bacteria, *Microbiol. Mol. Biol. Rev.*, **60**, 439.

Hausinger, R.P. (2004) Fe (II)/ -ketoglutarate-dependent hydroxylases and related enzymes, *Crit. Rev. Biochem. Mol. Biol.*, **39**, 21-68.

Hay, P.J. and Wadt, W.R. (1985) Ab initio effective core potentials for molecular calculations. Potentials for the transition metal atoms Sc to Hg, *J. Chem. Phys.*, **82**, 270-283.

Hayaishi, O. (1994) Tryptophan, oxygen, and sleep, *Annu. Rev. Biochem.*, **63**, 1-25.

Hayaishi, O. (2005) Fifty years of oxygen activation, *J. Biol. Inorg. Chem.*, **10**, 1-2.

Hayaishi, O., Takikawa, O. and Yoshida, R. (1990) Indoleamine 2, 3 Dioxygenase: Properties and Functions of a Superoxide Utilizing Enzyme, *Prog. Inorg. Chem.*, 75-95.

He, C., Mishina, Y. and Duguid, E.M. (2006) Direct reversal of DNA alkylation damage, *Chem. Rev.*, **106**, 215-232.

Heafield, M.T*., et al.* (1990) Plasma Cysteine and Sulfate Levels in Patients with Motor-Neuron, Parkinsons and Alzheimers-Disease, *Neurosci. Lett.*, **110**, 216-220.

Hegg, E.L. and Que, L., Jr. (1997) The 2-His-1-carboxylate facial triad--an emerging structural motif in mononuclear non-heme iron(II) enzymes, *Eur J Biochem*, **250**, 625-629.

Heisenberg, W. (1930) *The physical principles of the quantum theory*. Dover Publications, [New York].

Heisenberg, W., Eckhart, C.H. and Hoyt, F.C. (1930) *The physical principles of the quantum theory*. University of Chicago science series. The University of Chicago Press, Chicago, Ill.

Higgins, L.J*., et al.* (2005) Structural insight into antibiotic fosfomycin biosynthesis by a mononuclear iron enzyme, *Nature*, **437**, 838-844.

Hirao, H., *et al.* (2006) Two-state reactivity in alkane hydroxylation by non-heme iron-oxo complexes, *J. Am. Chem. Soc.*, **128**, 8590-8606.

Hirao, H., *et al.* (2008) A two-state reactivity rationale for counterintuitive axial ligand effects on the C–H activation reactivity of non-heme Fe IV= O oxidants, *Chem Eur J*, **14**, 1740-1756.

Hohenberg, P. and Kohn, W. (1964) Inhomogeneous Electron Gas, *Phys Rev B*, **136**, B864-&.

Horton, H.R. (1996) *Principles of biochemistry*. Prentice Hall, Upper Saddle River, NJ.

Horton, H.R. (2006) *Principles of biochemistry*. Pearson Prentice Hall, Upper Saddle River, N.J.

Jackson, T.A., *et al.* (2008) Axial ligand effects on the geometric and electronic structures of nonheme oxoiron (IV) complexes, *J. Am. Chem. Soc.*, **130**, 12394-12407.

Jaenicke, R. (1991) Protein folding: Local structures, domains, subunits, and assemblies, *Biochemistry*, **30**, 3147-3161.

Jensen, F. (2007) *Introd. comput. chem.* Wiley.

Jensen, K.P., *et al.* (2010) Experimentally calibrated computational chemistry of tryptophan hydroxylase: Trans influence, hydrogen-bonding, and 18-electron rule govern O(2)-activation, *J. Inorg. Biochem.*, **104**, 136-145.

Jensen, K.P., Roos, B.O. and Ryde, U. (2005) O2-binding to heme: electronic structure and spectrum of oxyheme, studied by multiconfigurational methods, *J. inorg. biochem.*, **99**, 45-54.

Jensen, M.P., *et al.* (2007) Kinetic analysis of the conversion of nonheme (alkylperoxo) iron (III) species to iron (IV) complexes, *Inorg. Chem.*, **46**, 2398-2408.

Jiang, Y., *et al.* (2010) Iron(II)-Thiolate S-Oxygenation by O2: Synthetic Models of Cysteine Dioxygenase, *J. Am. Chem. Soc.*, **132**, 12214-12215.

Joseph, C.A. and Maroney, M.J. (2007) Cysteine dioxygenase: structure and mechanism, *Chem. Commun.*, 3338-3349.

Kamachi, T., Shestakov, A.F. and Yoshizawa, K. (2004) How heme metabolism occurs in heme oxygenase: computational study of oxygen-donation ability of the oxo and hydroperoxo species, *J. Am. Chem. Soc.*, **126**, 3672-3673.

Karamzadeh, B., *et al.* (2010) Steric Factors Override Thermodynamic Driving Force in Regioselectivity of Proline Hydroxylation by Prolyl-4-hydroxylase Enzymes, *J Phys Chem A*, **114**, 13234-13243.

Karplus, P.A., *et al.* (2006) Crystal structure of mammalian cysteine dioxygenase - A novel mononuclear iron center for cysteine thiol oxidation, *J. Biol. Chem.*, **281**, 18723-18733.

Kataoka, H., Yamamoto, Y. and Sekiguchi, M. (1983) A New Gene (Alkb) of Escherichia-Coli That Controls Sensitivity to Methyl Methane Sulfonate, *J. Bacteriol.*, **153**, 1301-1307.

Kauzmann, W. (1957) *Quantum chemistry; an introduction*. Academic Press, New York,.

Keeler, J. and Wothers, P. (2008) *Chemical structure and reactivity : an integrated approach*. Oxford University Press, Oxford.

Knott, L. and Bailey, A.J. (1998) Collagen cross-links in mineralizing tissues: A review of their chemistry, function, and clinical relevance, *Bone*, **22**, 181-187.

Koehntop, K.D., Emerson, J.P. and Que, L. (2005) The 2-His-1-carboxylate facial triad: a versatile platform for dioxygen activation by mononuclear non-heme iron (II) enzymes, *J. Biol. Inorg. Chem.*, **10**, 87-93.

Kohn, W., Becke, A.D. and Parr, R.G. (1996) Density functional theory of electronic structure, *J. Phys. Chem.*, **100**, 12974-12980.

Kohn, W. and Sham, L. (1965) Self-consistent equations including exchange and correlation effects, *Phys. Rev. A*, **140**, 1133-1138.

Koivisto, P.*, et al.* (2003) Minimal methylated substrate and extended substrate range of *Escherichia coli* AlkB protein, a 1-methyladenine-DNA dioxygenase, *J. Biol. Chem.*, **278**, 44348.

Kovaleva, E.G.*, et al.* (2007) Finding Intermediates in the O2 Activation Pathways of Non-Heme Iron Oxygenases, *Accounts of chemical research*, **40**, 475-483.

Krebs, C.*, et al.* (2007) Non-heme Fe (IV)–oxo intermediates, *Acc. Chem. Res.*, **40**, 484-492.

Krebs, C.*, et al.* (2005) Rapid Freeze-Quench 57Fe Mössbauer Spectroscopy: Monitoring Changes of an Iron-Containing Active Site during a Biochemical Reaction, *Inorg. Chem.*, **44**, 742-757.

Kryatov, S.V., Rybak-Akimova, E.V. and Schindler, S. (2005) Kinetics and mechanisms of formation and reactivity of non-heme iron oxygen intermediates, *Chem. Rev.*, **105**, 2175-2226.

Kudrik, E.V. and Sorokin, A.B. (2008) N Bridged Diiron Phthalocyanine Catalyzes Oxidation of Benzene with H2O2 via Benzene Oxide with NIH Shift Evidenced by Using 1, 3, 5 [D3] Benzene as a Probe, *Chem.-Eur. J.*, **14**, 7123-7126.

Kumar, D., de Visser, S.P. and Shaik, S. (2005) Multistate reactivity in styrene epoxidation by compound I of cytochrome P450: Mechanisms of products and side products formation, *Chem.--Eur. J.*, **11**, 2825-2835.

Kumar, D.*, et al.* (2004) Radical clock substrates, their CH hydroxylation mechanism by cytochrome P450, and other reactivity patterns: what does theory reveal about the clocks' behavior?, *J. Am. Chem. Soc.*, **126**, 1907-1920.

Kumar, D.*, et al.* (2010) What Factors Influence the Rate Constant of Substrate Epoxidation by Compound I of Cytochrome P450 and Analogous Iron(IV)-Oxo Oxidants?, *J. Am. Chem. Soc.*, **132**, 7656-7667.

Kumar, D., Thiel, W. and de Visser, S.P. (2011) Theoretical Study on the Mechanism of the Oxygen Activation Process in Cysteine Dioxygenase Enzymes, *J. Am. Chem. Soc.*

Kumar, D.K., D., Thiel, W. and de Visser, S.P. (2011) Theoretical Study on the Mechanism of the Oxygen Activation Process in Cysteine Dioxygenase Enzymes, *J Am Chem Soc*, **133**, 3869-3882.

Lanzilotta, W.N.*, et al.* (2003) Substrate-induced conformational changes in *Escherichia coli* taurine/alpha-ketoglutarate dioxygenase and insight into the oligomeric structure, *Biochemistry*, **42**, 5547-5554.

Leach, A.R. (2001) *Molecular modelling: principles and applications*. Addison-Wesley Longman Ltd.

Lee, C., Yang, W. and Parr, R.G. (1988) Development of the Colle-Salvetti correlation-energy formula into a functional of the electron density, *Phys Rev B*, **37**, 785-789.

Lee, P.J.*, et al.* (1997) Hypoxia-inducible factor-1 mediates transcriptional activation of the heme oxygenase-1 gene in response to hypoxia, *J. Biol. Chem.*, **272**, 5375.

Lee, Y.-M.*, et al.* (2010) Dioxygen Activation by a Non-Heme Iron(II) Complex: Formation of an Iron(IV)−Oxo Complex via C−H Activation by a Putative Iron(III)−Superoxo Species, *J. Am. Chem. Soc.*, **132**, 10668-10670.

Levine, I.N. (2000) *Quantum chemistry*. Prentice Hall, Upper Saddle River, N.J.

Levine, R.D. (2005) *Molecular reaction dynamics*. Cambridge Univ Pr.

Liu, H., Llano, J. and Gauld, J.W. (2009) A DFT Study of Nucleobase Dealkylation by the DNA Repair Enzyme AlkB, *J Phys Chem B*, **113**, 4887-4898.

Lonsdale, R., Harvey, J.N. and Mulholland, A.J. (2009) Compound I reactivity defines alkene oxidation selectivity in cytochrome P450cam, *J Phys Chem B*, **114**, 1156-1162.

Lonsdale, R., Harvey, J.N. and Mulholland, A.J. (2010) Inclusion of Dispersion Effects Significantly Improves Accuracy of Calculated Reaction Barriers for Cytochrome P450 Catalyzed Reactions, *J. Phys. Chem. Lett.*, **1**, 3232-3237.

Lovell, T.*, et al.* (2003) Density functional methods applied to metalloenzymes, *Coord. Chem. Rev.*, **238**, 211-232.

Lutz, W.K. (1990) Endogenous Genotoxic Agents and Processes as a Basis of Spontaneous Carcinogenesis, *Mutat Res*, **238**, 287-295.

MacKerell Jr, A.*, et al.* (1998) All-atom empirical potential for molecular modeling and dynamics studies of proteins, *J Phys Chem B*, **102**, 3586-3616.

Marco, P.*, et al.* (2004) Novel pollutant resistant methylotrophic bacteria for use in bioremediation, *FEMS Microbiol. Lett.*, **234**, 75-80.

Maseras, F. and Morokuma, K. (1995) Imomm: A new ab initio+ molecular mechanics geometry optimization scheme of equilibrium structures and transition states, *J. Comp. Chem*, **16**, 1170-1179.

Matouschek, A.*, et al.* (1989) Mapping the transition state and pathway of protein folding by protein engineering, *Nature*, **340**, 122-126.

McQuarrie, D.A. (2008) *Quantum chemistry*. Univ Science Books.

Merkx, M.*, et al.* (2001) Dioxygen Activation and Methane Hydroxylation by Soluble Methane Monooxygenase: A Tale of Two Irons and Three Proteins, *Angewandte Chemie International Edition*, **40**, 2782-2807.

Mishina, Y., Chen, L.X. and He, C. (2004) Preparation and characterization of the native iron (II)-containing DNA repair AlkB protein directly from *Escherichia coli*, *J. Am. Chem. Soc.*, **126**, 16930-16936.

Mishina, Y., Duguid, E.M. and He, C. (2006) Direct reversal of DNA alkylation damage, *Chem. Rev.*, **106**, 215-232.

Mishina, Y. and He, C. (2003) Probing the structure and function of the *Escherichia coli* DNA alkylation repair AlkB protein through chemical cross-linking, *J. Am. Chem. Soc.*, **125**, 8730-8731.

Mishina, Y. and He, C. (2006) Oxidative dealkylation DNA repair mediated by the mononuclear non-heme iron AlkB proteins, *J. Inorg. Biochem.*, **100**, 670-678.

Mukherjee, A.*, et al.* (2010) Oxygen activation at mononuclear nonheme iron centers: A superoxo perspective, *Inorg. Chem.*, **49**, 3618-3628.

Mulholland, A.J. (2007) Chemical accuracy in QM/MM calculations on enzyme-catalysed reactions, *Chem Cent J*, **1**, 19.

Mulholland, A.J., Grant, G.H. and Richards, W.G. (1993) Computer modelling of enzyme catalysed reaction mechanisms, *Protein engineering*, **6**, 133.

Müller, J. and Bröring, M. (2008) Iron Catalysis in Biological and Biomimetic Reactions. In, *Iron Catalysis in Organic Chemistry*. Wiley-VCH Verlag GmbH & Co. KGaA, pp. 29-72.

Murrell, J.C., Gilbert, B. and McDonald, I.R. (2000) Molecular biology and regulation of methane monooxygenase, *Arch. Microbiol.*, **173**, 325-332.

Nakashima, H., Hasegawa, J. and Nakatsuji, H. (2006) On the O2 binding of Fe–porphyrin, Fe–porphycene, and Fe–corrphycene complexes, *J. Compu. Chem.*, **27**, 1363-1372.

Nam, W. (2007) High-Valent Iron (IV)–Oxo Complexes of Heme and Non-Heme Ligands in Oxygenation Reactions, *Acc. Chem. Res.*, **40**, 522-531.

Nam, W., Ryu, Y.O. and Song, W.J. (2004) Oxidizing intermediates in cytochrome P450 model reactions, *J. Biol. Inorg. Chem.*, **9**, 654-660.

Parr, R.G. (1983) Density functional theory, *Annu. Rev. Phys. Chem.*, **34**, 631-656.

Parr, R.G. and Yang, W. (1984) Density functional approach to the frontier-electron theory of chemical reactivity, *J. Am. Chem. Soc.*, **106**, 4049-4050.

Pavel, E.G.*, et al.* (1998) Circular dichroism and magnetic circular dichroism spectroscopic studies of the non-heme ferrous active site in clavaminate synthase and its interaction with alpha-ketoglutarate cosubstrate, *J. Am. Chem. Soc.*, **120**, 743-753.

Pechukas, P. (1981) Transition state theory, *Annu. Rev. Phys. Chem.*, **32**, 159-177.

Perdew, J.P. and Wang, Y. (1992) Accurate and simple analytic representation of the electron-gas correlation energy, *Phys Rev B*, **45**, 13244.

Perry, T.L.*, et al.* (1985) Hallervorden-Spatz Disease - Cysteine Accumulation and Cysteine Dioxygenase Deficiency in the Globus Pallidus, *Ann Neurol*, **18**, 482-489.

Phillips, G.N.*, et al.* (2006) Structure and mechanism of mouse cysteine dioxygenase, *P Natl Acad Sci USA*, **103**, 3084-3089.

Pierce, B.S.*, et al.* (2007) Characterization of the nitrosyl adduct of substrate-bound mouse cysteine dioxygenase by electron paramagnetic resonance: electronic structure of the active site and mechanistic implications, *Biochemistry*, **46**, 8569-8578.

Pinnell, S.R. and Martin, G.R. (1968) The cross-linking of collagen and elastin: enzymatic conversion of lysine in peptide linkage to alpha-aminoadipic-delta-semialdehyde (allysine) by an extract from bone, *P Natl Acad Sci USA*, **61**, 708.

Porro, C.S., Kumar, D. and de Visser, S.P. (2009) Electronic properties of pentacoordinated heme complexes in cytochrome P450 enzymes: search for an Fe (I) oxidation state, *Phys. Chem. Chem. Phys.*, **11**, 10219-10226.

Poulos, T.L. (1996) The role of the proximal ligand in heme enzymes, *J. Biol. Inorg. Chem.*, **1**, 356-359.

Poulos, T.L. (2005) Structural biology of heme monooxygenases, *Biochem Bioph Res Co*, **338**, 337-345.

Prokop, K.A., De Visser, S.P. and Goldberg, D.P. (2010) Unprecedented rate enhancements of hydrogen-atom transfer to a manganese(v)-oxo corrolazine complex, *Angew. Chem., Int. Ed.*, **49**, 5091-5095.

Proshlyakov, D.A.*, et al.* (2004) Direct detection of oxygen intermediates in the non-heme Fe enzyme taurine/ alpha-ketoglutarate dioxygenase, *J. Am. Chem. Soc.*, **126**, 1022-1023.

Purpero, V. and Moran, G.R. (2007) The diverse and pervasive chemistries of the -keto acid dependent enzymes, *J. Biol. Inorg. Chem.*, **12**, 587-601.

Que Jr, L. and Ho, R.Y.N. (1996) Dioxygen activation by enzymes with mononuclear non-heme iron active sites, *Chemical reviews*, **96**, 2607-2624.

Que, L. (2000) One motif - many different reactions, *Nat. Struc. Biol.*, **7**, 182-184.

Rappe, A.*, et al.* (1992) UFF, a full periodic table force field for molecular mechanics and molecular dynamics simulations, *J. Am. Chem. Soc.*, **114**, 10024-10035.

Rappe, A.K. and Casewit, C.J. (1997) *Molecular mechanics across chemistry*. Univ Science Books.

Reißner, T., Schorr, S. and Carell, T. (2009) Once Overlooked, Now Made Visible: ATL Proteins and DNA Repair, *Angew. Chem., Int. Ed.*, **48**, 7293-7295.

Riggs-Gelasco, P.J.*, et al.* (2004) EXAFS spectroscopic evidence for an Fe O unit in the Fe (IV) intermediate observed during oxygen activation by taurine: -ketoglutarate dioxygenase, *J. Am. Chem. Soc.*, **126**, 8108-8109.

Roelfes, G.*, et al.* (2003) End-on and side-on peroxo derivatives of non-heme iron complexes with pentadentate ligands: models for putative intermediates in biological iron/dioxygen chemistry, *Inorg. Chem.*, **42**, 2639-2653.

Roothaan, C.C.J. (1951) New Developments in Molecular Orbital Theory, *Rev Mod Phys*, **23**, 69-89.

Roothaan, C.C.J. (1951) A Study of 2-Center Integrals Useful in Calculations on Molecular Structure .1., *J Chem Phys*, **19**, 1445-1458.

Rosenzweig, A.C.*, et al.* (1995) Geometry of the soluble methane monooxygenase catalytic diiron center in two oxidation states, *Chem. Biol.*, **2**, 409-418.

Roy, T.W. and Bhagwat, A. (2007) Kinetic studies of Escherichia coli AlkB using a new fluorescence-based assay for DNA demethylation, *Nucleic Acids Res.*, **35**, e147.

Rydberg, P., Sigfridsson, E. and Ryde, U. (2004) On the role of the axial ligand in heme proteins: a theoretical study, *J. Biol. Inorg. Chem.*, **9**, 203-223.

Ryle, M.J. and Hausinger, R.P. (2002) Non-heme iron oxygenases, *Curr. Opin. Chem. Biol.*, **6**, 193-201.

Sanchez-Pulido, L. and Andrade-Navarro, M. (2007) The FTO (fat mass and obesity associated) gene codes for a novel member of the non-heme dioxygenase superfamily, *BMC biochemistry*, **8**, 23.

Sastri, C.V.*, et al.* (2007) Axial ligand tuning of a nonheme iron (IV)–oxo unit for hydrogen atom abstraction, *Proc. Natl. Acad. Sci. U. S. A.*, **104**, 19181-19186.

Schlegel, H.B. (1982) Optimization of equilibrium geometries and transition structures, *J. Comput. Chem.*, **3**, 214-218.

Schneider, I. (1998) Quantum achievements win Nobel Prize in chemistry, *Scientist*, **12**, 4-4.

Schofield, C.J.*, et al.* (2010) Structural studies on human 2-oxoglutarate dependent oxygenases, *Curr Opin Struc Biol*, **20**, 659-672.

Schofield, C.J. and Zhang, Z.H. (1999) Structural and mechanistic studies on 2-oxoglutarate-dependent oxygenases and related enzymes, *Curr. Opin. Stru. Biol.*, **9**, 722-731.

Schöneboom, J.C.*, et al.* (2004) Quantum mechanical/molecular mechanical investigation of the mechanism of CH hydroxylation of camphor by cytochrome P450cam: theory supports a two-state rebound mechanism, *J. Am. Chem. Soc.*, **126**, 4017-4034.

Schrodinger, E. (1994) 'Moe Mirovozzrenie' + Quantum-Mechanics, Metaphysics and Philosophy, *Vop Filos*, 70-94.

Schrödinger, E. (1926) An Undulatory Theory of the Mechanics of Atoms and Molecules, *Phys Rev*, **28**, 1049.

Schulz, G.E. and Schirmer, R.H. (1979) *Principles of protein structure*. Springer.

Scott, A.P. and Radom, L. (1996) Harmonic vibrational frequencies: An evaluation of Hartree-Fock, Møller-Plesset, quadratic configuration interaction, density functional theory, and semiempirical scale factors, *J. Phys. Chem.*, **100**, 16502-16513.

Senn, H. and Thiel, W. (2007) QM/MM Methods for Biological Systems. In Reiher, M. (ed), *Atomistic approaches in modern biology*. Springer Berlin / Heidelberg, pp. 173-290.

Senn, H.M. and Thiel, W. (2009) QM/MM methods for biomolecular systems, *Angew. Chem. Int. Ed*, **48**, 1198–1229.

Shaik, S.*, et al.* (1995) Two-State Reactivity in Organometallic Gas-Phase Ion Chemistry, *Helv. Chim. Acta*, **78**, 1393-1407.

Shaik, S.*, et al.* (2002) Two-state reactivity mechanisms of hydroxylation and epoxidation by cytochrome P-450 revealed by theory, *Curr. Opin. Chem. Biol.*, **6**, 556-567.

Shaik, S.*, et al.* (1998) Electronic structure makes a difference: Cytochrome P-450 mediated hydroxylations of hydrocarbons as a two-state reactivity paradigm, *Chem.--Eur. J.*, **4**, 193-199.

Shaik, S., Hirao, H. and Kumar, D. (2007) Reactivity of High-Valent Iron–Oxo Species in Enzymes and Synthetic Reagents: A Tale of Many States, *Acc. Chem. Res.*, **40**, 532-542.

Shaik, S., Kumar, D. and de Visser, S.P. (2008) Valence bond modeling of trends in hydrogen abstraction barriers and transition states of hydroxylation reactions catalyzed by cytochrome P450 enzymes, *J. Am. Chem. Soc.*, **130**, 10128-10140.

Shaik, S.*, et al.* (2005) Theoretical perspective on the structure and mechanism of cytochrome P450 enzymes, *Chem. Rev.*, **105**, 2279-2328.

Shaik, S.*, et al.* (2005) Theoretical Perspective on the Structure and Mechanism of Cytochrome P450 Enzymes†, *Chem. Rev.*, **105**, 2279-2328.

Shaik, S.*, et al.* (2005) The intrinsic axial ligand effect on propene oxidation by horseradish peroxidase versus cytochrome P450 enzymes, *J. Biol. Inorg. Chem.*, **10**, 181-189.

Siegbahn, P.E.M. (2001) O-O bond cleavage and alkane hydroxylation in methane monooxygenase, *J. Biol. Inorg. Chem.*, **6**, 27-45.

Siegbahn, P.E.M. (2003) Mechanisms of metalloenzymes studied by quantum chemical methods, *Q. Rev. Biophys.*, **36**, 91-145.

Siegbahn, P.E.M. (2006) O-O Bond Formation in the S4 State of the Oxygen-Evolving Complex in Photosystem II, *Chem.--Eur. J.*, **12**, 9217-9227.

Siegbahn, P.E.M., Bassan, A. and Borowski, T. (2004) Quantum chemical studies of dioxygen activation by mononuclear non-heme iron enzymes with the 2-His-1-carboxylate facial triad, *Dalton T*, 3153-3162.

Siegbahn, P.E.M. and Blomberg, M.R.A. (1999) DENSITY FUNCTIONAL THEORY OF BIOLOGICALLY RELEVANT METAL CENTERS, *Annu. Rev. Phys. Chem.*, **50**, 221-249.

Siegbahn, P.E.M. and Blomberg, M.R.A. (2010) Quantum Chemical Studies of Proton-Coupled Electron Transfer in Metalloenzymes, *Chem. Rev.*

Siegbahn, P.E.M. and Crabtree, R.H. (1997) Mechanism of C−H Activation by Diiron Methane Monooxygenases: Quantum Chemical Studies, *J. Am. Chem. Soc.*, **119**, 3103-3113.

Siegbahn, P.E.M., Crabtree, R.H. and Nordlund, P. (1998) Mechanism of methane monooxygenase – a structural and quantum chemical perspective, *J. Biol. Inorg. Chem.*, **3**, 314-317.

Siegbahn, P.E.M. and Himo, F. (2009) Recent developments of the quantum chemical cluster approach for modeling enzyme reactions, *J. Biol. Inorg. Chem.*, **14**, 643-651.

Siegel, R.C. and Martin, G. (1970) Collagen cross-linking, *J. Biol. Chem.*, **245**, 1653.

Solomon, E.I.*, et al.* (2000) Geometric and electronic structure/function correlations in non-heme iron enzymes, *Chem. Rev.*, **100**, 235-350.

Solomon, E.I. and Zhang, Y. (1992) The electronic structures of active sites in non-heme iron enzymes, *Accounts of chemical research*, **25**, 343-352.

Song, W.J.*, et al.* (2005) Oxoiron (IV) porphyrin -cation radical complexes with a chameleon behavior in cytochrome P450 model reactions, *J. Biol. Inorg. Chem.*, **10**, 294-304.

Sono, M.*, et al.* (1996) Heme-containing oxygenases, *Chem. Rev.*, **96**, 2841-2888.

Sorokin, A.B.*, et al.* (2009) Preparation and characterization of mu-nitrido diiron phthalocyanines with electron-withdrawing substituents: application for catalytic aromatic oxidation, *Dalton T*, 7410-7420.

Sorokin, A.B.*, et al.* (2010) Preparation of N-bridged diiron phthalocyanines bearing bulky or small electron-withdrawing substituents, *J. Porphyrins Phthalocyanines*, **14**, 324-334.

Sorokin, A.B.*, et al.* (2009) Preparation of iron phthalocyanine complex bearing four tetraazamacrocycles as a precursor for oxidation catalyst with two catalytic sites, *J. Porphyrins Phthalocyanines*, **13**, 747-752.

Sorokin, A.B., Kudrik, E.V. and Bouchu, D. (2008) Bio-inspired oxidation of methane in water catalyzed by N-bridged diiron phthalocyanine complex, *Chem Commun*, 2562-2564.

Stipanuk, M.H. (2004) Sulfur amino acid metabolism: pathways for production and removal of homocysteine and cysteine, *Annu. Rev. Nutr.*, **24**, 539-577.

Straganz, G.D. and Nidetzky, B. (2006) Variations of the 2-His-1-carboxylate theme in mononudear non-heme Fe-III oxygenases, *Chembiochem*, **7**, 1536-1548.

Strieker, M.*, et al.* (2007) Mechanistic and structural basis of stereospecific C -hydroxylation in calcium-dependent antibiotic, a daptomycin-type lipopeptide, *ACS chemical biology*, **2**, 187-196.

Szabo, A. and Ostlund, N.S. (1996) *Modern quantum chemistry: introduction to advanced electronic structure theory*. Dover Pubns.

Townsend, C.A. (2002) New reactions in clavulanic acid biosynthesis, *Curr. Opin. Chem. Biol.*, **6**, 583-589.

Trewick, S.C.*, et al.* (2002) Oxidative demethylation by Escherichia coli AlkB directly reverts DNA base damage, *Nature*, **419**, 174-178.

Vosko, S.H., Wilk, L. and Nusair, M. (1980) Accurate spin-dependent electron liquid correlation energies for local spin density calculations: a critical analysis, *Can. J. Phys.*, **58**, 1200-1211.

Wackett, L.P. (2002) Mechanism and applications of Rieske non-heme iron dioxygenases, *Enzyme Microb. Technol.*, **31**, 577-587.

Wadt, W.R. and Hay, P.J. (1985) Ab initio effective core potentials for molecular calculations. Potentials for main group elements Na to Bi, *J. Chem. Phys.*, **82**, 284.

Wang, J.*, et al.* (2004) Development and testing of a general amber force field, *J. Comput. Chem.*, **25**, 1157-1174.

Waterman, M.R. (2005) Professor Howard Mason and oxygen activation, *Biochem. Biophys. Res. Commun*, **338**, 7-11.

Wiener, M.C., Mohanty, A.K. and Simmons, C.R. (2003) Inhibition of tobacco etch virus protease activity by detergents, *Protein Expres Purif*, **27**, 109-114.

Wilson, K. and Walker, J.M. (2009) *Principles and techniques of biochemistry and molecular biology*. Cambridge University Press, Cambridge, UK New York.

Woggon, W.D. (2005) Metalloporphyrines as Active Site Analogues Lessons from Enzymes and Enzyme Models, *Acc. Chem. Res.*, **38**, 127-136.

Yamamoto, S. (2006) The 50th anniversary of the discovery of oxygenases, *IUBMB life*, **58**, 248-250.

Yang, L.*, et al.* (2009) DFT study on the mechanism of Escherichia coli inorganic pyrophosphatase, *J Phys Chem B*, **113**, 6505-6510.

Ye, S. and Neese, F. (2011) Nonheme oxo-iron (IV) intermediates form an oxyl radical upon approaching the C–H bond activation transition state, *Proc. Natl. Acad. Sci. U. S. A.*, **108**, 1228.

Ye, S*., et al.* (2007) An insight into the mechanism of human cysteine dioxygenase, *J. Biol. Chem.*, **282**, 3391.

Yi, C., Yang, C.G. and He, C. (2009) A non-heme iron-mediated chemical demethylation in DNA and RNA, *Acc. Chem. Res.*, **42**, 519-529.

Yoshizawa, K. and Shiota, Y. (2006) Conversion of methane to methanol at the mononuclear and dinuclear copper sites of particulate methane monooxygenase (pMMO): a DFT and QM/MM study, *J. Am. Chem. Soc.*, **128**, 9873-9881.

You, Z*., et al.* (2007) Crystal structure of the non-heme iron dioxygenase PtlH in pentalenolactone biosynthesis, *J. Biol. Chem.*, **282**, 36552.

Yu, B*., et al.* (2006) Crystal structures of catalytic complexes of the oxidative DNA, *RNA repair enzyme AlkB. Nature*, **439**, 879-884.

Yu, B. and Hunt, J. (2007) Crystal structures of catalytic complexes of the oxidative DNA/RNA repair enzyme AlkB, *life inspiring ideas*.

Yu, B. and Hunt, J.F. (2009) Enzymological and structural studies of the mechanism of promiscuous substrate recognition by the oxidative DNA repair enzyme AlkB, *Proc. Natl. Acad Sci.*, **106**, 14315-14320.

Yuryeva, E.I., Gabuda, S.i.a.P. and Pletnev, R.e.N. (2007) *Quantum chemistry and nuclear resonance spectroscopy data of natural and synthetic nanotechnological materials with ND-metal atoms participations*. Nova Science Publishers, New York.

Zhou, Y*., et al.* (2008) Contrasting cis and trans Effects on the Reactivity of Nonheme Oxoiron (IV) Complexes, *Angew. Chem., Int. Ed.*, **47**, 1896-1899.

Zhurko, G. and Zhurko, D. (2005) ChemCraft: Tool for treatment of chemical data, *Lite version build*, **8**, 2005.

Ziegler, T. (1991) Approximate density functional theory as a practical tool in molecular energetics and dynamics, *Chem. Rev.*, **91**, 651-667.

Zubay, G.L., Parson, W.W. and Vance, D.E. (1995) *Princ. Biochem.* William C. Brown, Dubuque, Iowa.